AD NUMBER
ADB004734
LIMITATION CHANGES

TO:

Approved for public release; distribution is unlimited.

FROM:

Distribution authorized to U.S. Gov't. agencies only; Test and Evaluation; MAR 1975. Other requests shall be referred to Federal Aviation Administration, Supersonic Transport Office, 800 Independence Avenue, SW, Washington, DC 20590. This document contains export-controlled technical data.

AUTHORITY

faa ltr, 26 apr 1977

SST Technology
Follow-On Program—Phase II
PERFORMANCE TECHNOLOGY
VOLUME VII

A GUIDE TO MULTITUBE SUPPRESSOR NOZZLE STATIC PERFORMANCES: TRENDS AND TRADES

D. B. Morden   R. S. Armstrong

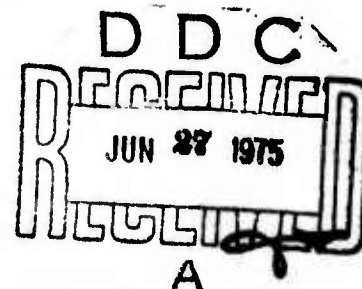Boeing Commercial Airplane Company
P.O. Box 3707
Seattle, Washington 98124

Volume VII

The contents of this report reflect the views of the Boeing
Commercial Airplane Company, which is responsible for the
facts and the accuracy of the data presented herein. The
contents do not necessarily reflect the official views or policy
of the Department of Transportation. This report does not
constitute a standard, specification, or regulation.

TECHNICAL REPORT STANDARD TITLE PAGE

1. Report No. FAA-SS-73-11-7	2. Government Accession No.	3. Recipient's Catalog No. 147 p.
4. Title and Subtitle SST TECHNOLOGY FOLLOW-ON PROGRAM—PHASE II NOISE SUPPRESSOR/NOZZLE DEVELOPMENT— Volume VII Performance Technology-- A Guide to Multitube Suppressor Nozzle Static Performance: Trends & Trades		5. Report Date Mar 75
		6. Performing Organization Code
7. Author(s) D. B. Morden R. S. Armstrong		8. Performing Organization Report No. D6-41961
9. Performing Organization Name and Address Boeing Commercial Airplane Company P.O. Box 3707 Seattle, Washington 98124		10. Work Unit No.
		11. Contract or Grant No. DOT-FA-72WA-2893
12. Sponsoring Agency Name and Address Federal Aviation Administration Supersonic Transport Office 800 Independence Avenue S.W. Washington, D.C. 20590		13. Type of Report and Period Covered Final Report Task III
		14. Sponsoring Agency Code

15. Supplementary Notes

16. Abstract

Five macroscopic geometric parameters and temperature are identified as the primary variable affecting static multitube jet noise suppressor thrust performance. The *a priori* knowledge about each variable is discussed, and reasonable ranges of interest are established. The results of an experimental investigation, treating each variable independently, are presented. Internal performance and base ventilation values are presented and analyzed.

The result of the investigation is a general static performance guide to multitube suppressor nozzles. Trends and tradeoffs are established for number, shape, length, and placement of tubes and nozzle area ratio.

SST Technology Follow-On Program-Phase II. Noise Suppressor/Nozzle Development. Volume VII. Performance Technology—A Guide to Multitube Suppressor Nozzle Static Performance: Trends and Trades.

— Volume VII

17. Key Words Supressor nozzle Aircraft propulsion Multitube suppressor Supersonic transport Nozzle performance, static Base ventilation Jet noise	18. Distribution Statement Approved for U.S. Government only. This document is exempted from public availability because of restrictions imposed by the Export Control Act. Transmittal of this document outside the U.S. Government must have prior approval of the Supersonic Transport Office.

19. Security Classif. (of this report) Unclassified	20. Security Classif. (of this page) Unclassified	21. No. of Pages	22. Price

Form DOT F 1700.7 (8-69)

390 145

PREFACE

This is one of a series of final reports on noise and propulsion technology submitted by the Boeing Commercial Airplane Company, Seattle, Washington, 98124, in fulfillment of Task III of Department of Transportation Contract DOT-FA-72WA-2893, dated 1 February 1972.

To benefit utilization of technical data developed by the noise suppressor and nozzle development program, the final report is divided into 10 volumes covering key technology areas and a summary of total program results. The 10 volumes are issued under the master title, "Noise Suppressor/Nozzle Development." Detailed volume breakdown is as follows:

This report is volume VII of the series and was prepared by the Propulsion Research Staff of the Boeing Commercial Airplane Company.

CONTENTS

CONTENTS (Continued)

FIGURES

FIGURES (Continued)

FIGURES (Continued)

ix

FIGURES (Concluded)

SYMBOLS AND ABBREVIATIONS

A, A_F, A_P Geometric flow area; measured at 70°F in inches.

A_B Base area in square inches. A (AR-1).

A_{eff} $C_D \cdot A$

amb   Ambient temperature.

A_P Geometric flow area of the nozzle at ambient temperature.

A_{PH} Geometric flow area of the nozzle including temperature induced area growth.

AR   Area ratio. Area inside a circle circumscribed around the outside of the outer most tubes in the nozzle divided by A.

(also physical area ratio)

A_S Measured area, in square inches, between the tubes in the outer row of a suppressor, see Figure 17.

A_S/l A_S per unit tube length. (inches)

A_V Total ventilation area. A_S + the calculated area between the jets in the outer row of a suppressor.

A_1 Internal cross-sectional area of a tube measured in square inches in the constant area portion of the tube.

C_D Discharge Coefficient accounting for temperature induced nozzle area growth.

$$WP / \left\{ \frac{A_{PH} \cdot PR \cdot P_\infty}{T_{TP}} \left[\frac{2g\gamma}{R(\gamma-1)} \left(PR^{-2/\gamma} - PR^{-(\gamma+1/\gamma)} \right) \right]^{1/2} \right\}$$

For this equation, if

$$PP \geqslant \left(\frac{\gamma+1}{2} \right)^{\frac{\gamma}{\gamma-1}} \qquad \text{let } PR = \left(\frac{\gamma+1}{2} \right)^{\frac{\gamma}{\gamma-1}}$$

C_f Skin friction coefficient

SYMBOLS AND ABBREVIATIONS (Continued)

C_{f_g}

Gross thrust coefficient. Measured (thrust-drag) $/\dot{m}$ VIP_o. (In the present test C_{f_g} is measured for configurations with constant internal tube length of six inches. $\Delta C_{V\,int}$ is added to this raw value of C_{f_g} to obtain the appropriate C_{f_g} for configurations with equal internal and external tube lengths.)

Close-packed

An arrangement of tubes so that there is approximately the same distance between any two adjacent tubes. (see Figure 7).

$C_{V\,int}$

Nozzle internal velocity coefficient. Measured: $C_{f_g} + D_{AFT}/FID \cdot 100$ or calculated using equation 5 in Section 5.1.

$\Delta C_{V\,int}$

Amount of internal performance lost due to excessive internal tube length (See Appendix). Calculated as the difference between $C_{V\,int}$ using L = 6 inches in equation 5, Section 5.1 and $L = L_T$ in the same equation.

d

Internal exit diameter of a tube in inches.

D

Representative diameter of constant internal tube area. Defined as $\sqrt{4A_{1}/\pi}$, see Figure 48 in Section 5.1.

D_{AFT}

Afterbody drag in pounds; $D_B + D_{RAMP}$

D_{AFT}/FID

Afterbody drag expressed as a percentage of ideal thrust.

D_B

Baseplate drag in pounds; calculated from static pressure measurements taken at area weighted taps on the baseplate.

DB/FID

Baseplate drag expressed as a percentage of ideal thrust.

D_{eq}

The exit diameter of a single round convergent nozzle having the same area as the *total* effective flow area of a multi-tube nozzle, inches.

D_{RAMP}

Drag in pounds calculated on the nozzle ramp using static pressure measured at area weighted taps.

FID

Ideal thrust in pounds; measured primary mass flow rate multiplied by the ideal, fully expanded velocity in VIP.

L

Length of the constant internal area portion of a tube in inches, see Figure 48 in Section 5.1.

SYMBOLS AND ABBREVIATIONS (Continued)

L_T — Tube length measured on the outside of the tube. Distance from the tube exit to the baseplate measured in inches.

$\dot{m}$ — Measured mass flow rate. WP/g.

N — Total number of tubes in a suppressor.

P_B — The average static pressure in PSIA obtained at area weighted taps on the nozzle baseplate.

PR — Nozzle pressure ratio. P_{T_o}/P_∞

P_{S_1} — Static pressure in the constant area portion of the tube. Function of PR and Mach number.

P_{T_P} — Nozzle charging total pressure, same as P_{T_o}.

P_{T_o} — The charging total pressure; i.e., total pressure PSIA at a station immediately upstream of the tube entrances.

P_{T_1} — Total pressure in PSIA at a station coincident with the tangent point between the tube entrance radius and the constant area portion of the tube.

P_{T_2} — Total pressure in PSIA at the station where the constant area portion of the tube is tangent to the convergent portion.

P_∞ — Ambient pressure.

ΔP_T — Inlet loss in total pressure (from ⓪ to ① in fig. 48, section 5.1).

q — Dynamic pressure.

R — Radius of the inlet to a tube in inches, see Figure 48 in Section 5.1.

Radial Array — An arrangement of tubes in radial lines to maximize ventilation. (see fig. 7).

R_b — Radius to outside of outer row tubes in inches.

Re — Reynolds number

SYMBOLS AND ABBREVIATIONS (Concluded)

R/C — Round convergent reference nozzle with 10° internal half-angle.

T_T, T_{T_p} — Average total temperature of the primary flow. ^oF unless otherwise noted.

VIP, VIP_o — Ideal velocity expanded to ambient pressure.

$$\left\{ (2gR)\left(\frac{\gamma}{\gamma-1}\right) T_{T_p} \left[1 - (PR)^{-(\gamma-1/\gamma)} \right] \right\}^{1/2}$$

WA — Measured weight flow rate of air in pounds/seconds.

WP — Measured weight flow rate of fuel and air in pounds/seconds.

a — Internal half-angle of the round convergent portion of the tube in degrees.

γ — Ratio of specific heats.

1.0 SUMMARY

The static performance of multitube jet noise suppressor nozzles (without ejectors) is investigated to provide a guide to optimize performance and quantify performance penalties and tradeoffs resulting from geometric constraints. Consideration of flow phenomena and the results of previous studies are used to establish constraints and ranges of interest for five geometric variables. A scale-model experimental investigation treats each parameter independently over a range of pressure ratios from two to four at ambient and 1150°F temperatures. Configurations tested include tube lengths compatible with the stowable suppressor concept (L_T/D_{eq} less than 0.35).

Optimum performance is shown to occur near pressure ratio 3.0 and area ratio 3.3. The most important result of the investigation is the placement of tubes on radial lines to optimize base ventilation. This is demonstrated in figure 1, where the performance of radial array multitube nozzles is compared to that of uniform (close-packed) array nozzles. A second and obvious result is that the number of tubes should be held to a minimum consistent with noise suppression requirements.

A semiempirical relationship is developed for internal performance and provides excellent agreement with data. The relationship is a function of ten geometric and flow parameters, including temperature and Reynold's number.

Figure 2 summarizes principle noise suppression results versus performance penalties relative to the noise and performance of a round convergent nozzle. Reference 1 presents the detailed results and analysis of concurrent acoustic testing.

1

2.0 INTRODUCTION

The static performance of multitube suppressor nozzles is investigated to provide a guide for optimizing performance and quantifying performance penalties and tradeoffs resulting from geometric constraints.

A parametric test and analysis are used to quantify the relative importance of five macroscopic geometric variables affecting the internal performance and external drag of a wide range of multitube suppressor nozzles, including stowable configurations compatible with supersonic transport requirements. Performance data and acoustic near- and far-field measurements were acquired simultaneously during the test. Acoustic characteristics are reported in detail in reference 1.

Supersonic cruise necessitates the use of engines with a high thrust-to-frontal-area ratio and high exhaust jet velocities. The noise associated with the high-velocity jet can be substantially reduced by placing hardware into the primary exhaust flow to break the jet into small elements. The extreme sensitivity of the supersonic aircraft mission to nozzle performance during supersonic cruise dictates that the suppressor hardware, with its inherent thrust loss, be retracted from the jet during cruise. SST technology (reference 2) demonstrated high suppression levels using multitube nozzle concepts that could be integrated into high cruise performance exhaust system (figure 3).

Previous test data (reference 3) have shown that the performance of multitube suppressor nozzles is strongly influenced by the lower-than-ambient pressure acting on the base area between elements. The reduced pressure is the result of air entrainment by each of the discrete primary jets. The extent of pressure reduction is largely dependent upon the ability to provide a sufficient quantity of ambient ventilating air to replace that entrained by the primary jets. The tube length and arrangement of the jet elements were shown to have a large effect on performance due to changes in base ventilation and thus base drag. The present work quantifies the affects of several major geometric parameters of multitube suppressors on base drag as well as internal and overall static performance.

The testing was conducted on families of suppressors with 7 to 61 equal sized tubes and a matrix of tube lengths, shapes, nozzle area ratios, and arrays (tube placements). The total effective flow area was 13.2 in. for each model. The investigation included pressure ratios from 2 to 4 at ambient and 1150°F temperatures. This analysis is the first portion of a program aimed at developing the technology necessary for the attainment of not more than 2% thrust loss for 20 PNdB static suppression relative to a round convergent nozzle. The effects of adding an ejector and forward velocity will be reported as a direct extension of the present work.

3.0 PHILOSOPHY, RANGES, LIMITATIONS, AND CONSTRAINTS

3.1 SUMMARY OF PARAMETERS

3.1.1 RANGE OF VARIABLES (See figs. 4 and 5)

- Tube number: 7-61

- Tube length (external): 1 to 4 in. (L_T/D_{eq} = .25 - 1.0)

- Area ratio: 2.75-6.0 (πR_b^2/geometric flow exist area)

- Base array: close-packed and radial

- Tube shape: round convergent, round nonconvergent, elliptical convergent (round exit)

- Ramp shape: circular arc and elliptical

- Pressure ratio: 2-4

- Primary temperature: ambient and 1150°F

3.1.2 CONSTRAINTS

- Total effective exist area 13.2 in.^{2} (geometric exist area $\approx$13.6 for convergent tubes; approximately 1/10 scale SST)

- Approximately 0.5 internal Mach number for convergent tubes

- Co-planar tube exists

- Flat baseplate

- All tubes within an array are the same (e.g., a 37-tube array has 37 tubes each with 0.36 in.^{2} effective flow area)

- Outside nacelle diameter held constant (8.89 in. to be respresentative of an actual scale SST nacelle)

3.2 PHILOSOPHY: VARIABLES, CONSTRAINTS, AND *A PRIORI* KNOWLEDGE

3.2.1 GENERAL

The study was confined to multitube suppressor nozzles operating at pressure ratios applicable to supersonic transports (i.e., between 2 and 4) at ambient and 1150°F temperatures. The suppressor, inserted into the primary flow, is inherently a thrust loss device. To

5

minimize the losses, one must understand the performance contribution of each of the various geometric parameters and temperatures. Quantifying the effects on performance due to constraining each variable is paramount for constructive interaction with the noise suppression and structural installation requirements.

Previous test data (reference 3) have shown that the performance of multitube suppressor nozzles is strongly influenced by the lower-than-ambient pressure acting on the base area between elements. The reduced pressure is the result of air entrainment by each of the discrete primary jets. The extent of pressure reduction is largely dependent upon the ability to provide a sufficient quantity of ambient ventilating air to replace the entrained by the primary jets. Air is removed from the base region by a combination of viscous and static pressure forces created by the primary flow exhausting into the surrounding air. The removal of air from the base creates a low static pressure region into which ambient air flows through the available ventilation inlet areas (between tubes and individual jet plumes). Thus, a flow field is produced consisting of air being removed from the base region by the primary flow entrainment process and ventilation air flowing into the base region. Another flow field consists of recirculation near the base. The factors which affect the magnitude of the base pressures can be grouped into two categories: those which affect the ability of the primary flow to entrain air from the base regions and those which affect the ability of the ventilation air to flow into the base regions.

The ability of the primary flow to entrain air is chiefly dependent on primary nozzle geometry and total pressure of the primary flow. As total pressure of primary flow is increased, the entrainment rate is increased. This causes the magnitude of the base pressure to be reduced.

The ability of ventilation air to get into the base regions is dependent on the shape and area of the ventilation flow path. As ventilation flow path restrictions are increased, pressure losses increase and base pressures are reduced. Ventilation inlet shape influences pressure losses and penetration potential of ventilation flow. The amount of ventilation area available is dependent on nozzle geometry and primary nozzle pressure ratio. As the primary nozzle pressure ratio is increased, the ventilation area between jet plumes is reduced and, as a consequence, base pressures are reduced. Therefore, as ventilation air loses its ability to get into the base regions, base pressures are reduced, resulting in increased base drag. Figure 6 illustrates typical ventilation flow paths.

Five geometric parameters (and temperature) were isolated as the principal variables governing the internal losses and external drag penalties. They are the number of tubes, tube length, tube shape, nozzle area ratio, and the arrangement of the tubes on the base (base array). The variables are not automatically independent, but the careful selection of models allows independent treatment of each variable without limiting the applicability of the results. To allow direct comparison of the models the total effective exist flow area for each model was 13.2 in.^{2}.

To make the separation of variables manageable and avoid "cut and try," constraints were introduced to give the nozzles a family relationship. At the outset of the program, Accoustic Technology believed that the optimum noise suppressor should have equal distance between all tubes. This criteria leads to hexagonal tube arrays having progressive rows of tubes

6

totaling 7, 19, 37, 61, 91, etc. with each additional row having six more tubes than the last. This exactly even spacing is altered slightly by placing all tubes in a given row on a fixed radius compatible with likely constraints for real installations. This type of array, as shown in figure 7, is referred to as a close-packed array. The other array in figure 7 is a radial array, deriving its name from the placement of tubes on radial lines to maximize the ventilation in the outer rows and minimize ventilating flowfield obstructions.

Another constraint to allow isolation of each parameter was maintaining identical tubes within each array (e.g., for an N-tube nozzle, each tube within the array handles N/13.2 square inches of flow). A composite model resulting from the technology will likely use different tube sizes and possibly uneven spacing between tubes, but it was felt that the additional complexity and endless possible combinations would negate the parametric nature of the study. If parameters can be established that accurately describe the internal performance and base drag of the parametric nozzles, then the hydraulic diameter and ventilation parameter should allow extension to other configurations.

In all but one nozzle the base plate was flat. The exception (R/37, figure 8) had a gentle boattail extending to the center tube to minimize separation. The outside nacelle diameter was held constant to simulate a realistic scale SST engine requirement. The tube exits were always co-planar, as suggested by previous testing (ref. 2). Installation constraints on actual stowable suppressors may require some variation in tube length.

It is instructive to examine the *a priori* knowledge of each parameter individually.

3.2.2 TUBE NUMBER

A single well-contoured tube provides the best bare (no ejector) nozzle performance possible; thus, increasing the number of tubes implies a decrease in performance due to internal losses associated with the additional wetted area (due to tube-length-to-diameter ratio increase) and increasing external drag. Generally, noise suppression increases with increasing tube number. By keeping all other parameters constant, this study quantifies the performance/noise tradeoffs due to tube number alone. The present report concentrates on performance, while reference 1 details the noise suppression characteristics of the nozzles.

A progression of close-packed arrays having 7, 19, 37, and 61 tubes and 31- and 37-tube radial arrays was tested to satisfy a reasonable range of tube numbers. A previously tested (ref. 4) 140-tube nozzle is also used to verify the analysis of internal performance described in this report.

3.2.3 TUBE LENGTH

Internal performance decreases and external performance increases as tube length is increased. Internal loss is primarily due to skin friction on the increased wetted area, while the external improvement is a result of the increasing ventilating air inlet area. The benefits of varying other parameters to decrease drag outweigh the internal loss trades for stowable tube lengths.

The study separates and quantifies the effects of tube length on internal and external performance. Tube lengths were incremented from stowable tube lengths to lengths sufficient to produce nearly the maximum C_{f_g}. The tube length nondimensionalized by the equivalent round convergent jet diameter (L_T/D_{eq}) was tested at 0.25, 0.50, 0.75, and 1.00. The total effective exit area tubes were held constant at approximately 13.2 in.^{2}, thus the tube lengths tested were 1, 2, 3, and 4.

To isolate the effects of base drag from internal losses, all models were designed with a constant internal tube length. External tube length (reflecting base ventilation) was varied using a sliding baseplate as shown in figures 9 and 10. The baseplate/ramp assembly was sealed to the tubes to prevent recirculation within the assembly. It was anticipated that an analysis would permit calculation of the performance decrement due to the internal losses in the long tubes. The analysis was completed and is presented as section 5 of this report. All values of performance shown are corrected to account for excess internal tube length.

3.2.4 BASE ARRAY

Two tube placement variations were studied. The close-packed array, used in the majority of model test configurations, consists of a number of equal-size tubes distributed on the baseplate in a manner which provides approximately the same distance between any two adjacent tubes. Unlike a true equidistant array, which produces a hexagonal group of tubes, the close-packed array maintains a constant radius to all tubes in a row. Figure 11 shows a 61-tube nozzle with a close-packed array. Observe that each successive row of the array contains six additional tubes. Thus, the natural progression for the family of close-packed arrays is 7, 19, 37, 61, 91, etc. Well-ventilated, close-packed arrays are of interest acoustically because the primary flow is uniformly distributed.

The other array investigated was the radial array, consisting of rows of tubes placed on radial lines. A 37-tube radial array is shown in figure 7. Notice that the elimination of the inner row of six tubes results in a 31-tube radial array which could be constructed in a much smaller area ratio without concentrating as much of the flow in the center of the array (fig. 12). A natural progression for radial arrays is 13, 31, 55, etc.

Radial arrays were expected to provide a performance advantage over close-packed arrays because of the increased physical ventilation parameter per unit tube length, the associated increase in jet wake ventilation area, and the unobstructed paths to the center of the base provide for ventilating flow. The difference in ventilation between the radial and close-packed array for nozzles of fixed area ratio can be seen in figure 13.

3.2.5 TUBE SHAPE

The effect of tube shape was well understood prior to the present study. Thus, the testing concentrated on the tube shapes which were known to optimize performance. The Mach number within the tube has a major effect on optimum tube length. Tubes with convergent ends minimize internal losses. If the constant area portion of the tube is round (round convergent tube), and the Mach number is near 0.5 to provide low internal losses, the substantial restriction to the ventilation distance between tubes requires increased tube length to provide the same base ventilation as a straight (nonconvergent) tube (see fig. 14). This

8

restriction becomes prohibitive for use with stowable concepts. The nonconvergent tube, with its high internal Mach number, has an ill-defined sonic line and relatively large boundary layer. To overcome the associated low-discharge coefficient, the size of the nonconvergent tubes must be increased to pass the required mass flow, again restricting the ventilation path though to a much smaller extent than the round convergent tube.

An alternate tube shape, elliptical converging to a round exit, is used in this study (fig. 4). As demonstrated in figure 14, the placement of the minor axis on the circumference increases the ventilation per unit tube length. A round exit provides the required hoop strength to make the shape structurally practical. The ellipse is defined as having a minor axis equal to the exit diameter and a major axis sufficient to provide the desired internal Mach number. Besides providing minimum internal losses and maximum ventilation area, two secondary benefits result from the elliptical shape. The point of minimum distance between tubes occurs nearer the center of the array than with other tube shapes and therefore the minimum pressure (maximum velocity) operates on a smaller annulus resulting in less drag. This effect is more noticeable when tube shapes are compared for a fixed nozzle area ratio as in figure 15. The elliptical shape also minimizes the size of separated regions on the side of the tubes toward the nozzle center. The only limitation on the use of elliptical tubes is area ratio (AR). It will be shown that for area ratios less than 2.7 the distance between the major axes of the tubes is insufficient to allow structural integrity of the base plate. The test concentrated on elliptical convergent tubes with round exits and internal Mach numbers of 0.5 because of their obvious performance benefits. Round convergent and round nonconvergent tubes were also tested on 37-tube AR-3.3 nozzles to allow comparison.

3.2.6 AREA RATIO

Throughout this study the area ratio (or nozzle area ratio) refers to the total area within a circle tangent to the outermost portion of the outside tubes divided by the geometric primary flow area. This definition is chosen to represent the physical area required to install the suppressor. Care should be taken not to confuse this definition with the effective area ratio (area inside a circle tangent to outside of outer jets, at the exit plane, divided by the primary geometric flow area). The latter area ratio is often used in acoustic analysis because the primary interest is the jet behavior rather than base drag or installation requirements. For example, when 37 elliptical convergent tubes are used, an AR-3.3 suppressor has an effective area ratio of 3.07. Figure 15 demonstrates the ventilation distance between tubes of various shapes for a fixed nozzle area ratio, while figure 14 presents the same shapes at constant effective area ratio.

For any number and type of tubes there is a minimum area ratio below which it is physically impossible to construct the nozzle. Figure 16 shows the minimum area ratio that can be constructed using three different tube shapes. The local minimums on the curve result in close-packed and radial arrays.

A convenient measure of the amount of ventilation on any given nozzle is the physical ventilation parameter A_S/A_B, where A_S is the total area between tubes in the outer row and A_B is the base area that must be ventilated. This parameter and another parameter including the area between the jet wakes have been used previously (ref. 5) in attempts to non-dimensionalize base drag parameters. Though the parameters are shown in this study

9

to be inadequate, the ventilation parameter does allow us to observe some interesting characteristics of various nozzles. Figure 17 shows the ventilation parameter per unit tube length as a function of tube number, area ratio, and tube shape. High ventilation parameters are associated with minimum base drag. It is most convenient that the physical ventilation parameter is reasonably independent of tube number. Tube length can be varied to acquire a wide range of A_S/A_B. The validity of the ventilation parameter as a base drag non-dimensionalizer can be tested easily by varying tube number at a fixed tube length and area ratio.

The effect of area ratio on ventilation is very pronounced. For very small area ratios the tubes touch and thus completely eliminate ventilation. The resulting $A_S/A_B=0$ has the physical significance that the base area, though small, is going to feel a very low pressure, resulting in high base drag. At the other extreme as rear ratio becomes very large, there is plenty of area between the tubes to allow ventilating air onto the base, but the base area becomes so large that small static pressure depressions due to the velocity of the air penetrating the base region result in a large base drag. Figure 17 shows that, for close-packed arrays, the optimum ventilation parameter is primarily a function of tube shape. Thus the minimum base drag could be expected to occur near AR 5 for round-convergent tubes (internal Mach number = 0.5) and AR 3 elliptical tubes (converging to round exists; M = 0.5) or round nonconverging tubes. The figure does not include a correction for the increased size required of the nonconvergent tube ($C_D \approx 0.91$) to pass the same mass flow as the convergent tubes ($C_D \approx 0.98$). If all configurations have the same mass flow rate (i.e., effective area) the family of curves for round nonconvergent tubes would fall between those shown for the elliptical and round convergent tube. Forty-five percent more tube length is required for an area-ratio 3, round-convergent-tube nozzle to have the same physical ventilation as a similar configuration incorporating elliptical convergent tubes.

Ventilation parameter is shown as a function of area ratio and number of tubes in the outer row in figure 18 for 37-tube nozzles. Again, an indicator of low-base drag is a high $A_S/(A_B L_T)$. Unlike the close-packed arrays, radial arrays are limited in ventilation parameter only by the minimum area ratio that it is possible to build. Even at area ratio 3 (where the close-packed array has its optimum performance), a radial array with twelve tubes in the outer row requires only half the tube length to produce the same ventilation parameter as a close-packed array. When the number of tubes in the outer row is less than the number used in a radial array (as defined), one of two disadvantages arise. If the maximum number of tubes in each row is less than or equal to the number in the outer row, the minimum area ratio that can be built becomes impractical (e.g., minimum possible area ratio for 37 tubes with six convergent tubes per row is seven). On the other hand, if the outer row contains fewer tubes than an interior row, the ventilation parameter is not representative, and a new ventilation parameter must be defined which weighs the physical ventilation in each of the rows.

All of the above considerations suggest that optimum ventilation for a fixed stowable tube length requires a small area ratio radial array. It is anticipated that the base drag becomes less sensitive to these parameters as tube length is increased beyond the stowable limits. The present study investigates area ratio 2.75 and 3.3 radial arrays and area ratio 2.75, 3.3, 4.5 and 6.0 close-packed arrays. Because ventilation is not a strong function of tube number the majority of the area ratio investigations were conducted on 37-tube nozzles.

10

3.2.7 RAMP SHAPE

Static bare-nozzle performance should be insensitive to ramp shape, with the possible exception of nozzles with very short tubes. Two types of ramps were investigated in preparation for suppressor/ejector and forward velocity investigations to follow, using the same hardware. The outside cowl diameter was maintained at 8.89 inches to represent a scale SST nacelle. One ramp shape, the circular arc ramp (fig. 19), consists of a 35.5 in.-radius circular arc, tangent to the nacelle and intersecting the base plate just outside of the outer tubes. A second ramp, referred to as an "elliptical ramp" (figs. 20 and 21), consists of a segment of an ellipse with foci on the nozzle centerline. The segment is tangent to the nacelle and extends to the center of the outer tube row. The elliptical ramp should provide more effective ejector inlet area with forward velocity and reduce primary afterbody drag by producing a smaller separated region on the base. Ramp shape is not treated on a par with the primary geometric variables. The two shapes were chosen to demonstrate that static, bare-suppressor performance is independent of ramp shape and to establish the extent to which performance depends on ramp shape for cases with restricted ventilation (i.e., short tubes).

11

4.0 APPARATUS AND TECHNIQUE

4.1 EXPERIMENTAL APPARATUS

4.1.1 FACILITY AND TEST PROCEDURE

The testing was conducted on the Boeing Hot Nozzle Test facility (fig. 22), a 2000-pound, single-axis thrust rig located at North Boeing Field, Seattle. As shown in figure 23, a variable slot inlet burner provided acceptable temperature profiles for testing at 1150°F. The air-flow rate was obtained using a critical flow venturi. Ambient and hot testing was conducted for pressure ratios from 2 to 4. Thrust measurements were the average of five one-second integrated samples for each test condition.

To increase the accuracy of the data, test conditions were always acquired in order of increasing pressure ratio. Repeat runs were made for each configuration. Any zero shifts were calculated into the data. Runs with excessive zero shift were rerun.

4.1.2 SUMMARY OF MODEL SPECIFICATIONS

Number of Tubes	Area Ratio	Array Type	A"	$A_S/1$"	Type of Tube*	Mean dia. to outside of outer jet"
1(R/C)	–	–	13.825	–	–	4.186
7-Tube	3.3	Close-packed	13.613	4.461	E.C.	
19-Tube	3.3	Close-packed	13.610	5.979	E.C.	7.262
37-Tube	3.3	Close-packed	13.543	6.197	E.C.	7.243
37-Tube	3.3	Close-packed	13.695	5.269	R.C.	7.432
61-Tube	3.3	Close-packed	13.616	6.064	E.C.	7.257
37-Tube	2.75	Close-packed	13.432	4.369	E.C.	6.703
37-Tube	4.5	Close-packed	13.571	10.395	E.C.	
37-Tube	6.0	Close-packed	13.532	14.425	E.C.	
31-Tube	2.75	Radial array	13.610		E.C.(M=.635)	6.703
37-Tube	3.3	Radial array	14.931	11.995	R.non C.	
37-Tube	4.5	Radial array	13.600	14.800	E.C.	

*E.C.–elliptical converging to round exit (M=0.5)
 R.C.–round converging to round exit (M=0.5)
 R Non C–round nonconverging

4.1.3 MODEL DESCRIPTION

4.1.3.1 Round Convergent Reference Nozzle (R/C) (fig. 8)

The R/C–a 10 degree half-angle, round convergent nozzle–was used as a noise and perform-ance referee throughout the program. The nozzle has an upstream-to-exit diameter ratio

13

(D/d) of 1.44 and a geometric exit area of 13.825 in.^{2}. The external contour consists of a 12-degree half-angle boattail tangent to a 35.5-inch-radius arc which in turn is tangent to the 8.89-inch nacelle diameter upstream. The R/C nozzle performance is reported in detail in reference 6*.

4.1.3.2 R/37, Reference 37-Tube Suppressor (fig. 8)

The R/37 configuration is a 13.695-square-inch, area-ratio-3.3, close-packed suppressor using 37 equal-diameter round convergent tubes of varying length. The nozzle was tested repeatedly throughout the program as a performance and noise referee. Two ramp/base contours were used.

To maximize the ventilation and minimize separation, a contoured baseplate was chosen which consisted of a 40-inch boattail radius tangent to the 8.89-inch nacelle and terminating in a central hole (fig. 8). All tube entrances have bellmouth radius-to-tube diameter ratios greater than 0.1 to minimize inlet ($\Delta P_T/q$) losses. All tube exits are co-planar, and the average length of the internal constant area portion of the tubes is 4.4 in. The tube internal upstream-area-to-exit-area ratio is maintained at 1.34 to produce a maximum Mach number of 0.5. The performance of the R/37 with contoured ramp is described in detail in Reference 6.

An elliptical ramp was also used on the R/37 (fig. 24) to provide an external contour compatible with the other nozzles being tested. Two- and three-inch external tube lengths were tested to provide the same ventilation parameter range being tested in the area ratio 3.3, close-packed, 37-tube nozzle using elliptical convergent tubes, thus allowing a comparison where tube shape is the only variable.

4.1.3.3 Seven Close-Pack Arrays: 7-, 19-, 37-, and 61-Tubes

Suppressors equipped with 7, 19, 37, and 61 tubes, each 13.6 in.^{2} and having area ratios of 3.3, were tested to investigate the natural progression of nozzles with approximately equal spacing between all tubes in the array. Figures 25-36 show key dimensions and photographs for each nozzle. All tubes are elliptical converging to round co-planar exits, have a tube internal area-to-exit area ratio of 1.34 (M = 0.5), and have tube inlet radius-to-tube diameter ratios greater than 0.1 to minimize inlet losses. Internal tube length was held constant at 6 in. Sealed ramps were used to vary the tube lengths from 1 to 4 in. (L_T/D_{eq} = 0.25-1.0). Nozzles were built with 37 tubes and area ratios of 2.75, 4.5, and 6.0, similar in other respects to the 37-tube, area-ratio-3.3 nozzle shown in figure 29. Variations in tube and ramp shape for 37-tube, area-ratio-3.3 nozzles are shown in figures 37 and 38.

---

*The actual hardware for this study is the same as that used in reference 6 except for the upstream cowl diameter which consisted of a 40-inch-radius arc connecting the 12-degree boattail to a 10-inch-diameter nacelle. Careful comparison resulted in no measurable changes in static nozzle performance due to the two external contours.

14

4.1.3.4 Three Radial Array Nozzles

A 37-tube, area-ratio-3.3 radial array was constructed using nonconvergent tubes (figures 39 and 40). To account for the inherently low discharge coefficient of nonconvergent tubes ($C_D \approx 0.91$), the total geometric flow area was 14.93 in.^{2}. As in the other nozzles the internal tube length was constant (6 in.), the tube inlet radii to tube diameter was greater than 0.1, and the external tube length was varied using a sealed ramp and baseplate assembly.

A second 37-tube radial array (figs. 41 and 42) was constructed using elliptical convergent tubes and an area ratio of 4.5. The tube size, shape, length, and internal characteristics were identical to the AR-4.5 close-packed nozzle. The geometric flow area was 13.514 in.^{2}. Again, external tube length was varied by repositioning the ramp and baseplate assembly.

Section 3.2.4 discussed the natural progression of radial array tube numbers. Figure 7 shows that the removal of the central row of six tubes results in a radial array with more evenly distributed flow. The resulting array could be constructed at a significantly smaller area ratio. The resulting 31-tube nozzle was constructed with an area ratio of 2.75 (figs. 12 and 13). Elliptical convergent tubes were formed from the same tube stock used for the 37 elliptical tube configurations. A total geometric flow area of 13.61 in.^{2} from 31 elliptical tubes (instead of 37) resulted in a tube upstream Mach number for this nozzle of 0.635. ($M = 0.5$ for all other elliptical tube nozzles). The effect of the difference in internal Mach number is treated in the section of chapter 5 dealing with C_V internal.

4.1.3.5 42-Tube Annular-Plug Nozzle

The 42-tube nozzle was constructed to be similar to the 61-tube close-packed array, except that the central 19 tubes were replaced by a 12-degree, half-angle movable plug and annulus (figures 43 and 44). A contoured boattail, like that used on the R/37, was tangent to the nacelle and terminated at the annulus, co-planar with the tube exists. The nozzle had a total flow area of 13.6 in.^{2} when the annulus height was set at 0.383 in. Figure 45 compares the 42-tube and 61-tube nozzles. The plug could be repositioned to result in any annulus height from zero to 1.59 in. (the latter with plug removed).

The nozzle was not intended to fit into the parametric format of this study but rather to test variations in noise suppression between tubular and tubular/annular nozzles and the effect on suppression of increasing the percentage of flow near the center.

Due to the fixed location of the outer row of tubes and the variation in primary flow area as the plug moves, the area ratio of the nozzle becomes a function of the annulus height. The nozzle area ratio varies from 4.8 for zero annulus to 2.1 when the plug is removed.

4.1.4 MODEL INSTRUMENTATION

4.1.4.1 Charging Station Instrumentation and Diffuser

Four co-planar rakes, located in the six-inch internal diameter instrumentation section (figure 22), were used to measure the primary flow temperature and total pressure profiles. Two horizontal rakes containing 14 thermocouples were area-weighted across the entire duct. Fourteen total-pressure probes, on two vertical rakes, were likewise area-weighted.

15

A four-degree, half-angle diffuser (figure 22) was used between the instrumentation section and the model to allow installation of the large area ratio suppressors. The round convergent referee nozzle was used with and without the diffuser to evaluate the total pressure loss in the diffuser. The appropriate total pressure correction was applied to all test configurations to remove the effect of the diffuser from the data.

4.1.4.2 Static Pressure Instrumentation

Each nozzle, with the exception of the 42-tube annular-plug nozzle, included area-weighted static pressure taps on the baseplate and elliptical ramps. The pressure lines were routed inside the baseplate/ramp assemblies, resulting in "clean" baseplates.

4.2 DATA ACQUISITION

Data was acquired on punched and printed paper tape using a Dymec system. Model static pressure and charging station pressures were obtained using Scannivalves with pressure transducers of appropriate range for each pressure group.

Accuracy of data for any single test condition:

Pressure: $\pm$ 0.25% full scale

Thrust: $\pm$ 0.5% full-scale (20 lb) for cold
3% to 4% of full-scale for 1150° runs
(Measured by averaging 5 1-second integrated samples for each condition)

Temperature: Below 100°F $\pm$ 2°
1150°F $\pm$ 5°

Weight Flow: within 0.1 pound/sec

To increase the accuracy of data presentation, conditions were always acquired in order of increasing pressure ratio, and repeat runs were made for each configuration. Any zero shifts occurring during a run were calculated into the data. Runs with excessive zero shift were rerun. As a result, final presented values of C_{f_g} and D_B/FID are within $\pm0.25\%$.

4.3 DATA REDUCTION AND PRESENTATION

Initial data was reduced on the SDS 92 and CDC 6600 computers using Boeing calibration and reduction programs LAB 475 and 553. Final data reduction was accomplished on the SDS 92 using LAB 606. In addition to paper output, the final reduction program produced a magnetic tape compatible with the CDC 243 grid system and the PDP 11/Vector General. In this manner, large quantities of data could be quickly displayed and compared.

As described in section 3.2.3 and shown in figure 9, the internal tube length was constant for all test configurations. To present the appropriate performance levels for nozzles with

16

internal tube length approximately equal to external tube length, a correction for the losses due to excessive internal tube length, $\Delta C_{V \, int}$, had to be applied (see section 5.1). The performance values stated within this report include the $\Delta C_{V \, int}$ and thus represent the performance of nozzles with internal tube length $\approx$ external tube length.

5.0 THEORY

5.1 INTERNAL VELOCITY COEFFICIENT

To isolate base drag effects on performance, all models were designed with a constant internal tube length. External tube length (reflecting base ventilation) was varied using a sliding baseplate as shown in figure 9. It was anticipated that an analysis would permit correction of the data obtained with long tube nozzles to reflect that representative of shorter tubes. The following internal loss analysis allows calculation of the appropriate internal performance as if internal and external tube lengths were approximately equal. $C_{V_{int}}$ is the nozzle static thrust performance with no penalty due to base or ramp drag.

Consider a single tube with a constant cross-section area, A_1, for a length L and having a convergent exit section with half-angle a as shown in figure 46.

Ignoring the higher order internal flow effects due to tube shape, the flow can be described as a function of the area. Thus, D is defined as $\sqrt{4A_1/\pi}$ where A_1 is the measured constant cross-sectional area of the tube being considered.

The losses within the tube occur in three regions: the inlet (⓪ - ① in figure 48), the constant area region ① - ② , and the convergent portion ② - ③ . Through examination of these regions, an expression for internal velocity coefficient is established. The expression is not rigorously derived from fundamentals. In fact, it appears to have an analytical redundancy by accounting for both the pressure loss and the skin friction drag force in the constant area region ① - ② . The expression is presented and used within this report because of its exceptional fit to the experimental data. Each region is discussed individually, then the resulting expression is presented.

The first to be considered are the Inlet losses in region ⓪ - ① Inlet losses, $\Delta P_T/q$, approach zero for $R/D > 0.1$ for incompressible flow (ref. 7). Though compressibility increases the losses slightly (ref. 8), the nozzles used in the present study maintained $R/D > 0.1$ and tube Mach number of 0.5. It will be shown that the assumption of $\Delta P_T/q \approx 0$ and thus $P_{T_1} = P_{T_0}$ provides good agreement between theory and experiment for the configurations tested; thus, the remainder of the analysis uses $P_{T_1} = P_{T_0}$.

The next region of tube flow loss to be considered is the constant area portion of the tube, ① - ② . Flow in this portion of the tube experiences losses due to skin friction, thus the total pressure is reduced from P_{T_1} to P_{T_2}. Because inlet losses are negligible ($P_{T_0} = P_{T_1}$) the pressure change between ① and ② can be expressed as $P_{T_0} - P_{T_2}$. The pressure ratio at ② expressed as a function of the charging pressure ratio at ⓪ (ref. 9) is

$$\frac{P_{T_2}}{P_\infty} = \frac{P_{T_0}}{P_\infty} \left(1 - 4C_f \cdot \frac{L}{D} \cdot \frac{q}{P_{S_1}} \right) \tag{1}$$

where,

C_f = appropriate skin friction value, a function of Reynold's number (to be discussed),

$$\frac{q}{P_{S_1}} = \frac{q}{P_T} \cdot \frac{P_T}{P_{S_1}}$$

function of Mach number. Note P_{S_1} is tube internal static not P_∞

The drag due to skin friction from ① - ②, expressed as a function of nozzle geometry and flow parameters, is

$$\text{Drag} \quad ① - ② \quad = 4 C_f A_1 \frac{L}{D} \frac{q}{P_{S_1}} \tag{2}$$

Finally, looses occur in the region depicted between ② and ③ in figure 48. The convergent portion of the tube acts as a round convergent nozzle, with a half-angle of a and contraction ratio of D/d, operating at pressure ratio P_{T_2}/P_∞ (where P_{T_2}/P_∞ can be obtained from equation 1). The measured thrust of a round convergent nozzle differs from the calculated ideal thrust due to viscous losses from ② to ③ and underexpansion losses due to the pressure difference between ③ and ∞ (fully expanded).

The internal velocity coefficient, $C_{V\ int}$, of the entire tube ⓪ - ③ by convention is

$$\frac{F \text{ internal measured*}}{VIP_0} \tag{3}$$

Where VIP_0 is an ideal fully expanded velocity calculated as a function of the upstream total pressure P_{T_0}.

In the present study all tubes of a given nozzle are alike in shape and length. Thus, the C_V internal of a single tube equals the C_V internal of the entire nozzle. This is most easily demonstrated by recalling that each tube of an N-tube nozzle produces 1/Nth of the total thrust and has 1/Nth of the total weight flow. Thus

$$C_{V_{nozzle}} = \frac{F \text{ measured total}}{\dot{m}_{total} \cdot VIP**} = \frac{N \cdot F \text{ measured for one tube}}{N \cdot \dot{m}_{one\ tube} \cdot VIP} = C_{V_{one\ tube}}$$

---

*In practice, the measured internal force is calculated by adding the magnitude of the external drag to the measured total force.

$$F_{internal\ measured} = F_{total\ measured} + \text{afterbody drag}$$

**VIP is a function only of the charging conditions (T_{T_0}, P_{T_0}, P_∞, a).

20

Recalling equation 2, the total drag force on an N-tube nozzle for the constant area portion of the tubes is

$$\text{Total Drag} \quad \textcircled{1} - \textcircled{2} \quad = 4C_f A_1 \cdot \frac{L}{D} \cdot \frac{q}{P_{S_1}} \cdot N \qquad (4)$$

The $C_{V\ int}$ of the convergent nozzle ($C_{V\ R/C}$) is well documented for various values of P_T/P_∞, a, D/d in reference 10. Since the upstream charging station of the convergent nozzle corresponds to Station $\textcircled{2}$ in figure 46, the $C_{V\ R/C}$ given in the reference is for pressure ratio P_{T_2}/P_∞.

Thus, to express the denominator in terms of FID for P_{T_0}/P_∞, the given $C_{V\ R/C}$ must be multiplied by the appropriate ideal velocity ratio VIP $(@P_{T_2})$/VIP $(@P_{T_0})$.

The $C_{V\ internal}$ for the nozzle can now be expressed as the sum of the $C_{V\ int}$ for the round convergent portion ($C_{V\ R/C}$) expressed in terms of FID@P_{T_0} and the internal loss term due to skin friction drag from $\textcircled{1}$ to $\textcircled{2}$ (equation (4)) expressed as a fraction of FID@P_{T_0}. The resulting expression is

$$C_{V\ int} \underset{@\frac{P_{T_0}}{P_\infty}}{} = \left\{ C_{V R/C} \underset{@\frac{P_{T_2}}{P_\infty}}{} \right\} \left\{ \frac{\text{VIP}_{@P_{T_2}}}{\text{VIP}_{@P_{T_0}}} \right\} - \left(4C_f A_1 \frac{L}{D} \frac{q}{P_{S_1}} \frac{N}{\text{FID@}P_{T_0}/P_\infty} \right) \qquad (5)$$

where P_{T_2} is obtained from equation 1. See section 5.2 for appropriate Reynold's number corrections. For configurations with irregular exit shape or variations in tube size use the hydraulic diameter relationship:

$$N = \frac{\text{total exit perimeter squared}}{\text{total exit area}}$$

The excellent agreement between the theory and experimental values is shown in figure 47 for a fixed pressure ratio. In the present experimental work, the tube length was held constant and the tube number and diameter were varied. (Effective total exit area was always 13.2 square inches.) As a result, experimental values for $C_{V\ int}$ were acquired for L/D ratio between 3.1 and 9.2 for the present test. Other nozzles are shown to provide a range of M_1 values from 0.37 to 0.64 and L/D ratios from 1.3 and 9.6.

For the scale of the present study, figure 48 shows the theory for various pressure ratios.

Within the range of interest, $C_{V\ internal}$ is a linear function of the tube length times the square root of the number of tubes for a fixed pressure ratio, allowing the equation to be reduced to

$$C_{V\ int} = C_{V\ R/C} - K L \sqrt{N} \qquad \text{where:}$$

21

L = internal length of tube excluding convergence
N = total number of tubes

For this test, the values of $C_{V\ R/C}$ and K are shown as a function of pressure ratio on figure 49. Experimental values of the quantity $L\sqrt{N}$ varied from 15.9 to 46.9.

5.2 REYNOLDS NUMBER CORRECTIONS NECESSARY FOR $C_{V\ R/C}$ AND C_f

Equation (5) can be used for flow areas that are greatly different from the present test if the following process is used to find C_f and $C_{V\ R/C}$. The C_f varies as a function of Reynold's number to the -0.25 power (ref. 11).

To calculate the appropriate C_f for use in equation (5), first calculate Reynolds number (Re) based on the equivalent tube diameter ($\sqrt{4A_1/\pi}$) and the velocity in the constant area portion of the representative tube. The value of C_f is then obtained from the following expression*

$$C_f = 0.003663 \left[\frac{Re}{3.88 \times 10^5} \right]^{-0.25} \tag{7}$$

The $C_{V\ R/C}$ corrected for use in equation (5) is a function of the size of the individual tubes.

$$(1 - C_{V\ R/C}\ corrected) = (1 - C_{V\ R/C}) \left[\frac{Re}{Re_{R/C}} \right]^{-0.2} \tag{8}$$

where $C_{V\ R/C}$ and $Re_{R/C}$ are known values (from reference 10). The Reynolds number based on the exit velocity 'd exit diameter of the tubes under consideration is expressed as Re. This relationship assumes a compressible, turbulent boundary layer.

5.3 TEMPERATURE EFFECTS ON $C_{V\ R/C}$ AND C_f

Temperature also produces a change in the $C_{V\ R/C}$ and C_f which are functions of the Reynolds number ratio (ambient to higher temperature). The $C_{V\ R/C}$ varies with the Reynolds number ratio raised to the 0.2 power.

$$\frac{(1 - C_{V\ R/C})\ X^O}{(1 - C_{V\ R/C})\ AMB} = \left[\frac{Re_{amb}}{Re_{x^O}} \right] \tag{9}$$

---

*The constants shown were derived experimentally for developing flow in a tube; see Reference 12.

22

For the present study this ratio ≈ 1.3 for $1150^\circ F$ flow.

$$C_{V\,R/C}@1150^\circ F = (1.3\,C_{V\,R/C\,AMB}) - .3 \qquad (10)$$

The C_f is found from equation 7 using Re at the appropriate temperature.

5.4 THE EFFECT OF L/D ON C_V INTERNAL

The effect on $C_{V\,int}$ of increasing L/D, besides decreasing the peak value of $C_{V\,int}$, is to shift the occurrence of the peak value to a higher pressure ratio. As L/D increases, P_{T_1} must be higher to actually produce choking at the nozzle exit. The under-expansion losses are a function of P_{T_2}/P_∞ and occur at pressure ratios above actual choking. Viscous losses, which dominate at low pressure ratios, are increased as L/D increases. The net result is the shifting of peak internal velocity coefficient to a higher nozzle pressure ratio (P_{T_0}/P_∞).

23

6.0 EXPERIMENTAL RESULTS

6.1 SUMMARY

This chapter presents the performance results of each of the nozzles tested. Close-packed arrays are shown first in order of increasing tube number for area ratio 3.3 nozzles. Then the performance of various 37-tube nozzles is presented in order of increasing area ratio. The radial array nozzles follow in order of increasing area ratio. Finally, the performance of the 42-tube annular-plug nozzle is presented.

Discharge coefficients, gross thrust coefficient, and afterbody drag as a percentage of ideal thrust are presented for each nozzle as a function of pressure ratio. Section 7 will compare the performance characteristics of the various nozzles and discuss performance trends and trade-offs.

6.2 DISCHARGE COEFFICIENT

The Discharge Coefficient, C_D , of each nozzle as a function of pressure ratio is shown on figure 50. The values include corrections for diffuser losses, when applicable. With or without diffuser the R/C nozzle C_D is 0.98 ±0.002 @PR=3.0, implying that the diffuser loss calculation is correct and the absolute value of C_D agrees with references 6 and 10.

At pressure ratio 3.0, the R/C, 7-tube, area ratio 3.3; 19-tube, area ratio 3.3 close-packed; 37-tube, area ratio 2.75 close-packed; and 37-tube, AR-4.5 radial nozzles all have C_D = 0.982±0.004. The 37-tube, area-ratio -3.3, -4.5, and -6.0 close-packed arrays; 31-tube radial; and the 61-tube, close-packed nozzles all have C_D = 0.969 at PR=3.0. As expected, the 37-tube radial array incorporating round nonconvergent (straight) tubes had a much lower discharge coefficient, C_D = 0.925, even with good inlet bellmouths. The C_D of the R/37, 37-tube, area ratio 3.3 close-packed array incorporating round convergent tubes of various lengths was 0.955 (average length 4.4 in.). All other multitube nozzles tested had internal tube lengths of six inches.

Temperature does not significantly affect C_D provided the geometric flow area increase due to thermal expansion is considered. For all test conditions the value at 1150° was within ±0.5% of the ambient value.

6.3 PERFORMANCE: C_{f_g} AND D_{AFT}/FID

6.3.1 GENERAL COMMENTS

Section 6.3 presents the static performance of the various nozzles tested as a function of pressure ratio. The gross thrust coefficient and the afterbody (baseplate and ramp) drag as a percentage of FID are presented for each nozzle at each tube length tested. Values of C_{f_g} are plotted from pressure ratio 2 to 4 at ambient temperature and at 1150°F, when available. Thrust values have been corrected for zero shifts on the test stand. The appropriate values for $\Delta C_{V_{int}}$ (see section 5) have been added to the measured C_{f_g} to yield a C_{f_g} value

25

that accurately represents the performance of nozzles with internal tube lengths equal to the external tube length plus a 0.3-in. baseplate thickness. External tube length is listed on the plots. When nondimensionalized to the nominal diameter of an equivalent round convergent nozzle, D_{eq}, the 1-, 2-, 3-, and 4-in. lengths tested have $L_T/D_{eq} = 0.25, 0.50, 0.75$, and 1.0 respectively (total effective flow area approximately 13.2 in.^{2}).

Baseplate and ramp drag as a function of ideal thrust, D_{AFT}/FID, is plotted for each configuration. This pressure drag is calculated using the static pressure values recorded at the area-weighted baseplate taps. Configurations incorporating circular arc ramps have a baseplate which extends to the outside of the outer row of tubes. The baseplate is connected to the nacelle by a very gentle (40-in. radius) circular arc segment. The drag on the small circular arc ramp does not significantly contribute to the measured static performance of the nozzles and is therefore neglected. Elliptical ramps extend from the nacelle to the center of the outer row of tubes. The drag on the elliptical ramps is noticeable and is added to the baseplate drag. The sum is expressed as a function of ideal thrust, resulting in D_{AFT}/FID.

6.3.2 R/C AND R/37 WITH CONTOURED RAMP

The two nozzles on figures 51 and 52 show C_{f_g} versus pressure ratio at ambient and 1150°F temperature. The R/37 has a contoured ramp extending to the center (recall figure 8) and is the only multitube nozzle within the present test that has varying internal tube lengths. The average constant area internal tube length is 4.4 in.

The afterbody external drag on the R/C nozzle is less than 0.1% and therefore is not plotted. Thus, within the accuracy of the data, $C_{V int}$ for the R/C equals the C_{f_g}.

The afterbody drag for the R/37 nozzle is shown on figure 53 for ambient and 1150° data to be a decreasing percentage of the ideal thrust for both ambient and 1150° data. The afterbody drag is independent of temperature for this configuration.

6.3.3 7-TUBE NOZZLE

The C_{f_g} of the 7-tube, area-ratio-3.3 array is shown in figure 54 for various tube lengths. The shape of the curve would indicate that beyond a small and nearly constant base drag loss (< 0.7%), the losses are due to underexpansion. The afterbody drag is shown in figure 55 for the range of tube lengths and pressure ratios. The 7-tube nozzle was tested with a circular arc ramp. The total drag is so small that the elliptical ramp would not have produced a measurably different value.

6.3.4 19-TUBE NOZZLE

Figure 56 shows the C_{f_g} of the 19-tube, area-ratio-3.3, close-packed nozzle as a function of tube length and pressure ratio. The drag penalty, due to insufficient ventilation, is noticeable for $L_T/D_{eq} = 0.25$. Ramp shape produces 0.5% change in performance for $L_T/D_{eq} = 0.5$.

26

Afterbody drag curves are shown on figure 57. The change in performance due to temperature (L_T/D_{eq} = 0.75) is entirely the result of changes in internal performance. Figure 57 shows that for the tube length tested, the ventilation is sufficient that temperature does not affect the afterbody drag.

6.3.5 37-TUBE, AREA-RATIO-3.3, CLOSE-PACKED ARRAY

Figure 58 presents C_{f_g} for the 37-tube, area-ratio-3.3, close-packed array incorporating elliptical convergent tubes. C_{f_g} as a function of pressure ratio is given for the range of tube lengths for configurations using circular arc ramps and a configuration using the elliptical ramp. The elliptical ramp provides a slight (< 0.5%) increase in performance relative to the circular arc ramp for well ventilated case of L_T/D_{eq} = 0.75. Afterbody drag as a percentage of ideal thrust is shown on figure 59 to be a strong function of tube length and a nearly constant percentage of ideal thrust. An elliptical ramp case is shown with sealant between the baseplate and tubes, which was the usual practice, and without sealant. The difference in C_{f_g} is less than 0.1% for this L_T/D_{eq} = 0.75 configuration.

6.3.6 37-TUBE, AREA-RATIO-3.3, CLOSE-PACKED ARRAY WITH ROUND CONVERGENT TUBES

An elliptical ramp was added to R/37 nozzles to make an area-ratio-3.3 close-packed array with elliptical ramp and round convergent tubes. It is the only nozzle in the test series to use round convergent tubes. The internal tube length varied but had an average of 4.4 in. The $C_{V\ int}$ between 4.4 in. and the external tube length tested was calculated as described in chapter 5, and the appropriate correction was added to the C_{f_g}. Thus, the values of C_{f_g} shown in figure 60 properly depict the performance of a nozzle with a flat baseplate and approximately equal internal and external tube lengths.

The afterbody drag as a percentage of ideal thrust is presented on figure 61 for the L_T/D_{eq} = 0.5 configuration. For this tube length the ventilation reduction of the round convergent tubes relative to the elliptical convergent tubes result in a 1% increase in base drag. (Compare figures 59 and 61). The discharge coefficient is 0.5% below that given in section 6.2 for the R/37 and is presented as figure 62.

6.3.7 61-TUBE, AREA-RATIO-3.3, CLOSE-PACKED ARRAY

Figure 63 presents the gross thrust coefficient, C_{f_g}, of the 61-tube, area-ratio-3.3, close-packed array. The stowable suppressor concept requires tube lengths which scale to approximately L_T/D_{eq} = .35. The C_{f_g} associated with such a tube length is less than 0.93. This low performance is a result of the high base drag, shown in figure 64 to be a strong function of tube length.

For a fixed tube length, the drag is a slight function of pressure ratio with a minimum occurring at or above pressure ratio 3.0. Figure 65 shows the decrease in afterbody drag as a percentage of FID due to increased temperature as a function of nondimensional tube length (L_T/D_{eq}) at pressure ratio 3.0. The effect of the decreased base drag at 1150°F on overall performance is offset by the reduced internal performance of the nozzle as shown in figure 63.

27

6.3.8 37-TUBE, AREA-RATIO-2.75, CLOSE-PACKED ARRAY

Area ratio is the only variable for the nozzles described in Section 6.3.5, 6.3.8, 6.3.9, and 6.3.10. The gross thrust coefficients for the area-ratio-2.75 configurations are presented in figure 66. Afterbody drag as a percentage of ideal thrust for these configurations is presented on figure 67. The effect of the ramp shape on performance for short tubes should be noted. For short tube (L_T/D_{eq} = 0.25), the elliptical ramp provides 1.6% less drag than the circular ramp. At this tube length, the drag of the circular arc configuration is reduced by 1.5% at 1150°F.

6.3.9 37-TUBE, AREA-RATIO-4.5, CLOSE-PACKED ARRAY

The gross thrust coefficient for the 37-tube area-ratio-4.5 close-packed array is given on figure 68. The nozzle, which has a larger than practical area ratio, was only tested using the circular arc ramp. The afterbody drag as a percentage of FID is presented as a function of tube length and pressure ratio in figure 69. As predicted in section 3.2.6, the area ratio is large enough to create severe base drag for short tubes making it an unacceptable configuration for the stowable tube concept (D_{AFT}/FID = 7% @ Pressure Ratio = 3.0).

6.3.10 37-TUBE, AREA-RATIO-6.0, CLOSE-PACKED ARRAY

The area-ratio-6.0 nozzle was tested primarily to show the effects of area ratio on noise suppression. Its extreme size required that it use a 10-in. nacelle diameter, larger than the 8.89-in. constraint placed on all other models. The only tube length tested was three in. The nozzle is listed as having a circular arc ramp because the baseplate extends outside of the tubes. In fact, no circular arc is necessary, since the nacelle diameter is equal to the diameter of the baseplate.

Figure 70 shows C_{f_g} as a function of pressure ratio. Afterbody drag as a percentage of ideal thrust, presented on figure 71, is approximately 2.0% for L_T/D_{eq} = 0.75. Section 7 shows that the drag penalty is a strong function of area ratio for short tubes, and thus the expected drag for a stowable tube configuration would be approximately 8% of ideal thrust.

6.3.11 31-TUBE, AREA-RATIO-2.75 RADIAL ARRAY

The 31-tube, area-ratio-2.75 radial array performance for all tube lengths is shown in figure 72. Unlike close-packed arrays, the drag as a percentage of ideal thrust decreases with increasing pressure ratio (figure 73). The internal velocity coefficient is less than for 37-tube nozzles because the tube internal Mach number is 0.65 instead of 0.5, as explained in Section 4.1.3.4. Thus, due to the difference in $C_{V_{int}}$, the C_{f_g} of a nozzle constructed with M = 0.5 tubes would be higher than the values shown by 0.2% at pressure ratio 3.0 and L_T/D_{eq} = 0.25 and 0.01% for L_T/D_{eq} = 1.0 at the same pressure ratio.

6.3.12 37-TUBE, AREA-RATIO-3.3 RADIAL ARRAY

The 37-tube, area-ratio-3.3 radial array was the only configuration tested using round non-convergent tubes. The expected low-discharge coefficient (figure 50) was accounted for by using a larger geometric flow area for the nozzle. The gross thrust coefficient is shown in

figure 74. Because of the nonconvergent tubes the C_V int cannot be corrected using the method described in section 5. For this case the C_V int for each tube length was acquired by assuming a straight-line correction between the value of zero tube length (1, an orifice) and the measured value for the 6-in. internal tube length tested.

The exceptional performance of the nozzle is due to the base ventilation provided by the radial array. The base drag is less than 1% of ideal thrust even for stowable tube lengths (fig. 75).

The 37-tube radial array with round nonconvergent tubes can be compared with other nozzles having convergent tubes by "constructing" the gross thrust coefficient of a similar array with elliptical tubes. The internal performance of all 37-tube nozzles with elliptical convergent tubes where M = 0.5 is essentially the same and agrees with the value calculated using equation (6), section 5.1. As discussed in section 3.2.5, round nonconverging tubes should result in less ventilation and hence more afterbody drag than the elliptical tubes. Figure 75 shows the afterbody drag to be less than 1% of FID. Thus, a gross thrust coefficient obtained by subtracting the drag values of figure 75 from the C_V int calculated from equation (6) for elliptical convergent tubes (fig. 76) results in an accurate and slightly conservative representation of 37-tube, area-ratio-3.3 radial array with elliptical convergent tubes. The resulting gross thrust coefficient is shown in figure 77.

6.3.13 37-TUBE, AREA-RATIO-4.5 RADIAL ARRAY

The performance of the 37-tube, area-ratio-4.5 radial array is shown in figure 78 as a function of pressure ratio and tube length. Even with its increase in drag (fig. 79) relative to the area-ratio-3.3 radial configuration, the drag is less than 2% of ideal thrust for all tube lengths.

6.3.14 42-TUBE ANNULAR/PLUG NOZZLE

The 42-tube nozzle, incorporating a variable height annular and plug, did not have static pressure instrumentation because the primary function of the nozzle was acoustic evaluation. The performance of the nozzle is shown as a function of pressure ratio and annulus height. Notice that the flow area increases with increasing annulus height. The diameter to the outside of the outer tubes remains constant, resulting in decreasing area ratio as annulus height increases. (For details see section 4.1.3.5.)

The discharge coefficient as a function of annulus height and pressure ratio is presented in figure 80. The gross thrust coefficient is shown in figure 81 as a function of annulus height and pressure ratio. Notice that the use of small annulus provides 2.5% better performance than the configuration using a plug surrounded by tubes with no annular flow. The decrease is due to separation on the plug that is avoided by using a flow annulus. Recall that the 42-tube nozzle with an annulus height of 0.383 inches is similar to the 61-tube, area-ratio-3.3 nozzle (fig. 45). Figure 81 shows that the performance of the nozzle with the 0.383-in. annulus is the same as that of a 61-tube nozzle with 3-in. tubes. The close agreement between data at ambient, 1150°F and 1500°F temperatures is shown in figure 82. Based on the results of the other nozzles with instrumentation, it is likely that the agreement in C_{f_g} at various temperature is due to a one-for-one trade-off between decreasing base drag and increasing internal losses as the temperature rises.

7.0 ANALYSIS: TRENDS AND QUANTITATIVE TRADE-OFFS

7.1 SUMMARY

Based on the results of the experimental investigation, it is now possible to establish quantitative performance trends and trades for each of the geometric parameters and temperatures. Each parameter will be addressed individually, but the major effects are nearly self-evident from figure 83, which presents performance as a function of tube number, tube length, and nozzle array. Figure 84 adds the influence of area ratio. In both of these curves the high performance of radial arrays is obvious. Carpet plots are used to allow easy interpolation to desired conditions.

The effective flow area used in the present study was maintained at 13.2 in.^{2}, making the nominal equivalent round jet diameter equal to four in. The relative performance quoted for any two configurations applies to nozzles tested at any other scale, but the actual value of the performance must be corrected for Reynold's number effects if the scale change is substantial. Reynold's number effects on tube internal performance are specified in section 5.2. Base drag, a separated flow phenomena, will decrease very slightly as the nozzle scale increases (ref. 13). The value of this decrease cannot be quantified but should be better understood at the end of the entire DOT/SST contract when a geometrically similar model and full-scale nozzles will be tested. The effect is expected to be negligible.

7.2 PRESSURE RATIO

Throughout section 6 the experimental results were expressed as a function of pressure ratio with a range from 2 to 4. This encompasses the operating range for candidate SST engines and includes the value required to produce optimum performance for every nozzle tested.

The nozzle performance, C_{f_g}, is the net result of the internal performance, $C_{V \, int}$, and the external drag, D_{AFT}/FID. As discussed in section 5, the $C_{V \, int}$ for a single tube has a peak value near pressure ratio 2. The value of $C_{V \, int}$ is lower on either side of the peak due to viscous and underexpansion losses. Since the pressure ratio is defined as a ratio of nozzle upstream (charging) total pressure to ambient pressure, the pressure loss in the tubes of a multitube nozzle requires that the pressure ratio be higher to produce choking at the end of the tubes. As a result the peak internal velocity coefficient decreases in magnitude and moves to higher pressure ratio as the number of tubes is increased. For the configurations tested the peak values occur in the pressure ratio range of 2.5 to 3. Section 7 demonstrates that drag as a percentage of ideal thrust is either independent of or decreases with increasing pressure ratio.

The resulting overall performance, C_{f_g}, is at or very near its optimum value at a pressure ratio of 3 for all nozzles tested. Therefore, the remainder of the analysis will address itself to pressure ratio three. Section 6 provides sufficient information for the reader to construct curves with the same format as the following figures for any pressure ratio constraint necessary from 2 to 4.

31

7.3 NUMBER OF TUBES

A single well-contoured tube provides the best base nozzle performance possible. Increasing the number of tubes, with other parameters held constant, causes a decrease in performance due to both increased internal losses and increased drag. On the other hand, noise suppression generally increases with increasing tube number by breaking the flow into small elements, each of which requires less distance to mix with surrounding air. Thus, to meet specified suppression requirements, the number of tubes often becomes a constraint, and the performance must be optimized by varying the other parameters. Fortunately, within the range of variables investigated, noise suppression is reasonably insensitive to nozzle internal performance and external ventilation. Reference 1 shows that the suppression is independent of ventilation for the most restricted configuration tested (i.e., 61-tube, area-ratio-3.3 close-packed) as demonstrated in figure 2.

The performance of nozzles with between 7 and 61 tubes is summarized on figure 83. A carpet plot is used to allow interpolation of values. As tube number increases, the use of radial arrays and increasing tube length become increasingly important. To equal the performance of a 19-tube nozzle with stowable tubes ($L_T/D_{eq} = 0.25$), a 61-tube, close-packed array would require three times the tube length of the 19-tube nozzle.

The seven-tube nozzle can be classified as either a close-packed or a radial array. The steep slope of C_{f_g} from the 7- to the 19-tube nozzle is an indication of the increased losses due to the obstruction in the ventilation flow path caused by the close-packed tube arrangement. Phantom lines connecting the 7- and 37-tube radial array demonstrate the increased performance available from the larger amount of base ventilation per unit tube length provided by the radial array. For example, a stowable-tube-length ($L_T/D_{eq} = 0.25$), 37-tube nozzle using a radial array produces 3.5% more thrust than a similar close-packed array.

A summary of internal performance, $C_{V\ int}$, of elliptical convergent tube nozzles is shown in figure 85 for ambient temperature cases and in figure 86 for 1150°F configurations. The $C_{V\ int}$ is proportional to the square root of the number of tubes (equation 6, section 5.1) and is independent of nozzle array; and the shorter the tube, the higher the internal performance. For short ($L_T/D_{eq} = 0.25$) elliptical convergent tube nozzles, internal losses account for only 0.4% thrust loss when the number of tubes is increased from 7 to 61. For tube lengths $L_T/D_{eq} = 1$, an equal amount of thrust loss occurs when the tube number increases from 37 to 61. Of course, tubes with higher Mach numbers would have greater losses. Baseplate drag due to incomplete ventilation accounts for the majority of thrust loss in most multitube nozzles, as shown in figure 87. Since internal losses are independent of the base array, the entire performance difference between radial and close-packed arrays, shown as A in figures 83 and 84, is due to the difference in base drag. Thrust losses due to incomplete ventilation amounted to as must as 8.5% for the configurations tested.

7.4 TUBE LENGTH

Tube length is nondimensionalized by the diameter of a single round convergent jet having the same flow area as the total effective flow area of the multitube configuration. For the present study, the nominal equivalent jet diameter, D_{eq}, is 4 in. Present mechanical concepts for stowable tubes require nondimensional tube lenths, L_T/D_{eq}, of less than 0.35. The

32

present study investigated L_T/D_{eq} values from 0.25 to 1.0 The longer tubes were tested to provide performance values for fixed suppressors, for business jet applications for instance, and to demonstrate the asymptotic nature of base drag as tube length increases.

Increasing tube length results in a linear increase in tube internal losses and a nonlinear decrease in base drag. The rate of internal loss with increasing tube length increases, as shown in figures 85 and 86, due to increased tube L/D. Incomplete ventilation results in high base drag for short tubes. The effect becomes dominant as tube number increases. Tube lengths necessary for stowable concepts are so critically dependent on ventilation that the radial array becomes the obvious choice from a performance point of view.

The tradeoff between internal and external performance results in an optimum tube length for each configuration. The location of the optimum tube length and the tradeoff between internal performance and base drag are demonstrated in figure 88. For the elliptical convergent tubes used in the present study, the radial array has nearly optimum performance at stowable tube lengths while the close-packed array requires a nondimensional tube length, L_T/D_{eq}, of 0.8. The use of nonconvergent tube or tubes with higher internal Mach number will produce an optimum performance with shorter tubes (figure 89). Of course, the level of performance will not be as high as for the elliptical tube case. For very short tubes ($L_T/D_{eq} < 0.25$), the straight tube C_V int becomes nonlinear and highly dependent on inlet shape. In this region the internal performance of the nonconvergent tube is better than that of the convergent tube. However, the increase in tube size required for the nonconvergent tube to pass the same mass flow as the elliptical convergent tube would result in sufficient ventilation reduction that the gain in internal performance would be easily negated by the increased drag.

7.5 BASE ARRAY

The most significant test result is the performance increase due to using radial instead of close-packed arrays. Figures 83 and 84 compare the performance of the two arrays for various tube lengths and area ratios. The higher performance of radial array nozzles is mostly due to the larger amount of base ventilation available per unit tube length. This is of particular significance when short tubes are required. For example, the gross thrust coefficient gain of the radial over the close-packed array for 37 one-inch elliptical convergent tube configurations ($L_T/D_{eq} = 0.25$) is 3.3% for an area ratio of 3.3 and 5% for an area ratio 4.5 at a pressure of 3.0.

The increase in performance of the radial over the close-packed array becomes even more important as tube number increases due to the increasing obstruction to penetration of ventilating flow caused by multiple rows of tubes in a close-packed array.

Radial ventilation flow paths should be provided on any suppressor being considered even if tube size or shape is not being held constant.

Internal performance is not affected by the arrangement of tubes on the base. Therefore, the entire benefit of radial arrays is a result of decreased base drag resulting from better ventilation. To provide good suppression characteristics, the flow in a radial array should be distributed, thus tubes should not be concentrated into a core at the center. The problem is

33

easily avoided by using a radial array with tube progression like the 31-tube nozzle. The distribution of pressure on the base plate is demonstrated on figure 90 for the area-ratio-2.75, 37-tube, close-packed array and on figure 91 for the area-ratio-2.75, 31-tube radial array. Notice that the pressure variations correspond to variations in area between tubes. The increased drag per unit area due to close-packed tubes is noticeable by comparing the pressure between the nonradial tubes of the close-packed array (shown as diamonds on figure 90) and those on the somewhat radial gutter on the same figure (shown as solid circles). The substantial increase is pressure relief due to a pure radial array becomes obvious by comparing figures 90 and 91. Pressure ratio does not alter the relative pressure distribution as shown in figure 92. The pressure distribution of two area-ratio-4.5 nozzles which are similar in all respects except base array is shown on figure 93. The path shown is the best-ventilated gutter for each case. The difference in pressure is a direct result of the velocity of the air moving toward the center to ventilate the base. The figure shows the minimum pressure (maximum velocity) for the close-packed array at the minimum area between the outer row tubes. Besides creating a low pressure per unit area, the occurrence of the maximum velocity at a large radius causes low pressure on a large area, resulting in the worst possible drag situation. (Note: This phenomenon is area-ratio-dependent.)

7.6 AREA RATIO

Internal performance is independent of area ratio. Area ratio produces performance changes by affecting ventilation. Nozzle performance and afterbody drag as functions of area ratio are shown on figures 84 and 94 respectively. As predicted in Section 3.2.6, the peak performance of close-packed arrays occurs at an area ratio of 3.3. Thus, the crossplots, such as figure 83, shown at area ratio 3.3 are representative of the maximum performance possible.

Figure 95 provides an insight into the effect of area ratio on the performance (e.g., close-packed arrays with short tubes). For the area-ratio-2.75 nozzle, the ventilation is poor due to the close proximity of the tubes. This results in a low static pressure on the base because ventilating air cannot get to the center of the base at a sufficient rate to replace the air entrained by the jets. However, the small area ratio means the low pressure acts on a relatively small area, resulting in a drag of 6.5% of ideal thrust. The area-ratio-4.5 nozzle, on the other hand, has an average base pressure 6.5% higher than the area-ratio-2.75 of nozzle. The air moving toward the center has a maximum velocity—and hence minimum pressure—between the outer row tubes, producing a maximum drag on a large annulus. The large base area operated on by the moderate pressure results in nearly the same total drag as the area-ratio-2.75 nozzle (7.0% of ideal thrust). Area ratio 3.3 offers the best compromise between these two extremes. The minimum pressure occurs nearer the center and hence acts on a smaller annulus. The average pressure is almost identical to that of the area-ratio-4.5 nozzle, but area ratio is sufficiently less than that of either of the others that the resultant drag is only 60% of each of theirs (4.0% of ideal thrust).

Radial arrays are less sensitive to area ratio and, even at area ratio 3.3, the radial array has 3.5% more thrust that the close-packed array for 37-tube nozzles with short ($L_T/D_{eq} = 0.25$) tubes. For the same configurations the difference in performance has grown to 5% at area ratio 4.5 (figure 84).

34

7.7 TUBE SHAPE

Elliptical convergent tubes were selected for most of the test configurations because of the benefits discussed in section 3.2.5. The present investigation quantifies the choice. The area ratio providing maximum ventilation and thus maximum performance was accurately predicted in section 3.2.6 for elliptical convergent tubes. The same analysis predicts that the optimum performance of nozzles with round convergent tubes should occur near area ratio 5, a ratio too large for practical consideration. The restricted ventilation per unit tube length assures that the level of performance for round convergent tubes is less than for elliptical convergent tubes in all cases. The difference in performance of two 37-tube, area-ratio-3.3 nozzles, one with round convergent and the other with elliptical convergent tubes (both having an internal tube Mach number of 0.5), is shown in figure 96 to be 1% of FID for $L_T/D_{eq} = 0.5$ and 0.75 tubes at PR = 3.0.

Round nonconvergent tubes must be larger than elliptical convergent tubes in order to pass the same mass flow. For very short tube lengths ($L_T/D_{eq} < 0.25$) the internal performance of nonconvergent tubes can be higher than for convergent tubes. However, for the short tubes the ventilation restriction due to larger tubes far outweighs the small gain in internal performance.

7.8 RAMP SHAPE

The ramp shape becomes increasingly important as tube length decreases due to the increased velocity of the ventilating air. The elliptical ramp provides 1.5% less drag/FID than the circular arc ramp for a configuration with a severe ventilation restriction (37-tube, area-ratio-2.75, close-packed array, see figure 67). For all nozzles investigated, the effect of the ramp on afterbody drag/FID was less than 0.5% for $L_T/D_{eq} \geqslant 0.75$. Because ramp shape is increasingly important as ventilation needs increase, the elliptical ramp will be used for the extension of the present study to include ejectors and forward velocity.

7.9 VENTILATION PARAMETER

Ventilation parameters, as defined in reference 5, were established for the nozzles under investigation in an attempt to nondimensionalize the base drag. For the various parameters tested, base drag as a function of geometric ventilation parameter, A_S/A_B, shown in figure 97, does not nondimensionalize the data. If the ventilation area between the jets is included (assuming an average expansion angle of 1/2 the Prandtl-Meyer turning angle at the appropriate pressure ratio) the ventilation parameter, A_V/A_B, does an adequate job of nondimensionalizing the drag for various tube numbers at a fixed area ratio (fig. 98). The nondimensionalization does not extend to all area ratios, nor is it the same for radial and close-packed arrays.

7.10 TEMPERATURE EFFECTS

7.10.1 DISCHARGE COEFFICIENT

Thermal expansion of the nozzle exit area is accounted for by assuming a linear expansion of the nozzle perimeter. The effect of change in Reynold's number due to increased temperature

35

is considered to be very small and is ignored. The excellent agreement between ambient and 1150°F discharge coefficient shown in section 6 confirms that it is sufficient to account only for thermal expansion, as above.

7.10.2 INTERNAL THRUST COEFFICIENT

A temperature of 1150°F causes a 35% increase in the skin friction coefficient for the present test resulting in increased losses within the constant area portion of the tubes and a decrease in the pressure ratio available to the convergent portion of the tubes. The change in C_f due to temperature (calculated as a function of Reynold's number using equation 7, section 5.2) is sufficient to accurately predict pressure losses within the tubes. The momentum thickness within the convergent portion of the tube increases so that θcold = 0.72 (θ @ 1150°F). For the convergent portion of the tubes, the internal velocity coefficient is approximately

$$C_{V\,R/C} = 1\,\frac{-2\theta}{r}$$

Thus, the $C_{V\,R/C}$ for use in $C_{V\,int}$ calculations for multitube nozzles (equation 5, section 5.1) is

Pressure Ratio	2.0	2.5	3.0	3.5	4.0
$C_{V\,R/C}$ @ Ambient	0.9955	0.9960	0.9930	0.9875	0.9815
$C_{V\,R/C}$ @ 1150°F	0.9948	0.9955	0.9913	0.9825	0.9786

Equation 5, section 5.1 is sufficient for calculating $C_{V\,int}$ at any desired temperature provided the appropriate Reynold's number corrections (section 5.3) are made to C_f and $C_{V\,R/C}$.

7.10.3 AFTERBODY DRAG

Afterbody drag becomes a decreasing percentage of ideal thrust, FID, as temperature increases. Figure 99 demonstrates that the amount of decrease is dependent on both the tube length and array. The amount of change in afterbody drag does not nondimensionalize to the ventilation parameter, nor is the change a constant percentage of the ambient drag.

7.10.4 GROSS THRUST COEFFICIENT

The partially compensating effects of temperature-induced changes in internal performance and afterbody drag result in relatively small changes in gross thrust coefficient with temperature for the configurations tested with convergent tubes. For cases with restricted ventilation (short tube, close-packed arrays), the drag dominates and hence the gross thrust coefficient is slightly higher for elevated temperatures. As tube length increases the internal losses dominate, and the elevated temperature results in a slightly lower gross thrust coefficient than that of the geometrically similar case tested at ambient temperature. For straight tubes

less length is required for the internal losses to dominate; hence, increased temperature results in a slight decrease in performance for even the shortest tube tested.

7.11 SUMMARY OF SUPPRESSION VERSUS THRUST LOSS

The complete results and analysis of the suppression characteristics are covered in detail in reference 1. A summary of suppression versus thrust loss for the multitube nozzles is presented using suppression values quoted from the reference. The noise suppression and thrust loss characteristics at pressure ratio = 3.0 are shown (relative to a single round jet) in figure 100. The suppression values are for $1150^{\circ}F$ jet temperature. The curves show thrust loss values for ambient jet temperatures because hot jet thrust measurements were not available for most configurations. The available values of thrust loss at $1150^{\circ}F$ are plotted on the figure to produce a skeleton version of suppression versus thrust loss with both measured at the elevated temperature. As shown in section 7.10 the temperature effect on the gross thrust coefficient is small and thus the curves on figure 102 are expected to be representative of hot jet thrust versus noise characteristics for all configurations.

Radial arrays provide the best suppression to thrust loss ratio. Within the range of interest, increasing tube length results in large performance gains without measureable changes in suppression. The effect of area ratio on suppression and thrust loss is summarized in figure 101.

8.0 CONCLUSIONS AND RECOMMENDATIONS

- The single most important performance parameter investigated is the radial array. The increased ventilation and uniform base pressure distribution provide a strong incentive for recommending the use of radial arrays, particularly for nozzles having tube lengths compatible with the stowable tube concept.

- Elliptical tubes converging to a round exit proved to be the best tube shape studied.

- Optimum nozzle area ratio is at or near 3.3.

- Configurations incorporating elliptical convergent tubes and a radial array provide near-optimum performance with stowable tube lengths.

- Optimum performance of all nozzles occurs near pressure ratio 3.0.

- Increasing jet temperature increases internal losses while decreasing afterbody drag.

- The semiempirical relationship developed for calculating the internal velocity coefficient, as a function of 10 geometric and flow parameters, provides an excellent correlation with experimental values.

39
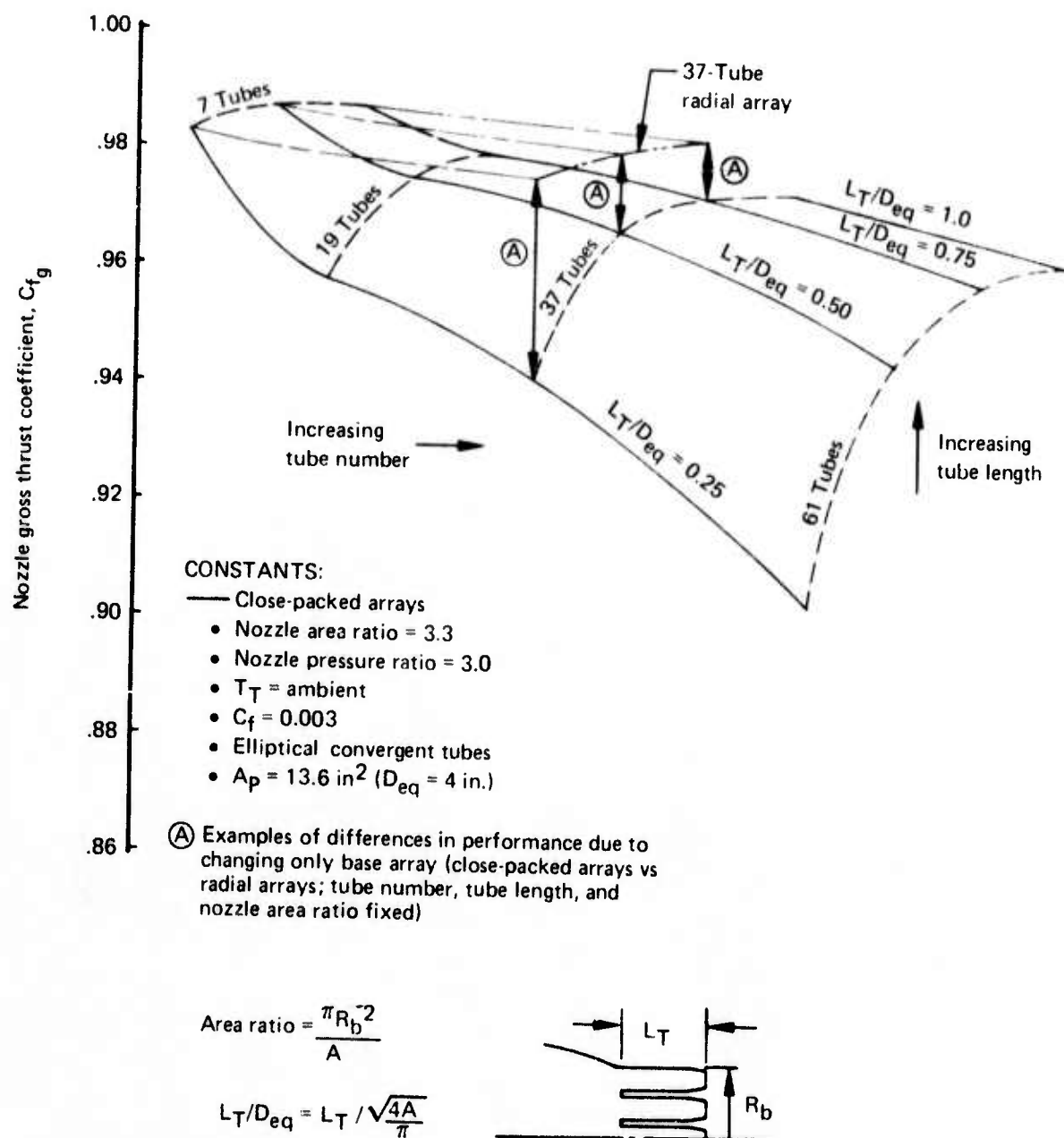
Figure 1.—Effect of Tube Number, Base Array, and Tube Length on Suppressor Performance
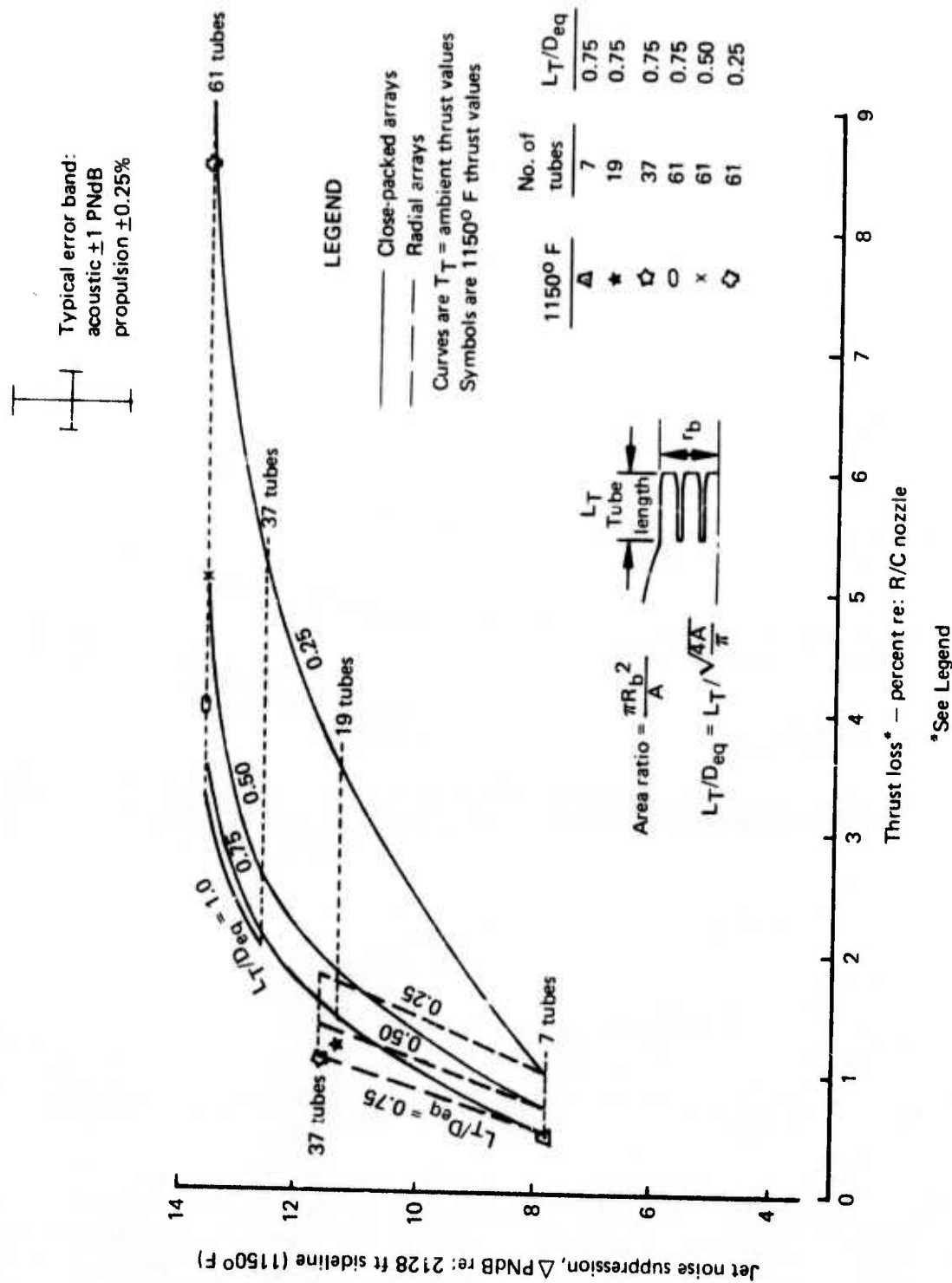
Figure 2.—Summary of Suppression Versus Thrust Loss, Area Ratio 3.3, Pressure Ratio 3.0

42

Thrust
reverser

Primary
nozzle

Ejector

Takeoff mode

Cruise mode
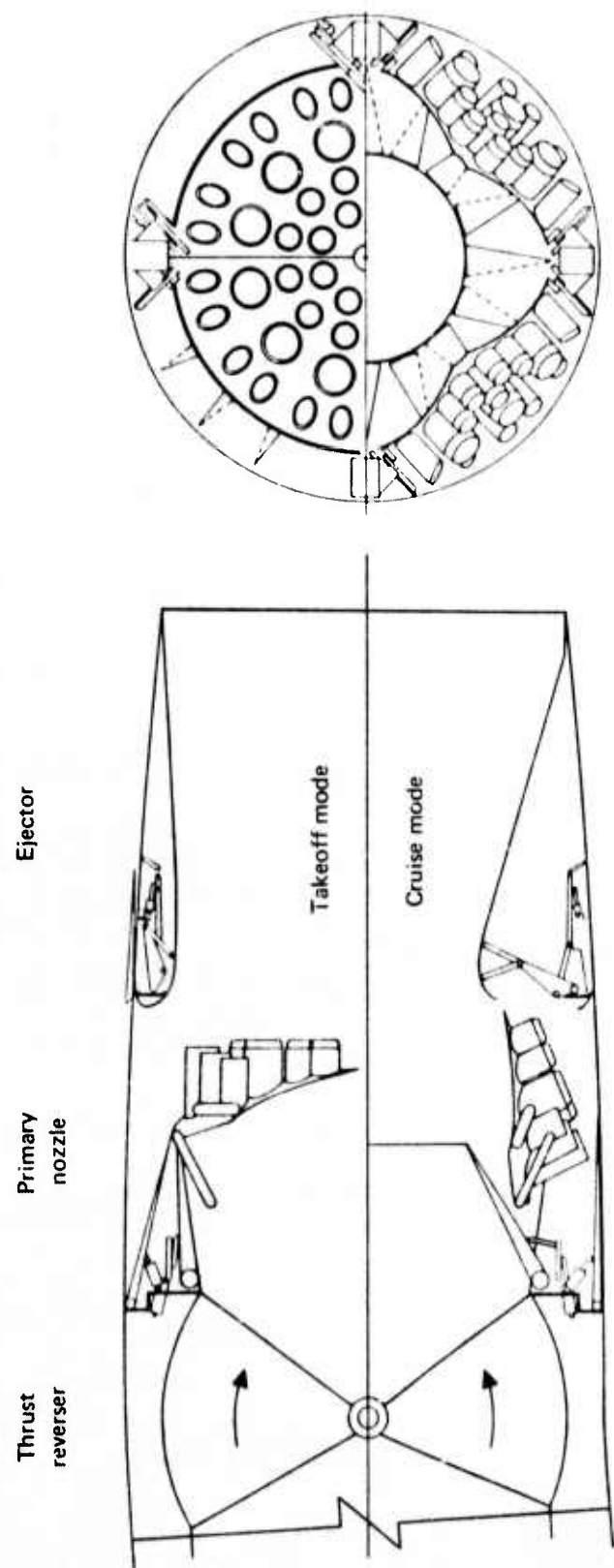
Figure 3. – Application of Stowable Suppressor to an Advanced SST Exhaust System

43

Objective: Isolate the contribution of each of the following parameters to multitube suppressor performance
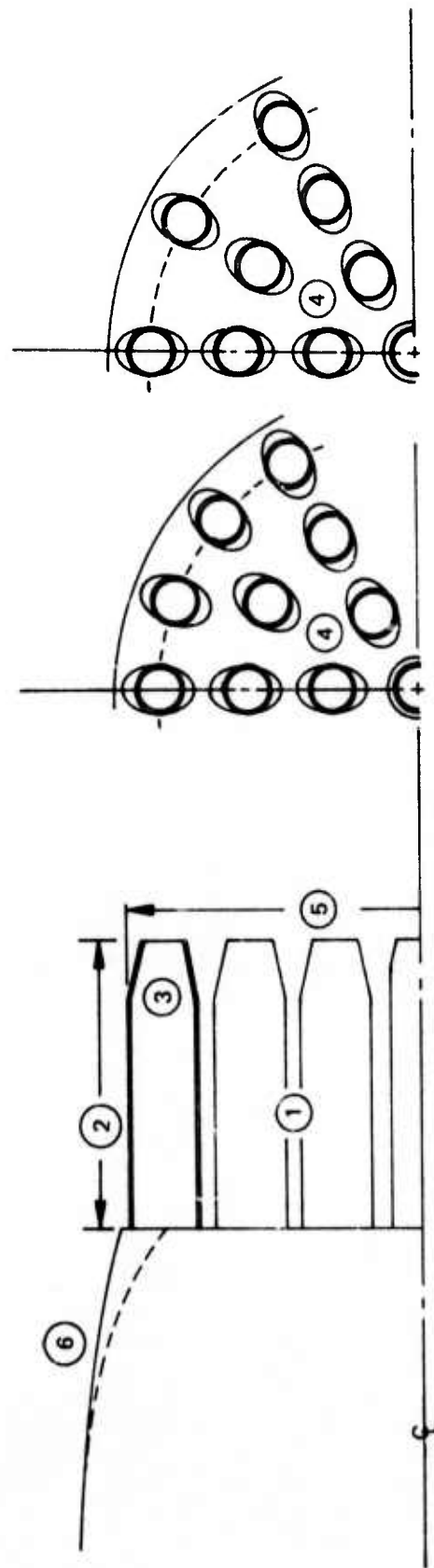
Variables and ranges:

1. Tube number: 7, 19, 37, 61
2. Tube length: 1- to 4-in. ($L_T/D_{eq} = 0.25 - 1.0$)
3. Tube shapes: round, elliptical
4. Base arrays: close-packed, radial
5. Primary area ratios: 2.75, 3.3, 4.5, 6.0
6. Primary ramp shapes: circular arc, elliptical

- Pressure ratio: 2 - 4
- Temperatures: ambient, 1150°F

Figure 4.—Summary of Parameters

44
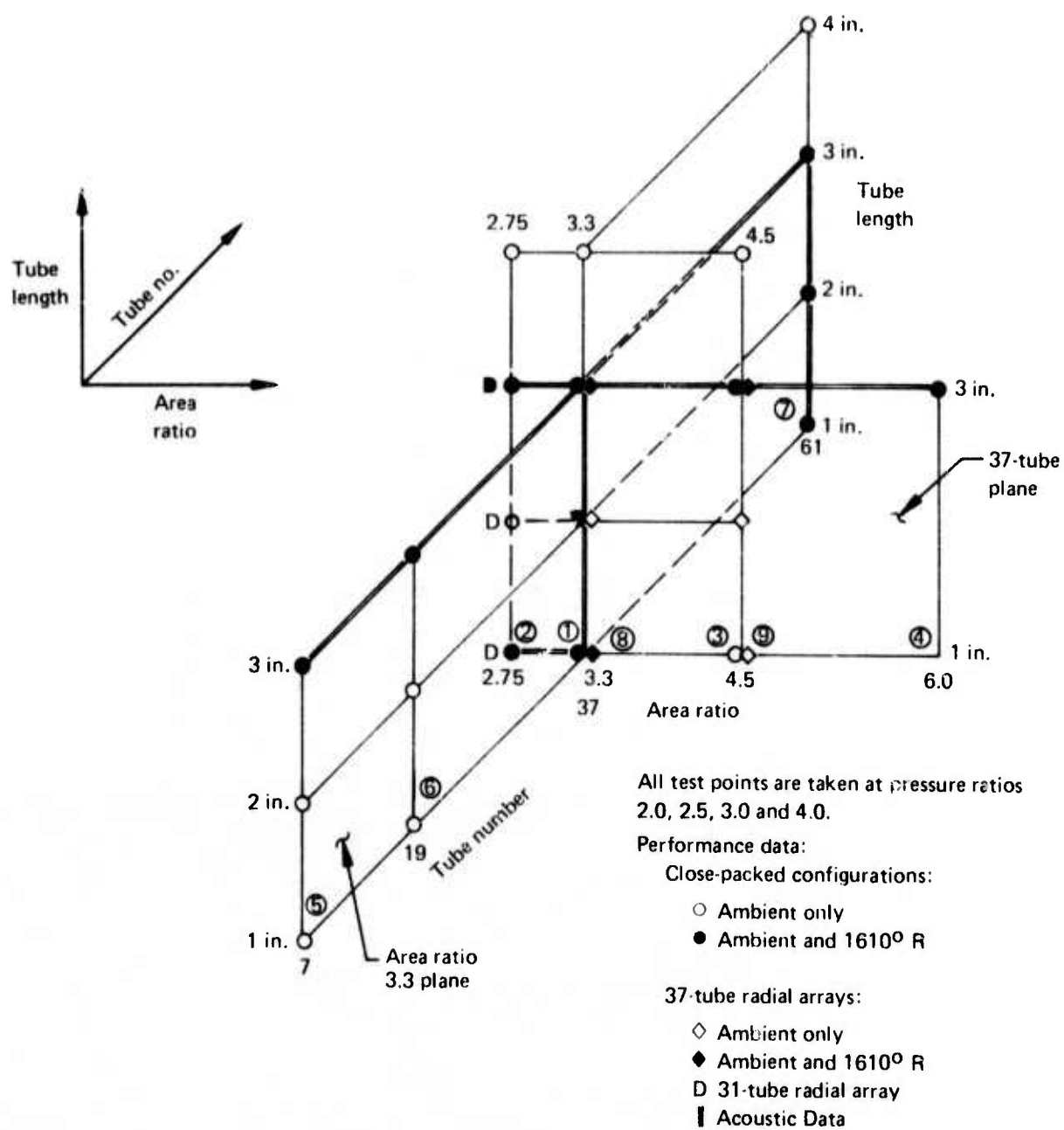
Figure 5.—Matrix of Configurations and Conditions for Mechanism Studies

45
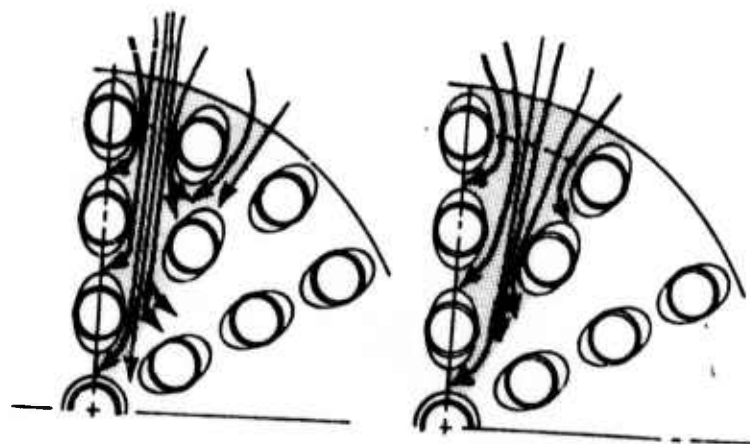
Figure 6.—Typical Ventilation Flow Paths

Closed-packed array
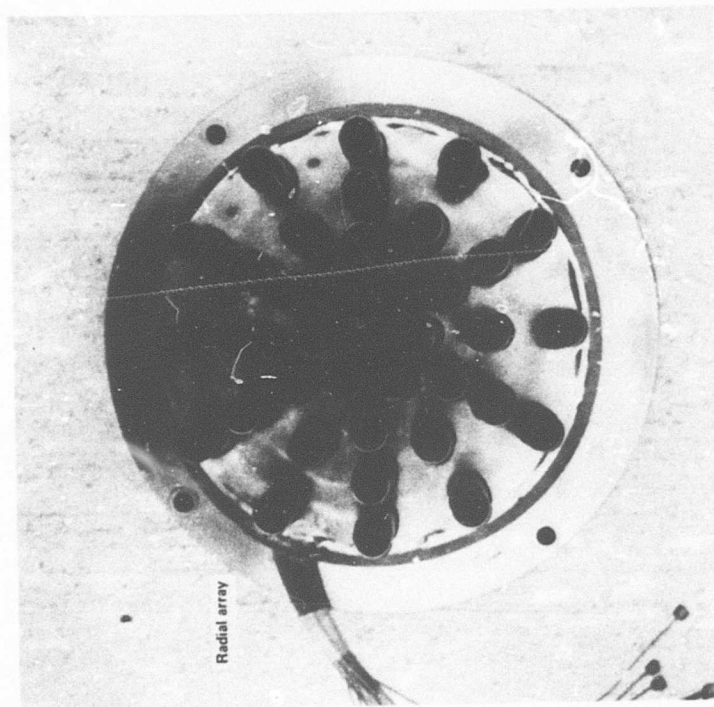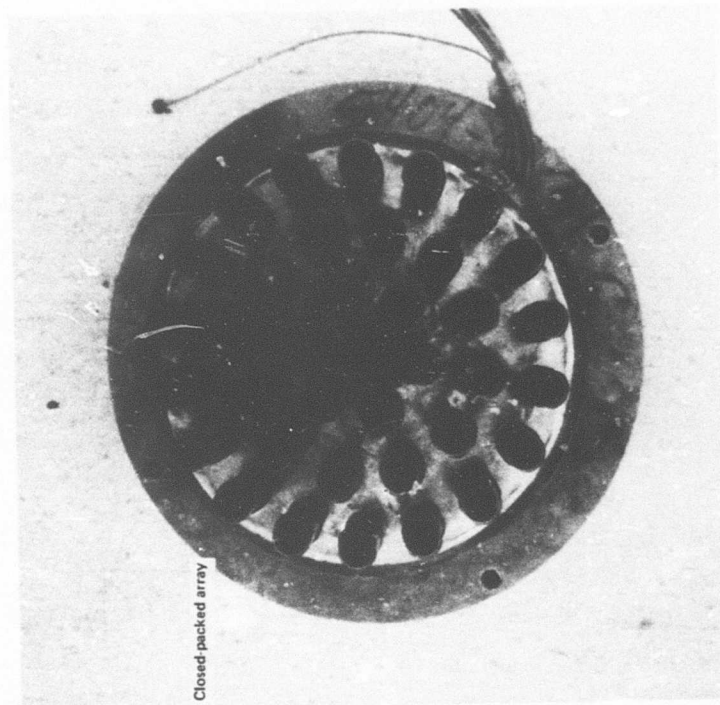
Radial array

Figure 7.—Example of Radial and Close-Packed Arrays

47
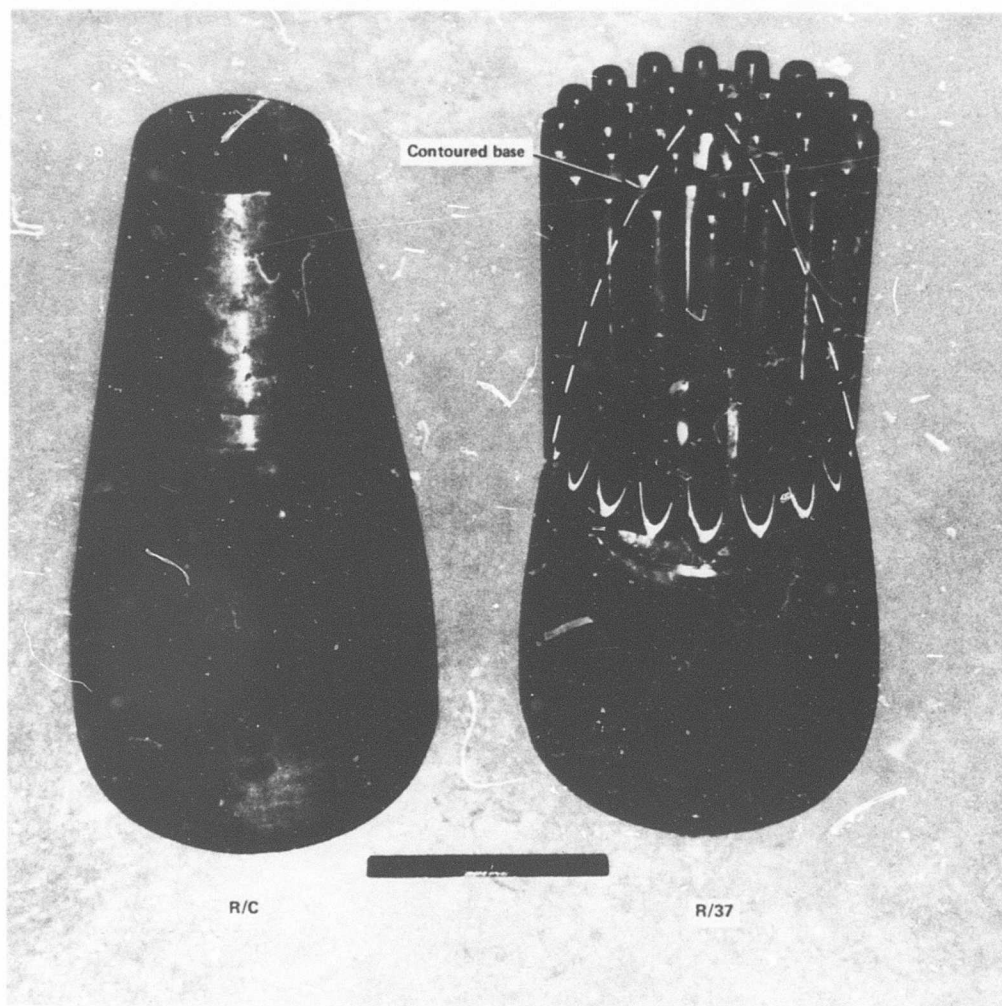
Round-convergent
reference nozzle

37-tube area ratio 3.3
close-packed with
round-convergent tubes

Figure 8. – R/C and R/37 Nozzles

48
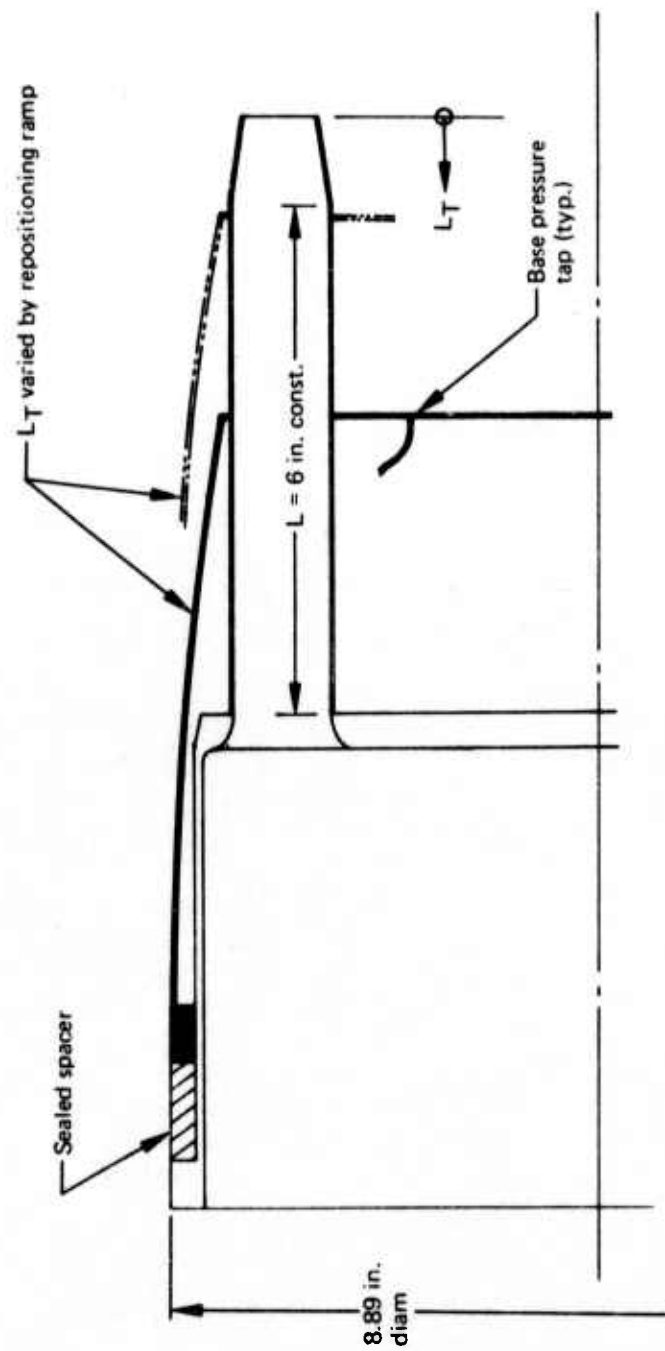
Figure 9.—Method for Varying External Tube Length, L_T (Constant Internal Tube Length)

49
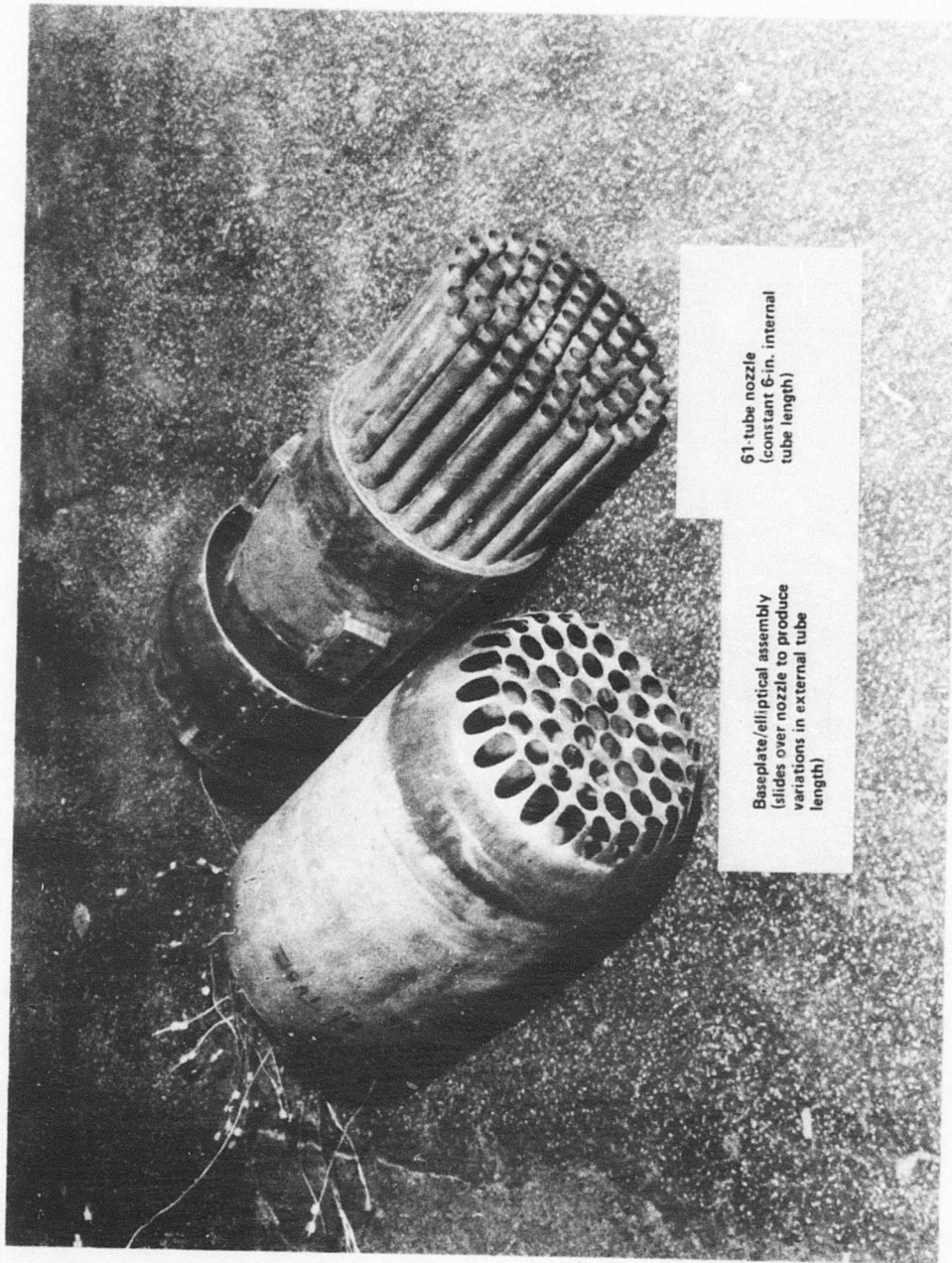
61-tube nozzle
(constant 6-in. internal
tube length)

Baseplate/elliptical assembly
(slides over nozzle to produce
variations in external tube
length)

Figure 10.—61-Tube Nozzle and Associated Baseplate/Elliptical Ramp Assembly
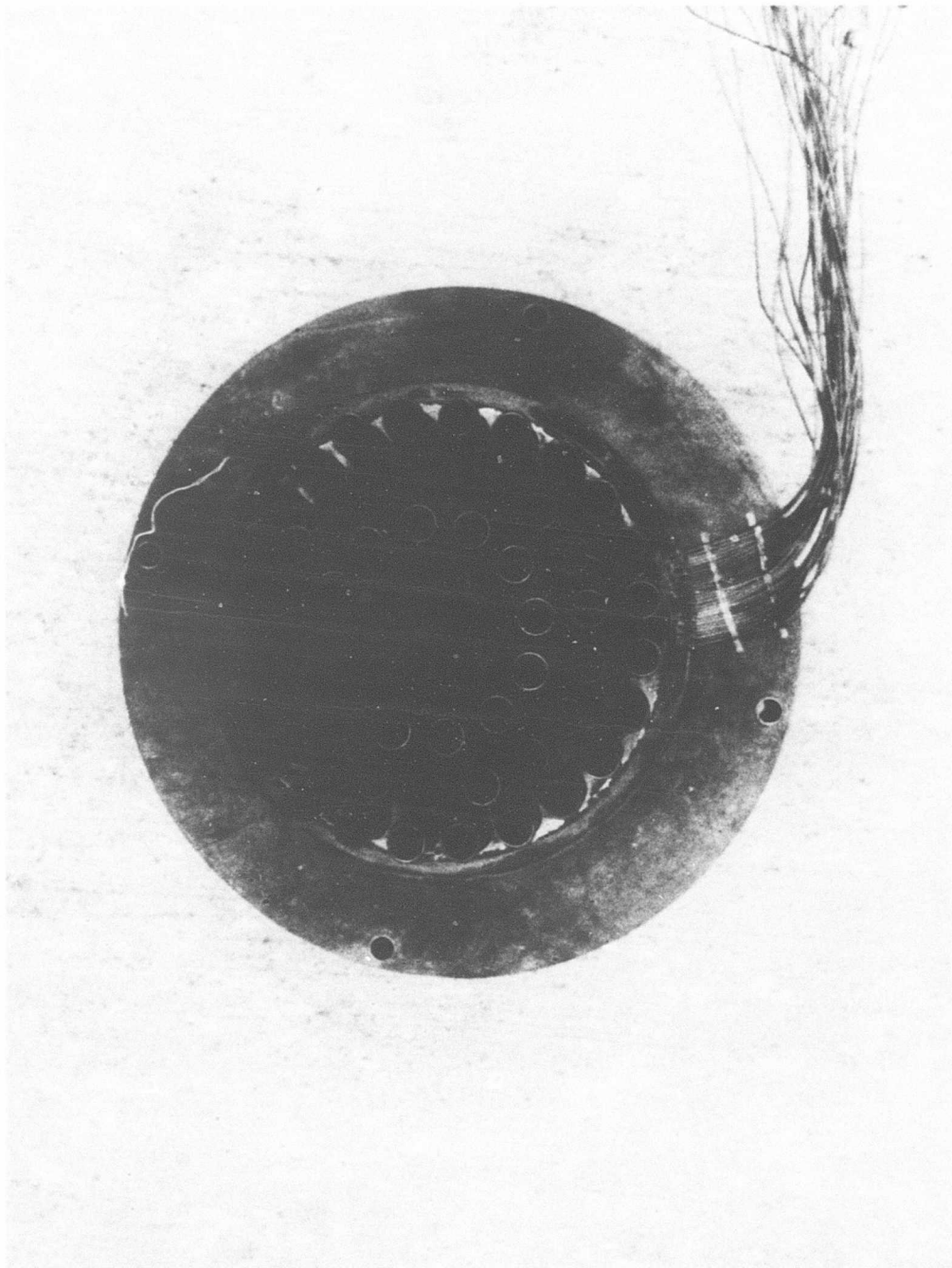
Figure 11. — 61-Tube, Area Ratio 3.3, Close-Packed Array With Elliptical Convergent Tubes

51

Material: 321 CRES

NOTE: Center tube is 0.875-in. dia, tube with 0.020-in. wall
(0.835-in. i.d.) with a 12° nom. convergence to 0.747-
in. diam exit.

12° nom.   0.035-in. wall

0.937-in.   0.747-in.

6.0-in.
(Tube exit plane to
tube holder plate)
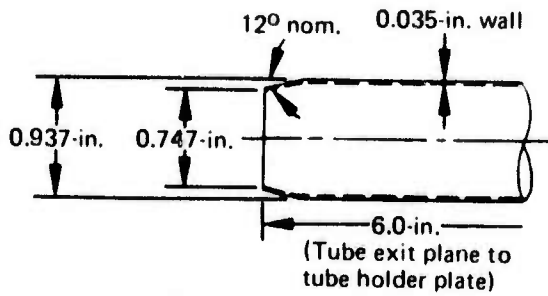
(30 elliptical
tubes req'd)

30°
(typ.)

3.45-in. R

2.975-in. R

1.971-in. R

0.967-in. R

0.747-in. I.D.
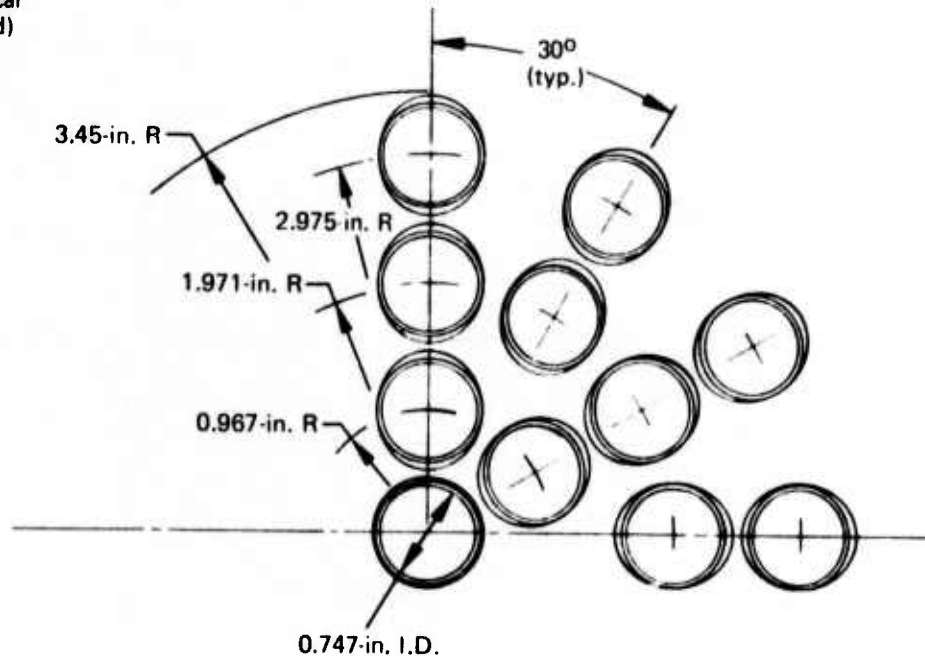
Figure 12.—31-Tube, Area Ratio 2.75, Radial Array With Elliptical Convergent Tubes

52

Close-packed array
(37 tubes)

Radial array
(31 tubes)
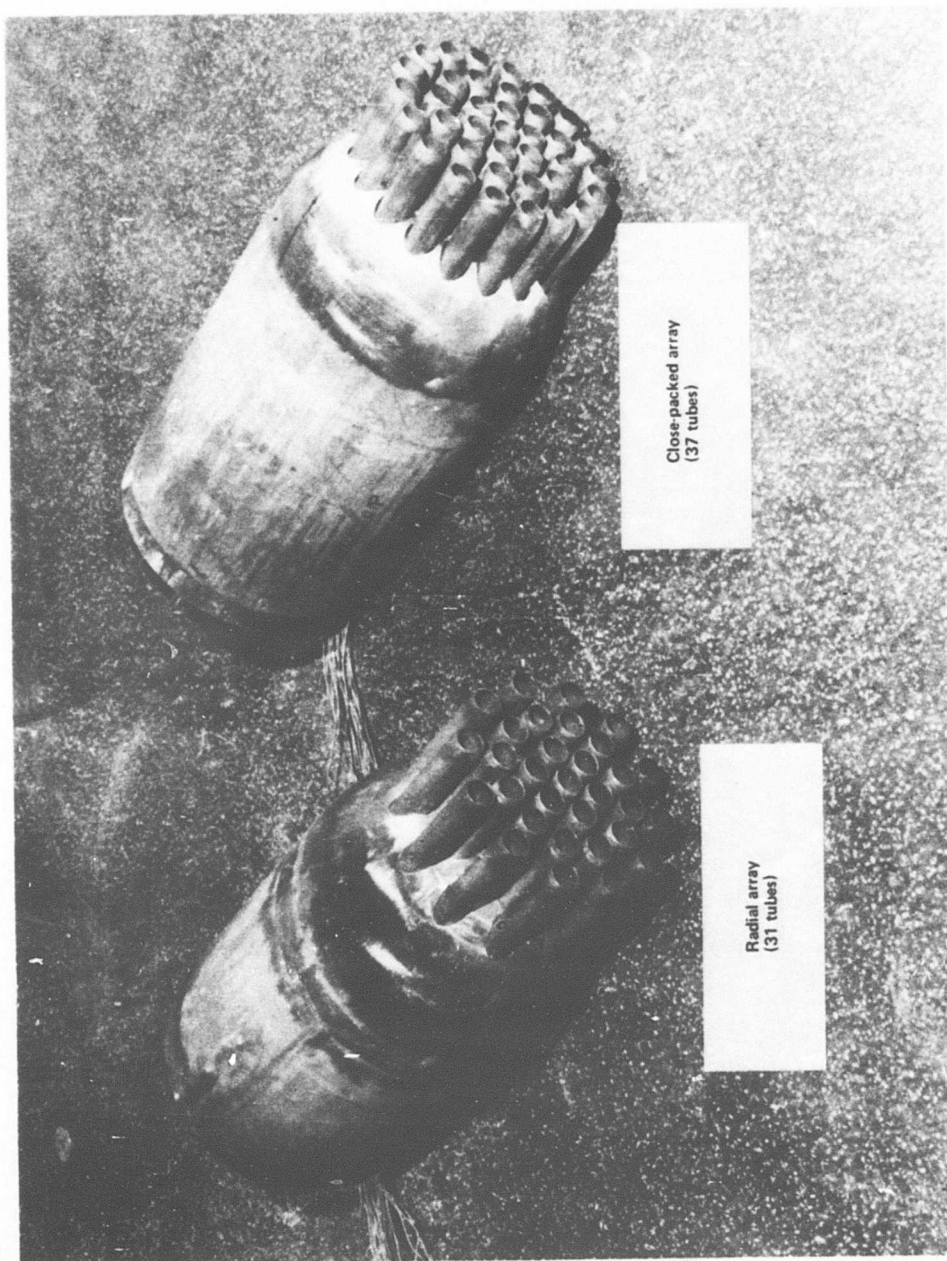
Figure 13.—Area Ratio 2.75 Nozzles: 31-Tube Radial Array and 37-Tube Close-Packed Array

53

Round convergent

Round non-convergent

Elliptical converging
to round exit*

All tubes pass the same mass flow.

* Elliptical convergent tubes produce
largest ventilation area and move
the minimum area toward the center
to effectively minimize base area to
be ventilated.
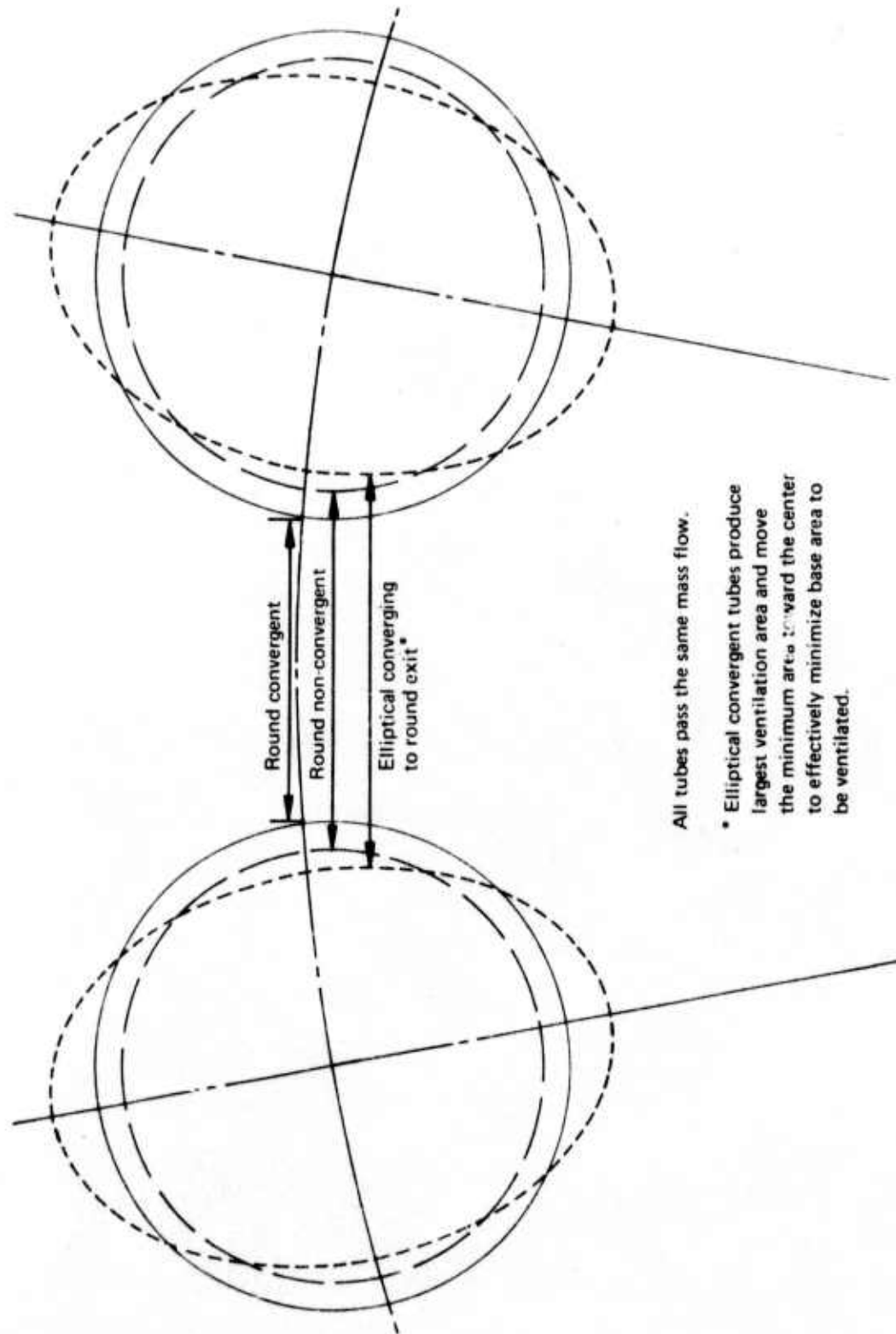
Figure 14.—Minimum Distance Between Tubes for Various Tube Shapes

54

All tubes pass the same mass flow.

- Elliptical convergent tubes produce largest ventilation area and move the minimum area toward the center to effectively minimize base area to be ventilated.

Round convergent

Round non-convergent

Elliptical converging to round exit*
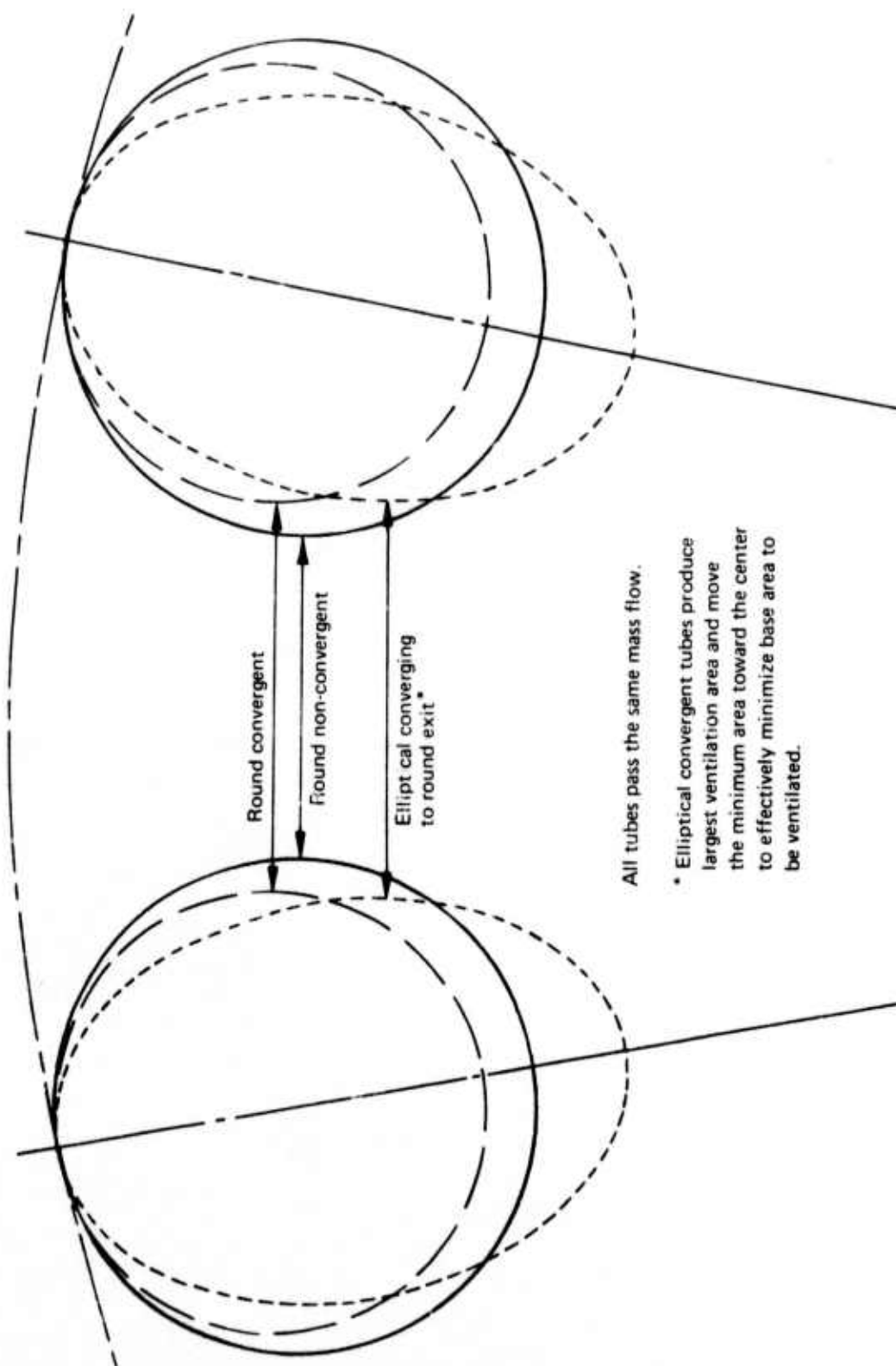
Figure 15.—Location of Minimum Distance Between Tubes for Various Tube Shapes and Constant Area Ratio

55
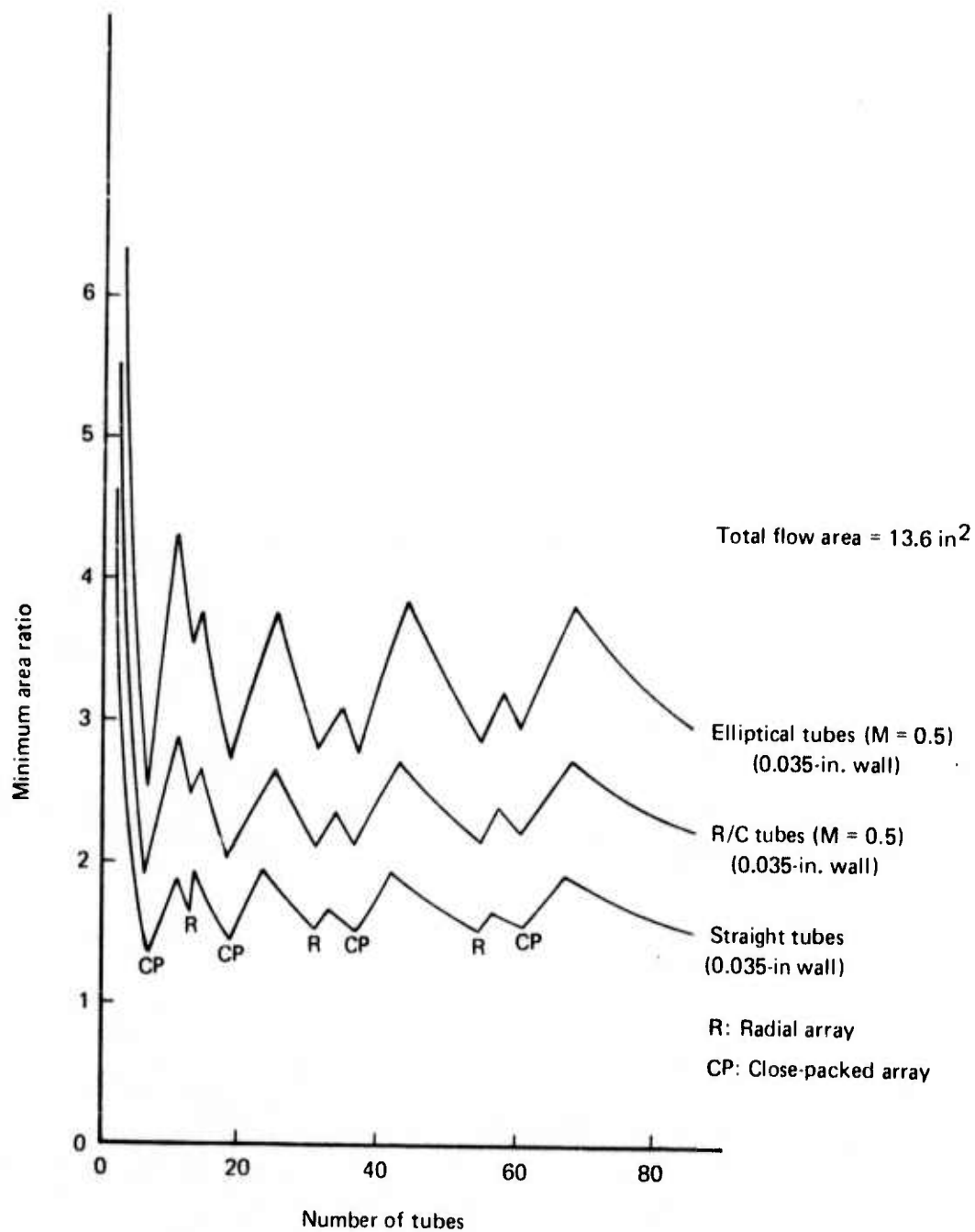
Figure 16.--Minimum Possible Area Ratio

56
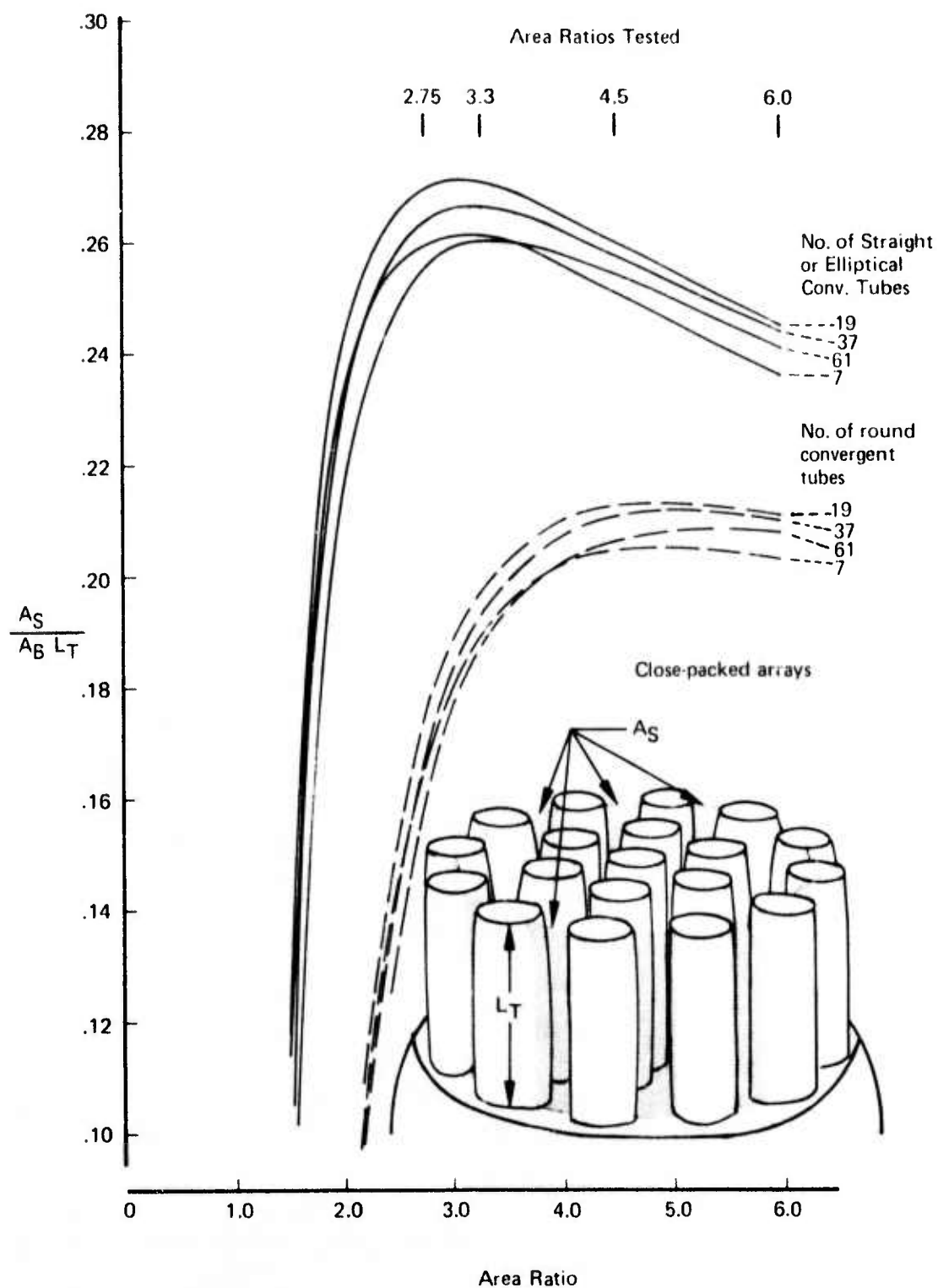
Figure 17.—Physical Ventilation Parameter (Per Unit Tube Length) as a Function of Area Ratio, Tube Number, and Tube Shape

57
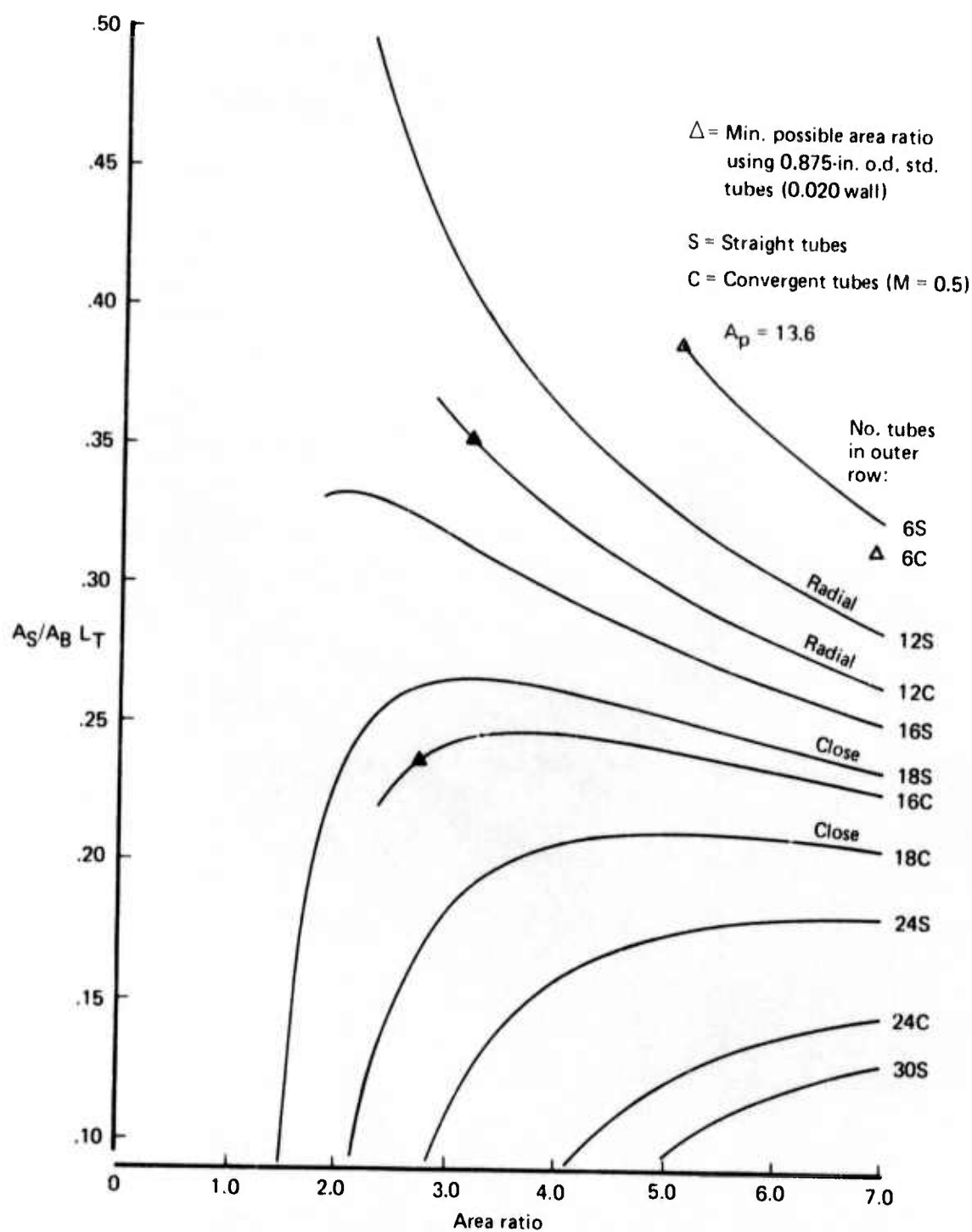
Figure 18.— Ventilation Parameter Per Unit Tube Length Versus Physically Possible Area Ratios for 37-Tube Configurations

58
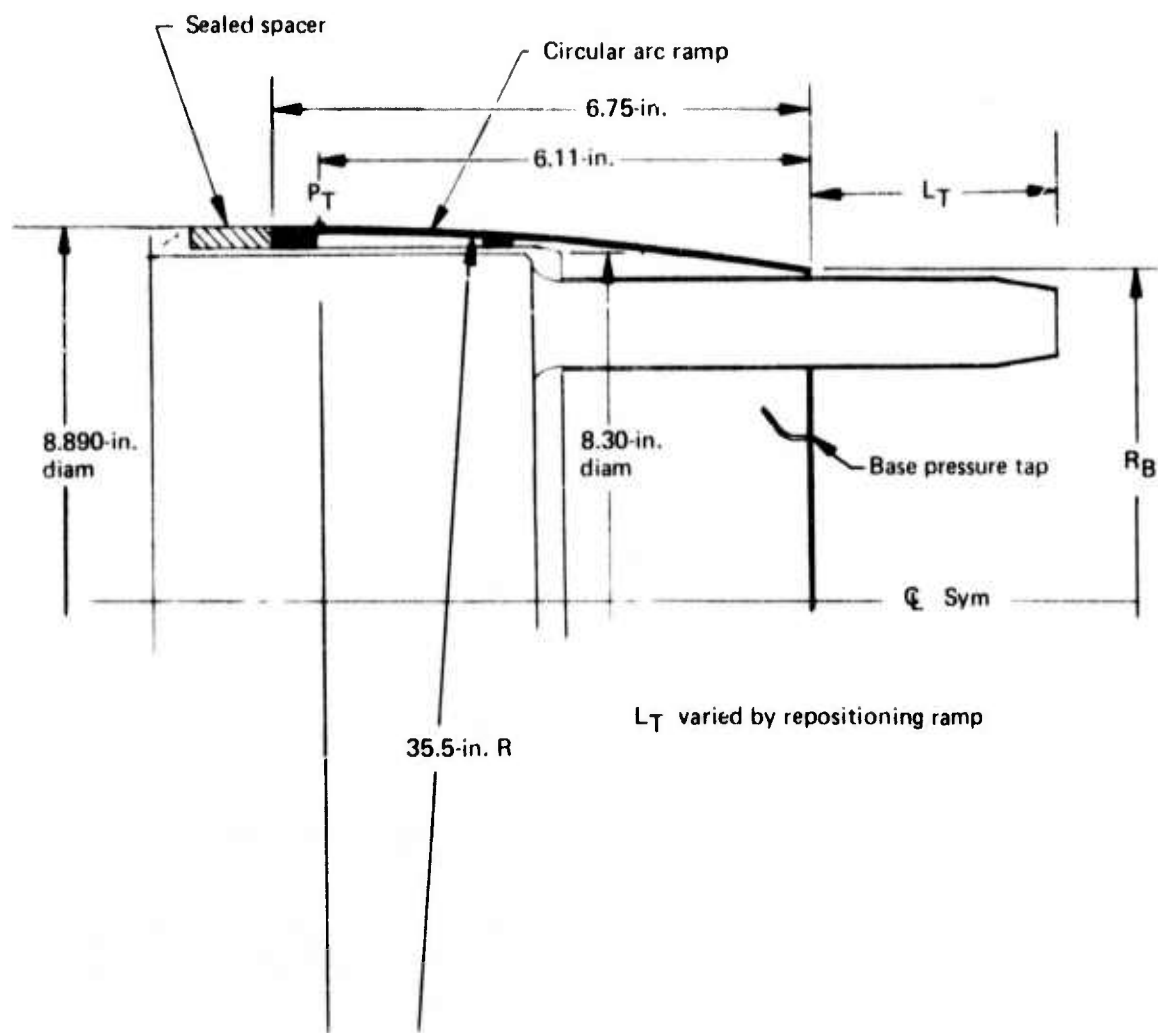
Figure 19.—Circular Arc Ramp
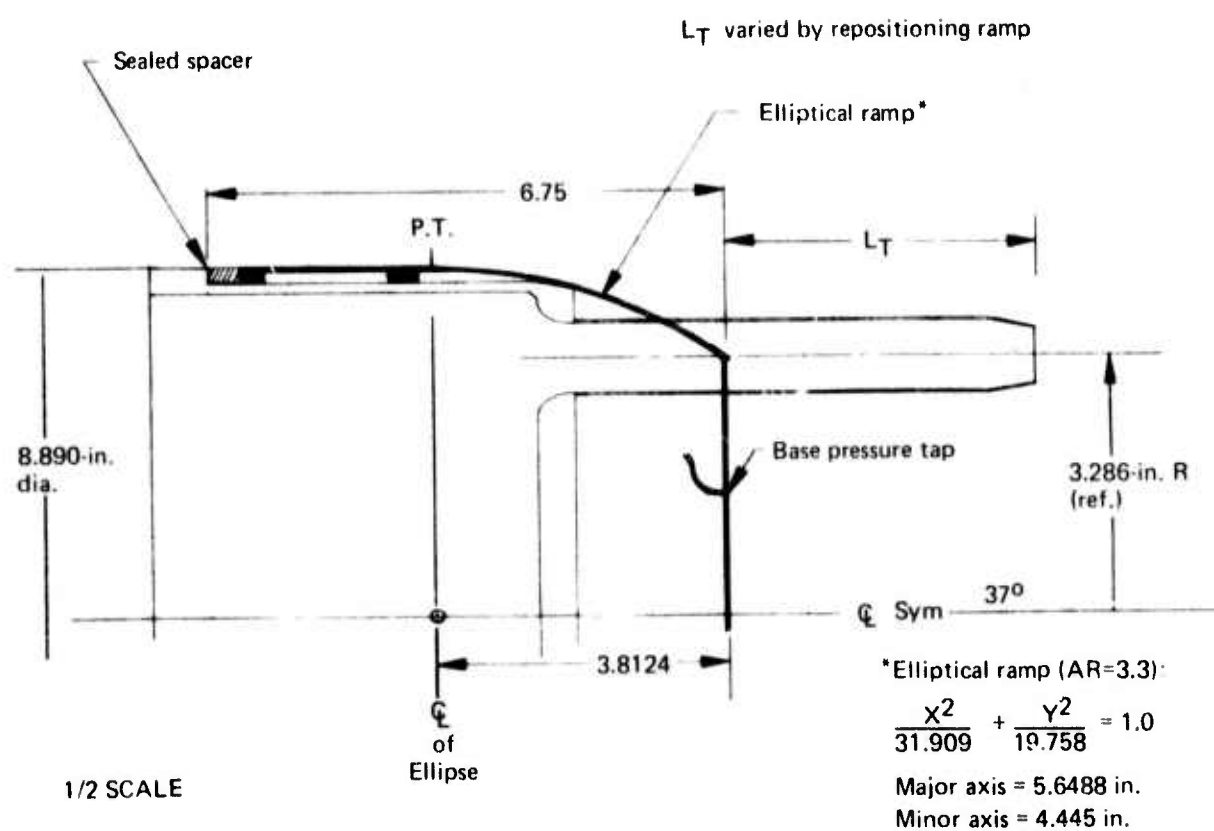
Figure 20.—Elliptical Ramp for Area Ratio 3.3 Nozzles

L$_T$ varied by repositioning ramp

Figure 21.—Elliptical Ramp for Area Ratio 2.75 Nozzles
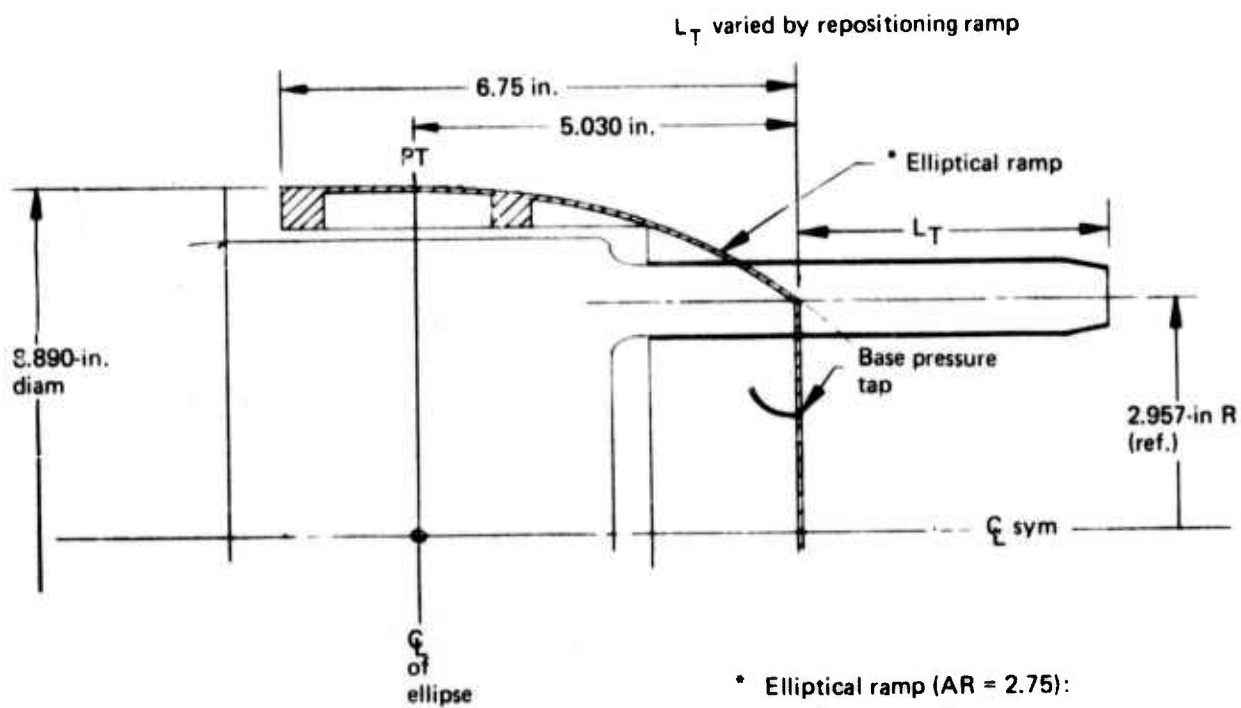
* Elliptical ramp (AR = 2.75):

$$\frac{X^2}{45,394} + \frac{Y^2}{19.758} = 1.0$$

Major axis = 6.7375 in.
Minor axis = 4.445 in.

61
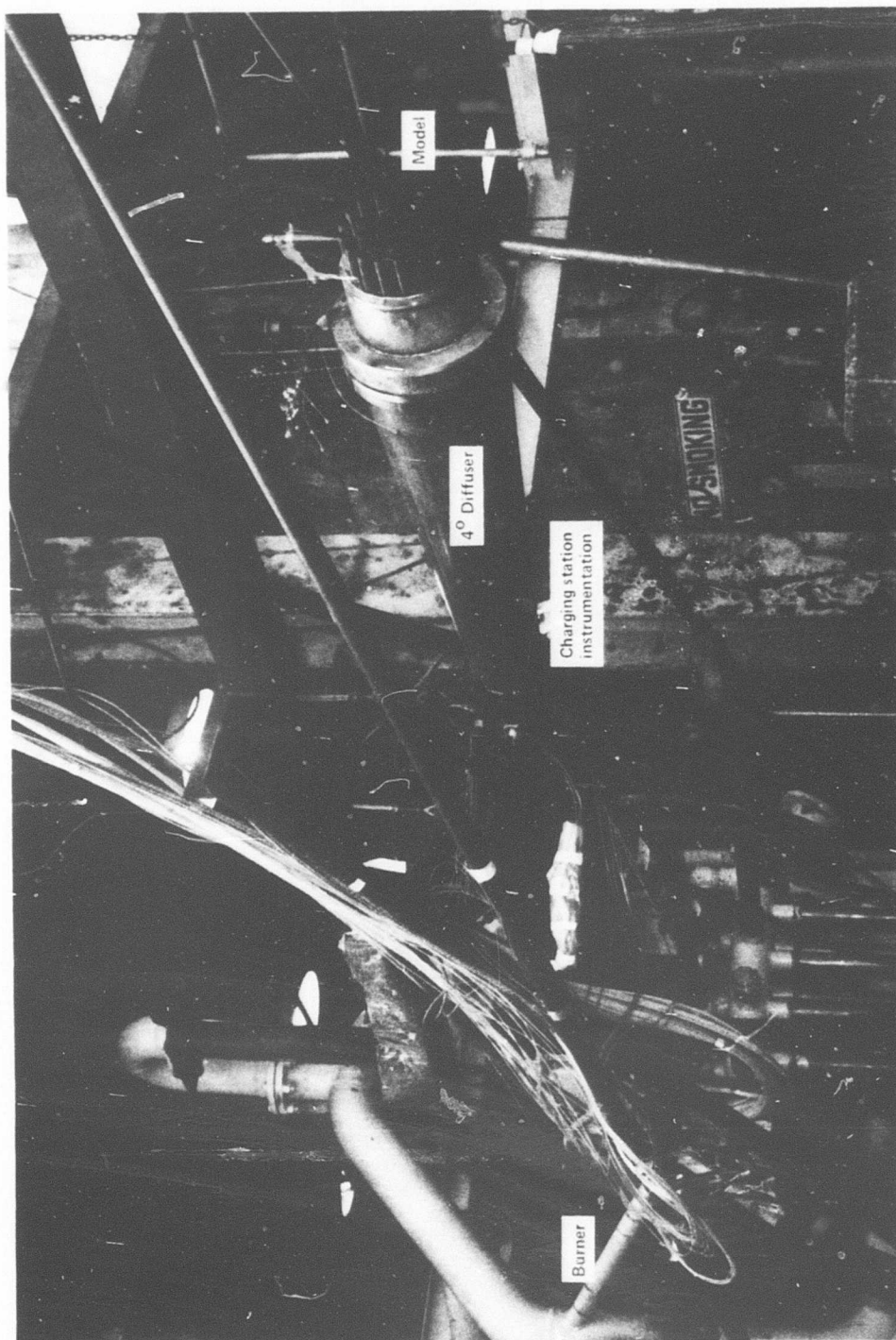
Figure 22.—Boeing Hot Nozzle Test Facility

Material: .035 in. wall, 321 CRES
Tube length—6.0 in. to tube holder plate

A—A
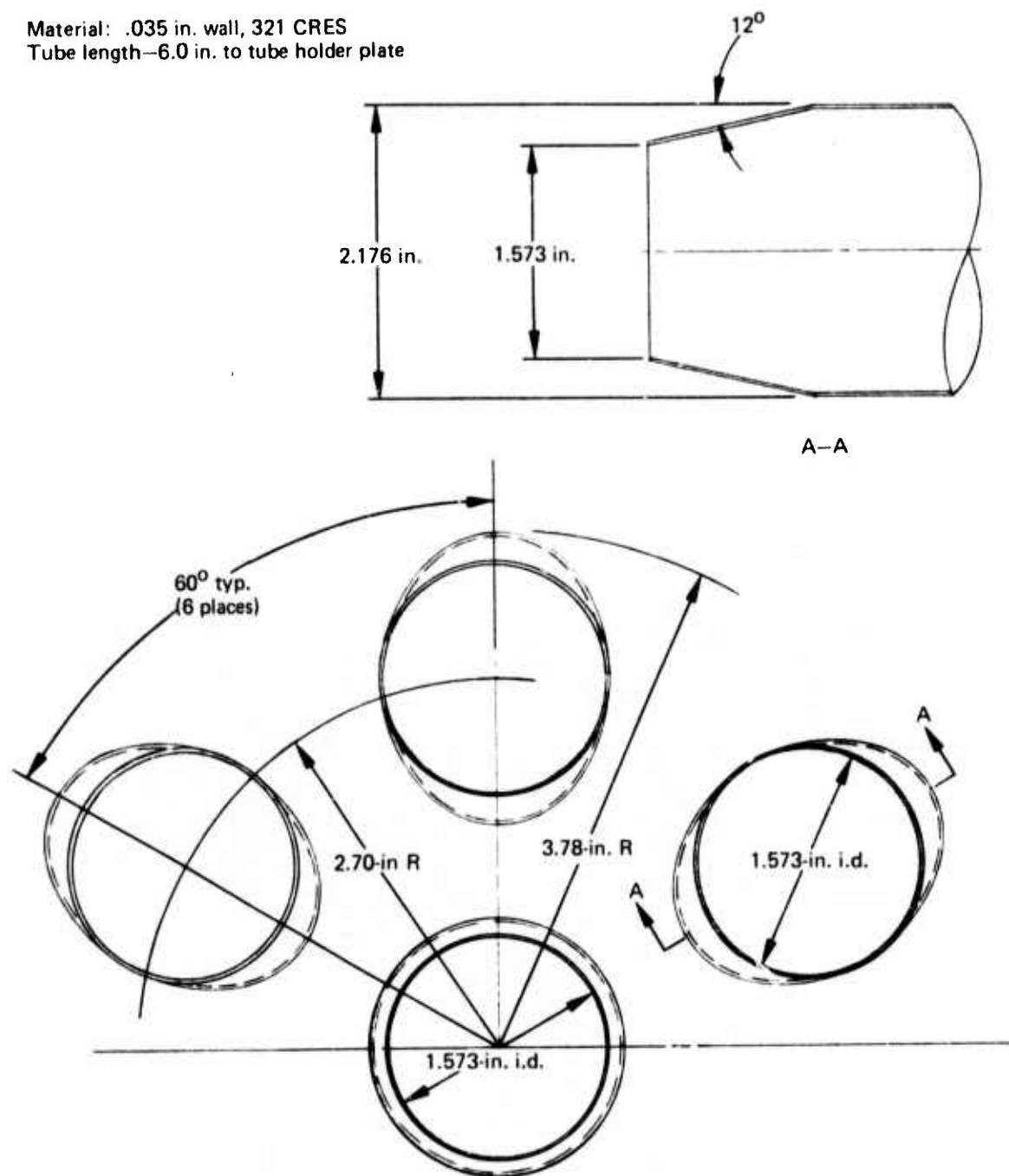
Note: Actual tubes are slightly squared (See figure 26).

Figure 25.—7—Tube Area, Ratio 3.3, Close-Packed Array With Elliptical Tubes (See Note.)
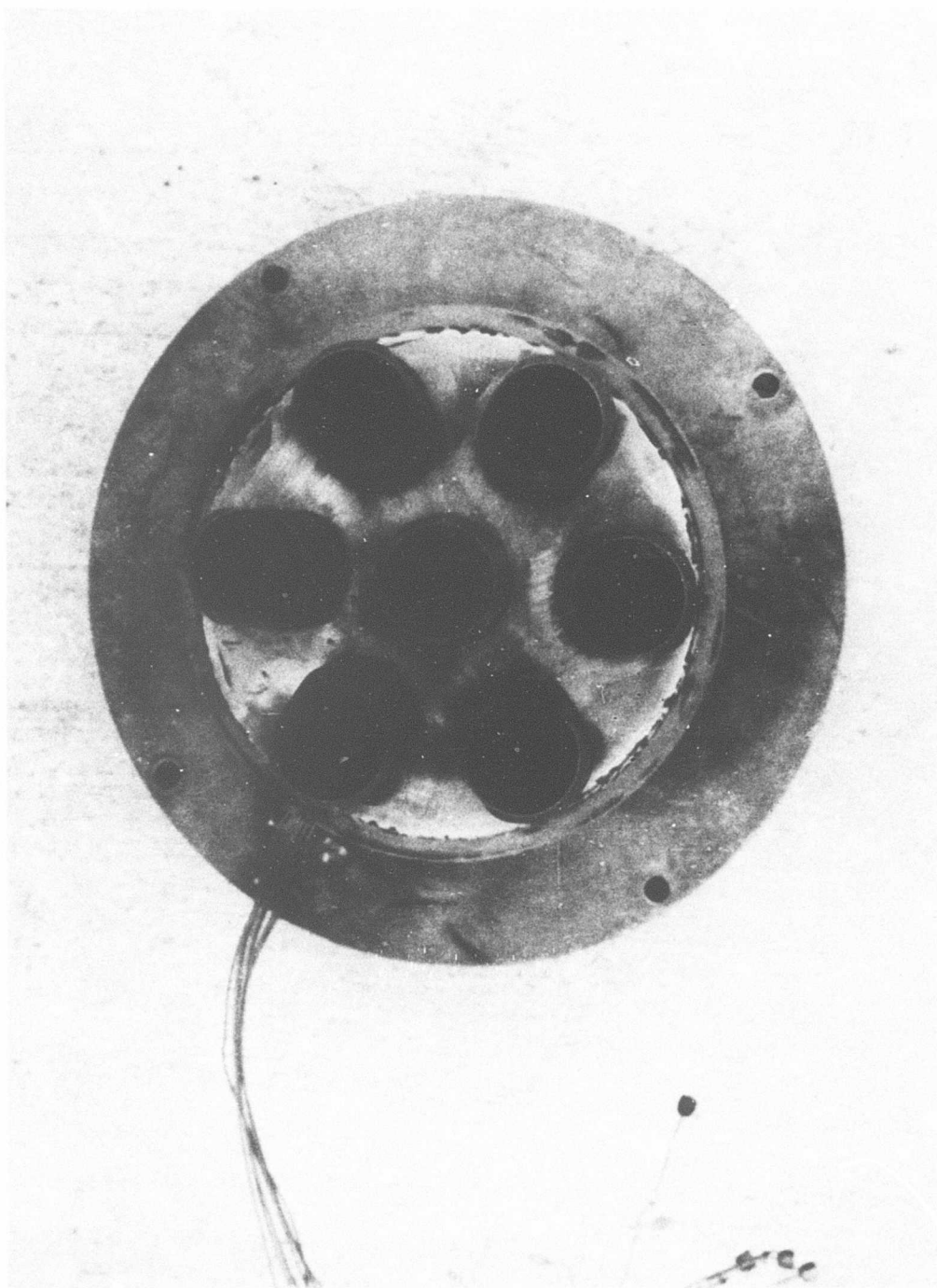
Figure 26.—7-Tube, Area Ratio 3.3 Nozzle

NOTE: Material: 0.035-in. wall, 321 CRES
Center tube is a 1.125-in.-diam tube
with a 12° nom. convergence to
0.955 in. i.d. exit.
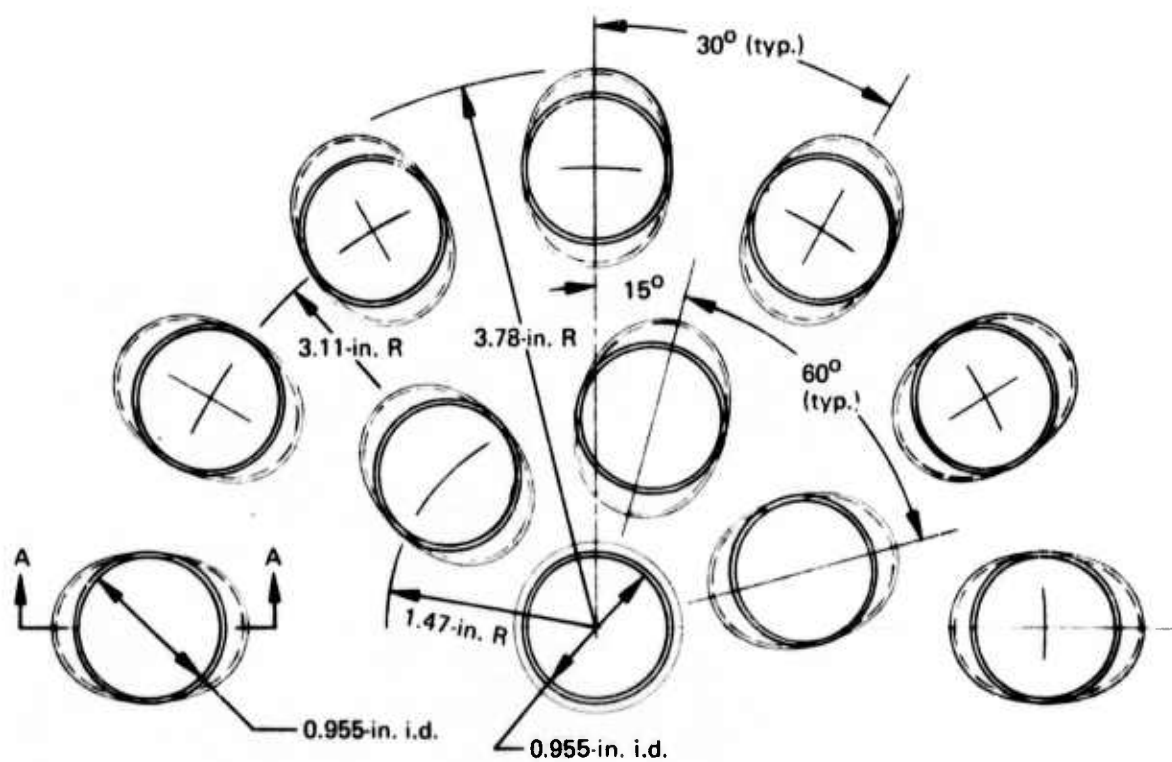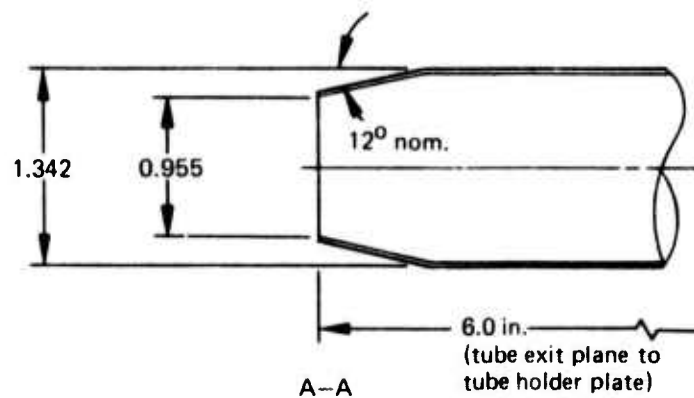
Figure 27.—19-Tube, Area Ratio 3.3, Close-Packed Array With Elliptical Convergent Tubes

67
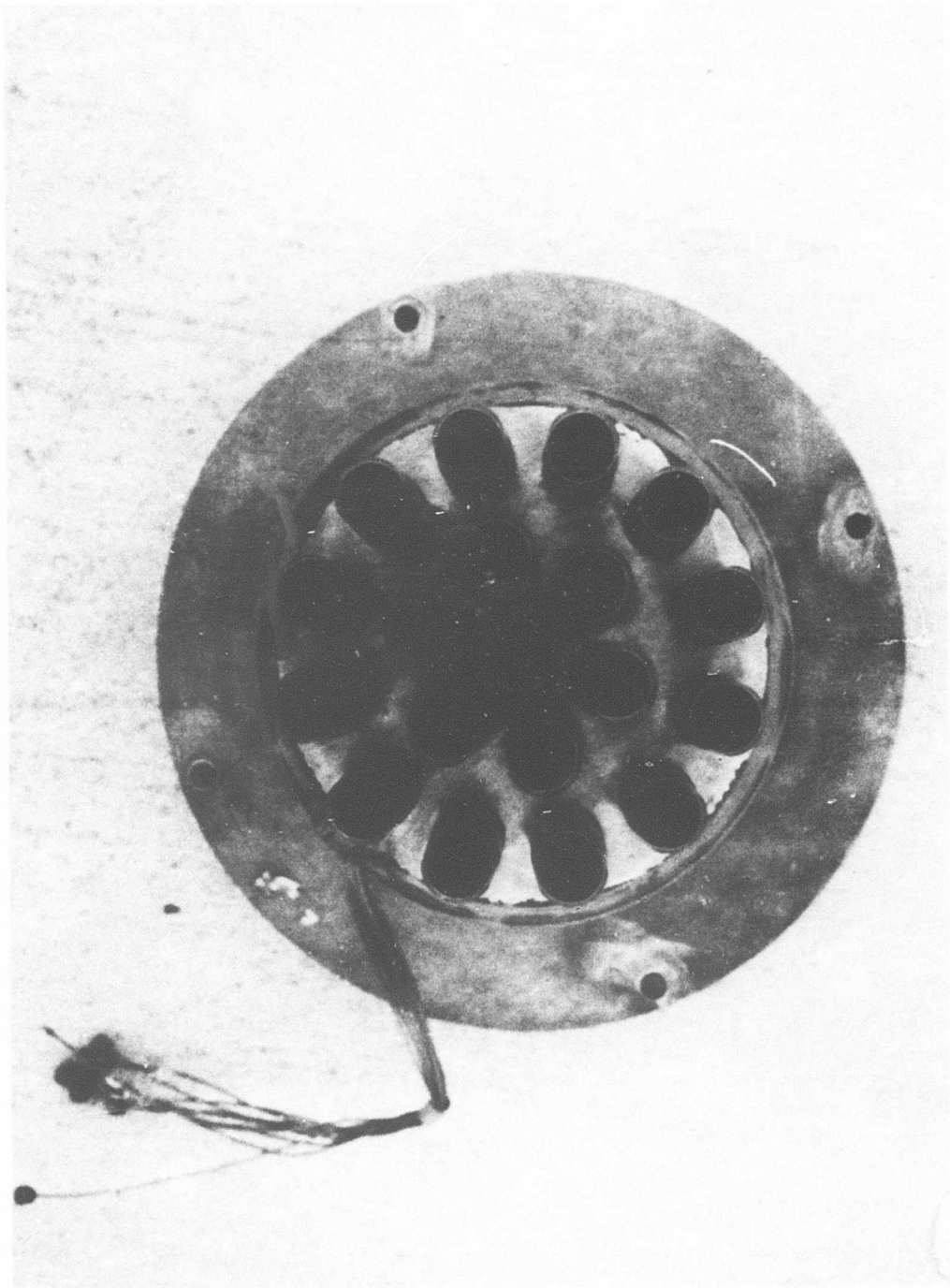
Figure 28.—19-Tube, Area Ratio 3.3, Close-Packed Array With Elliptical Convergent Tubes

No.	Area Ratio	R_1	R_2	R_3	R_{max}
1	3.3	1.058	2.172	3.286	3.78
2	2.75	See fig. 33			
3	4.5	1.268	2.592	5.917	4.41
4	6.0	1.498	3.052	4.607	5.10

NOTE: Center tube is 0.875-in.-diam tube with 12° nom. convergence to 0.684 in. i.d. exit.
Mat'l.—0.035-in. wall, 321 CRES
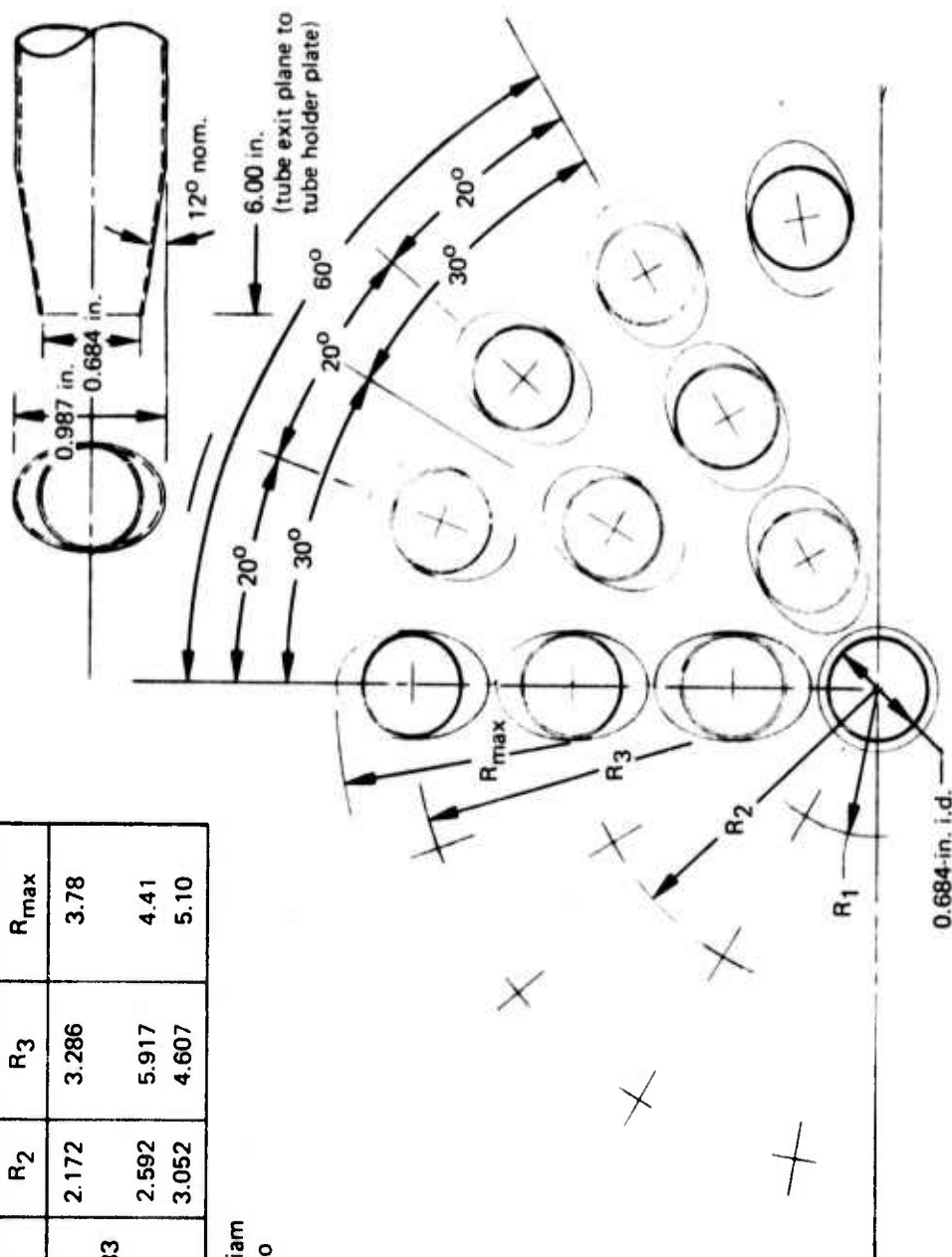
Figure 29.—37-Tube, Area Ratio 3.3, 4.5, 6.0, Close-Packed Array With Elliptical Convergent Tubes.

69
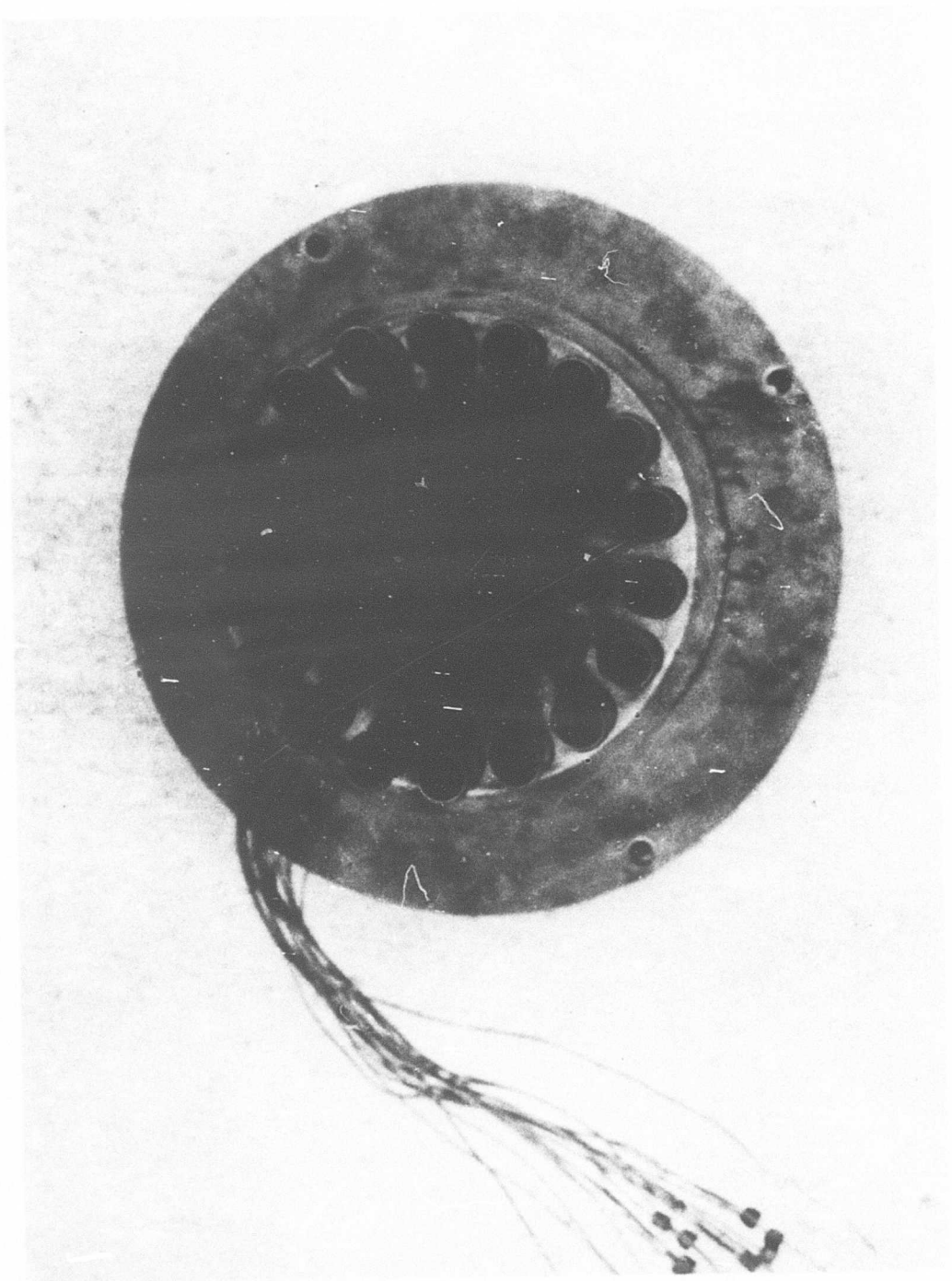
Figure 30. – 37-Tube Area Ratio 3.3 Close-Packed Array With Elliptical Convergent Tubes
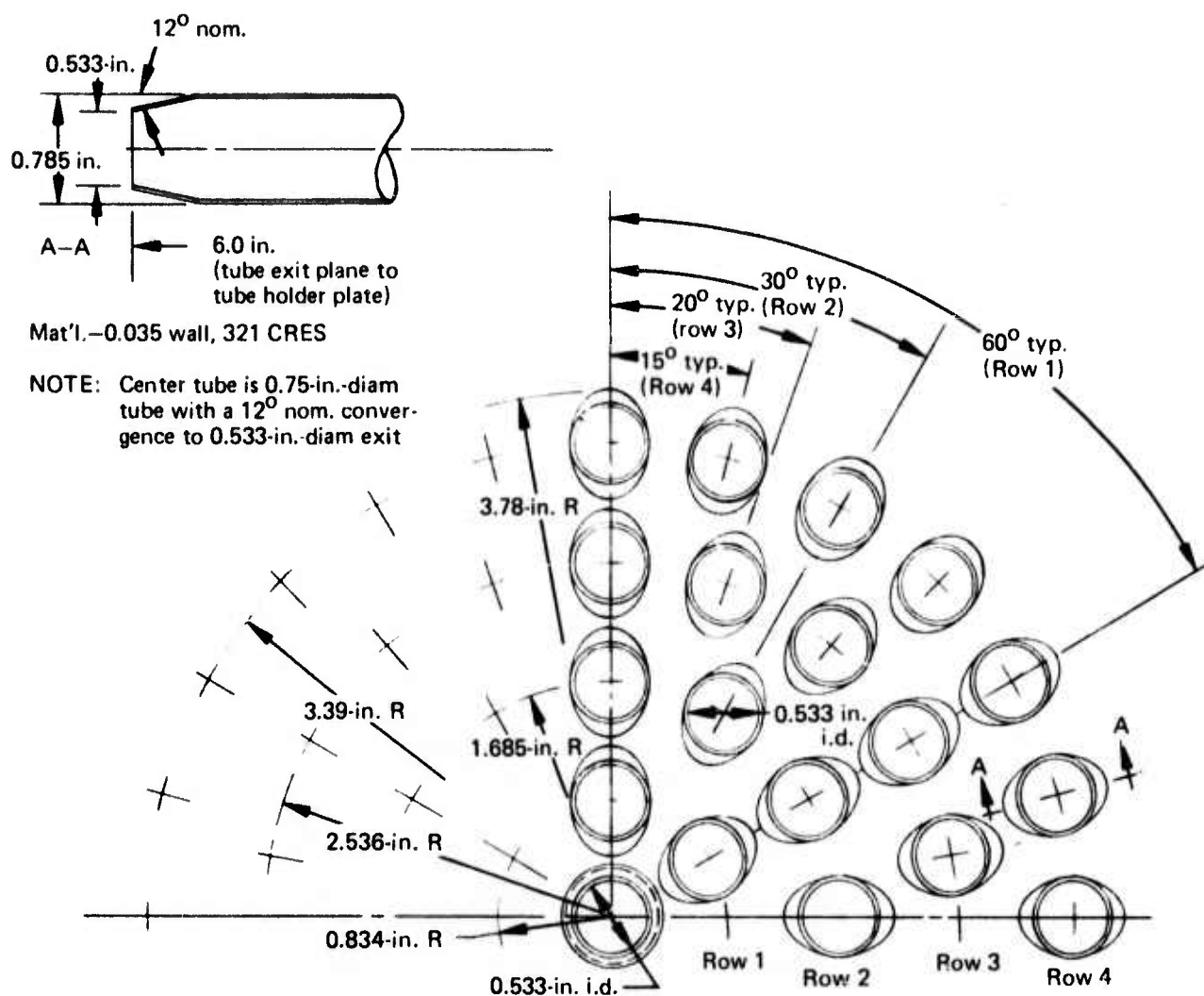
Figure 31.—61—Tube, Area Ratio 3.3 Close-Packed Array With Elliptical Convergent Tubes

71
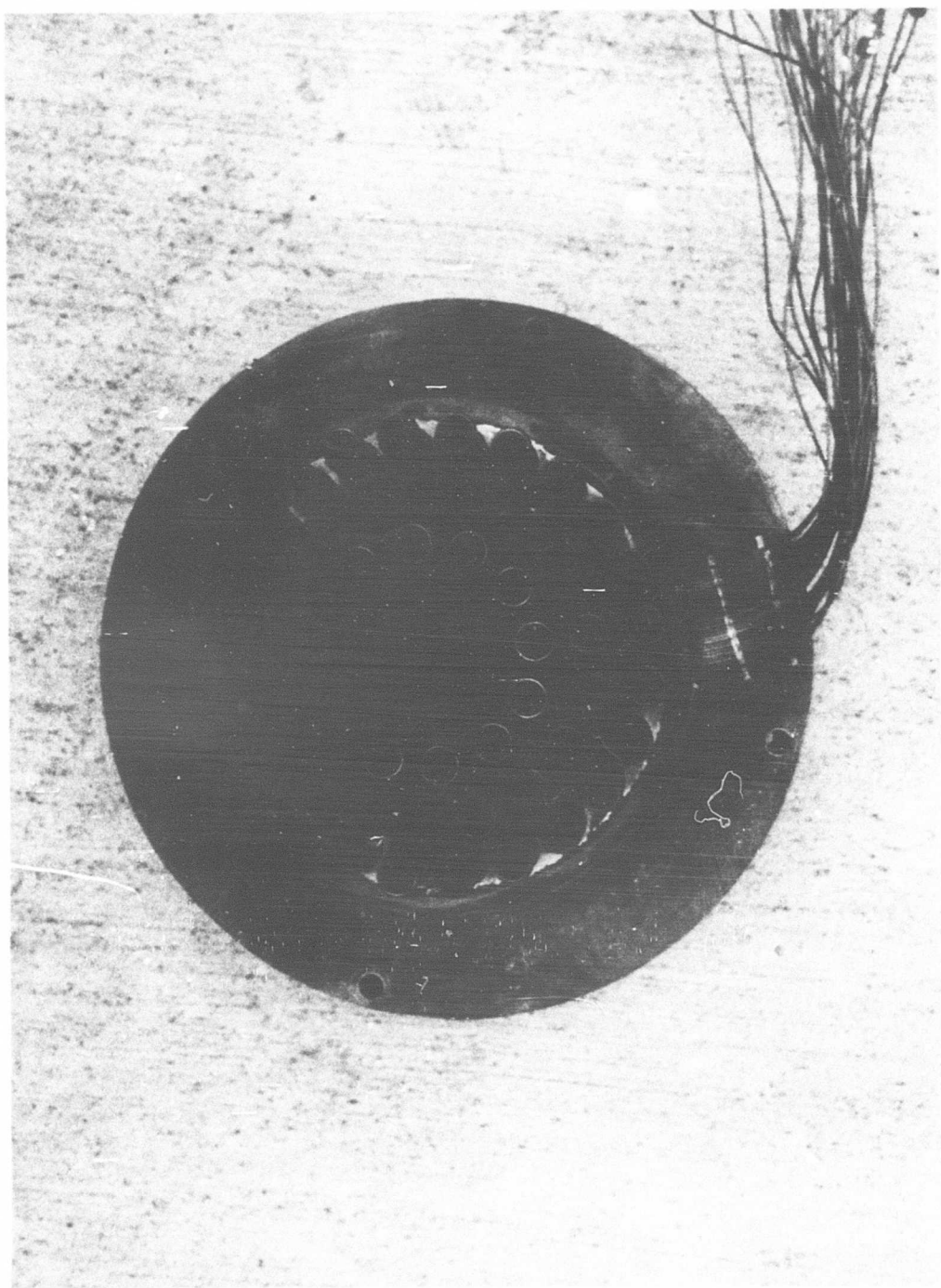
Figure 32.—61-Tube, Area Ratio 3.3, Close-Packed Array With Elliptical Convergent Tubes
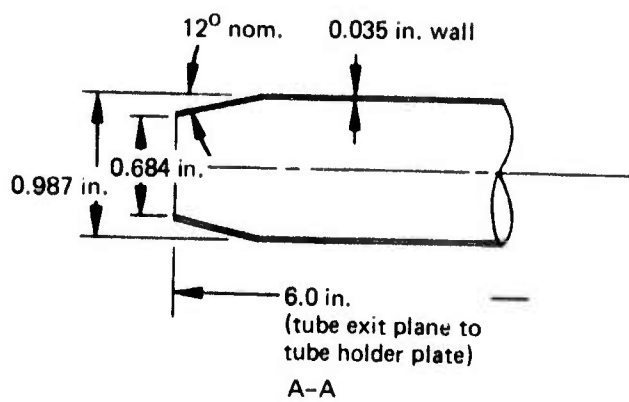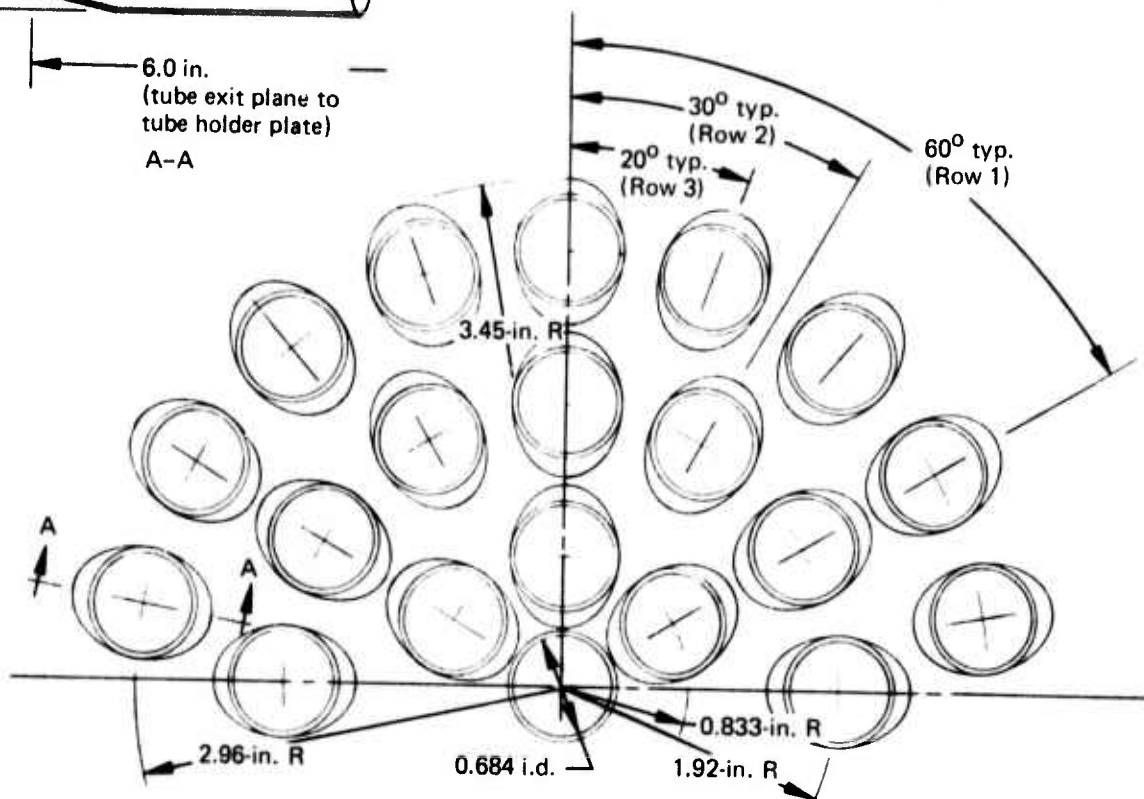
Figure 33.—37-Tube, Area Ratio 2.75, Close-Packed Array With Elliptical Convergent Tubes
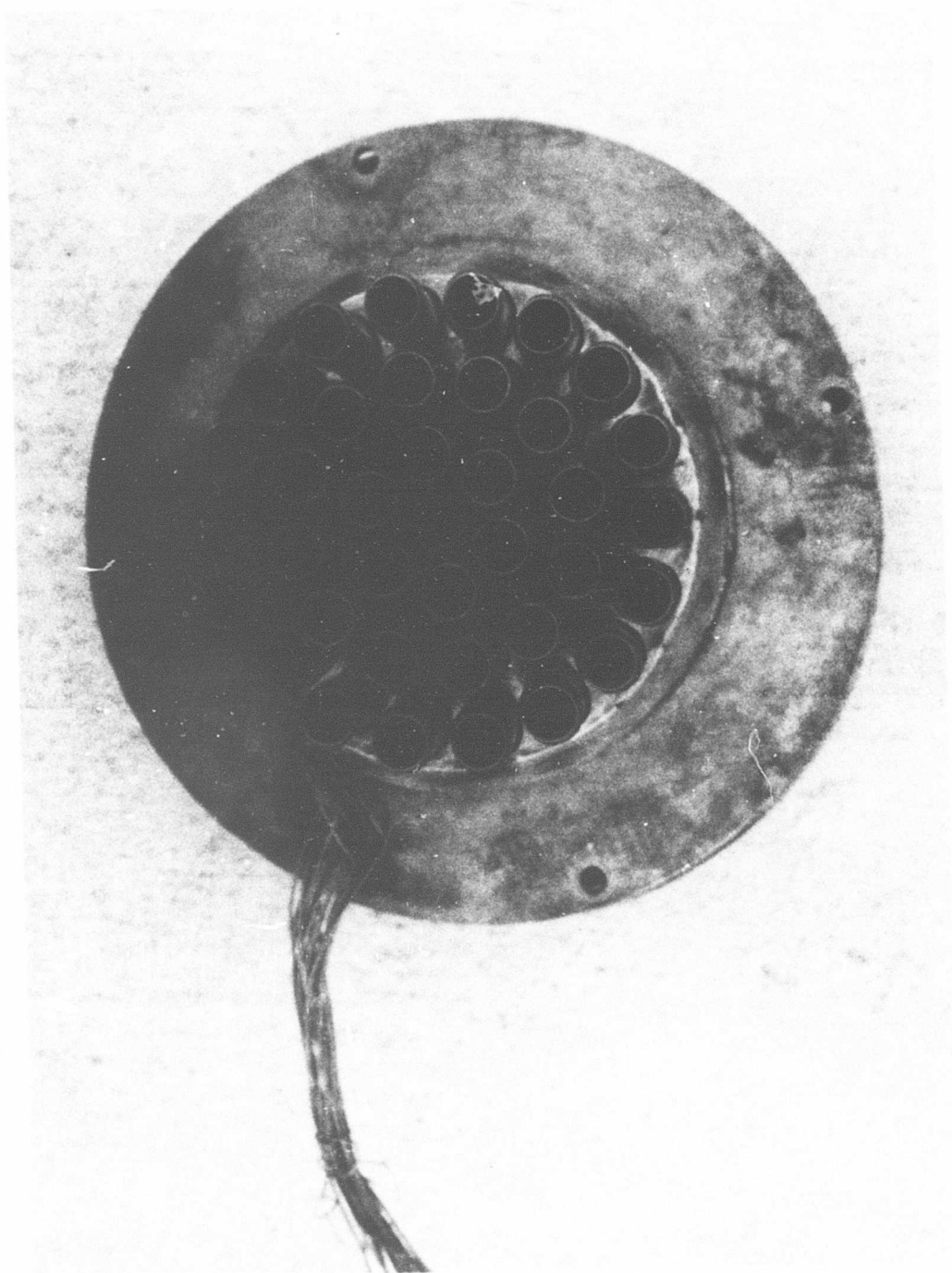
Figure 34.—37-Tube, Area Ratio 2.75, Close-Packed Array With Elliptical Convergent Tubes
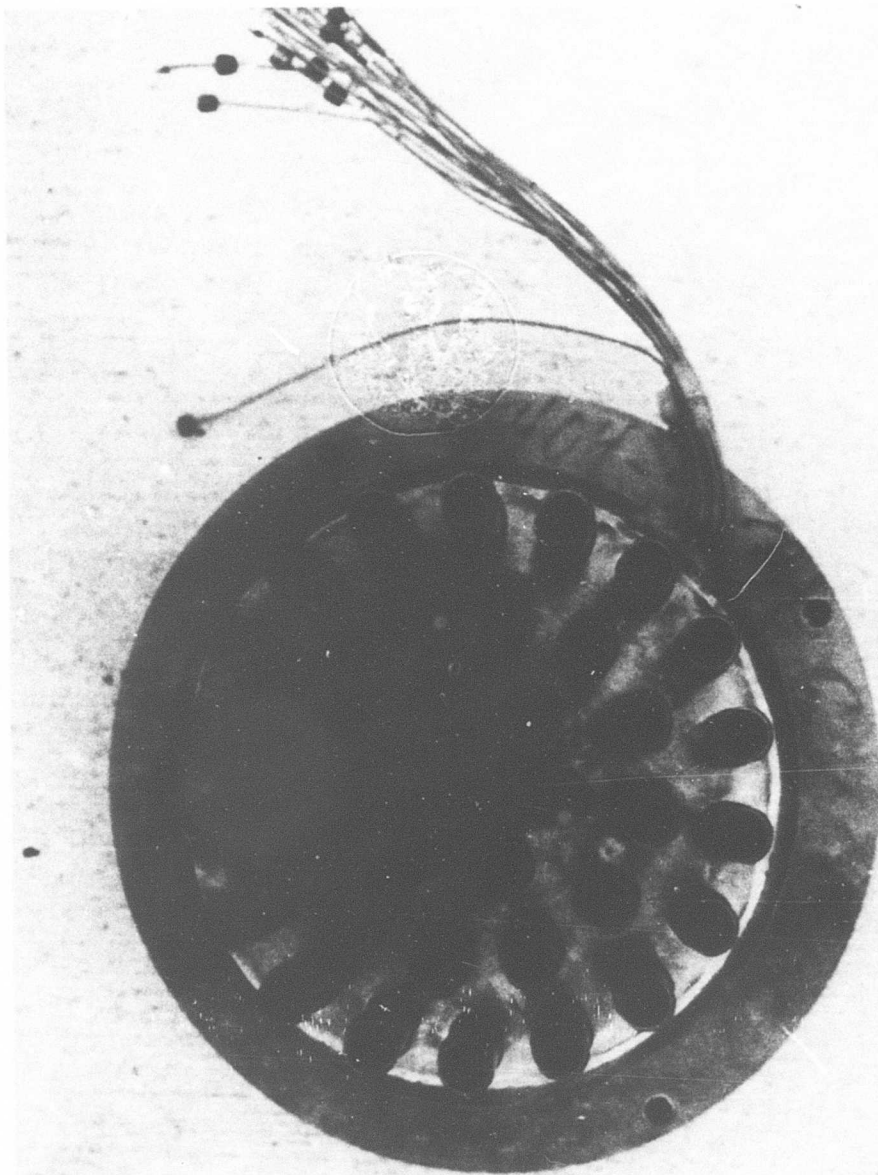
Figure 35.—37-Tube, Area Ratio 4.5, Close-Packed Array With Elliptical Convergent Tubes
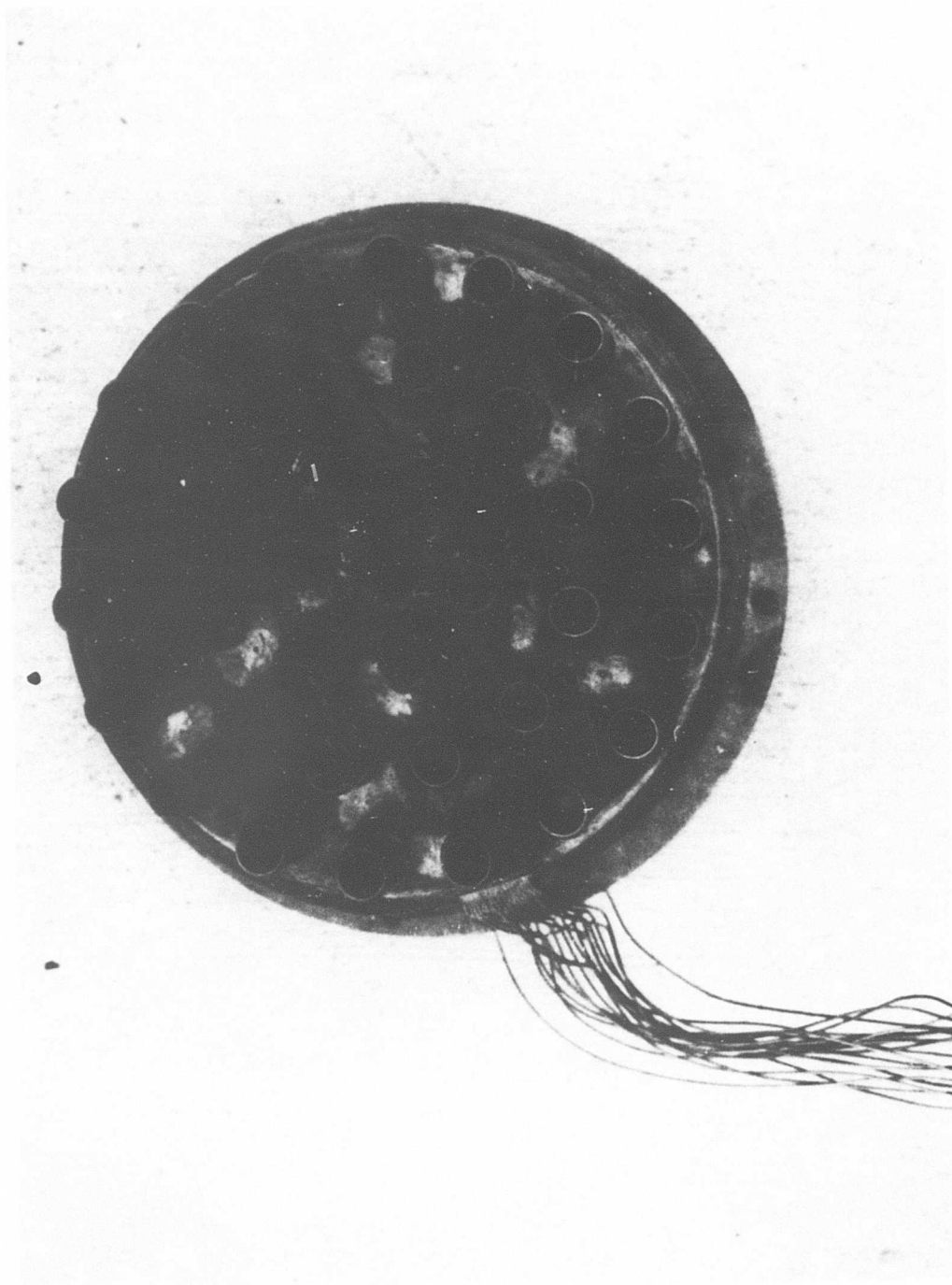
Figure 36.—37-Tube, Area Ratio 6.0, Close-Packed Array With Elliptical Convergent Tubes

37-tube, area ratio 3.3,
close-packed array with
elliptical ramp
(round convergent tubes)

37-tube, area ratio 3.3,
close-packed array with
circular arc ramp
(elliptical convergent tubes)

37-tube, area ratio 3.3,
close-packed array with
elliptical ramp
(elliptical convergent tubes)
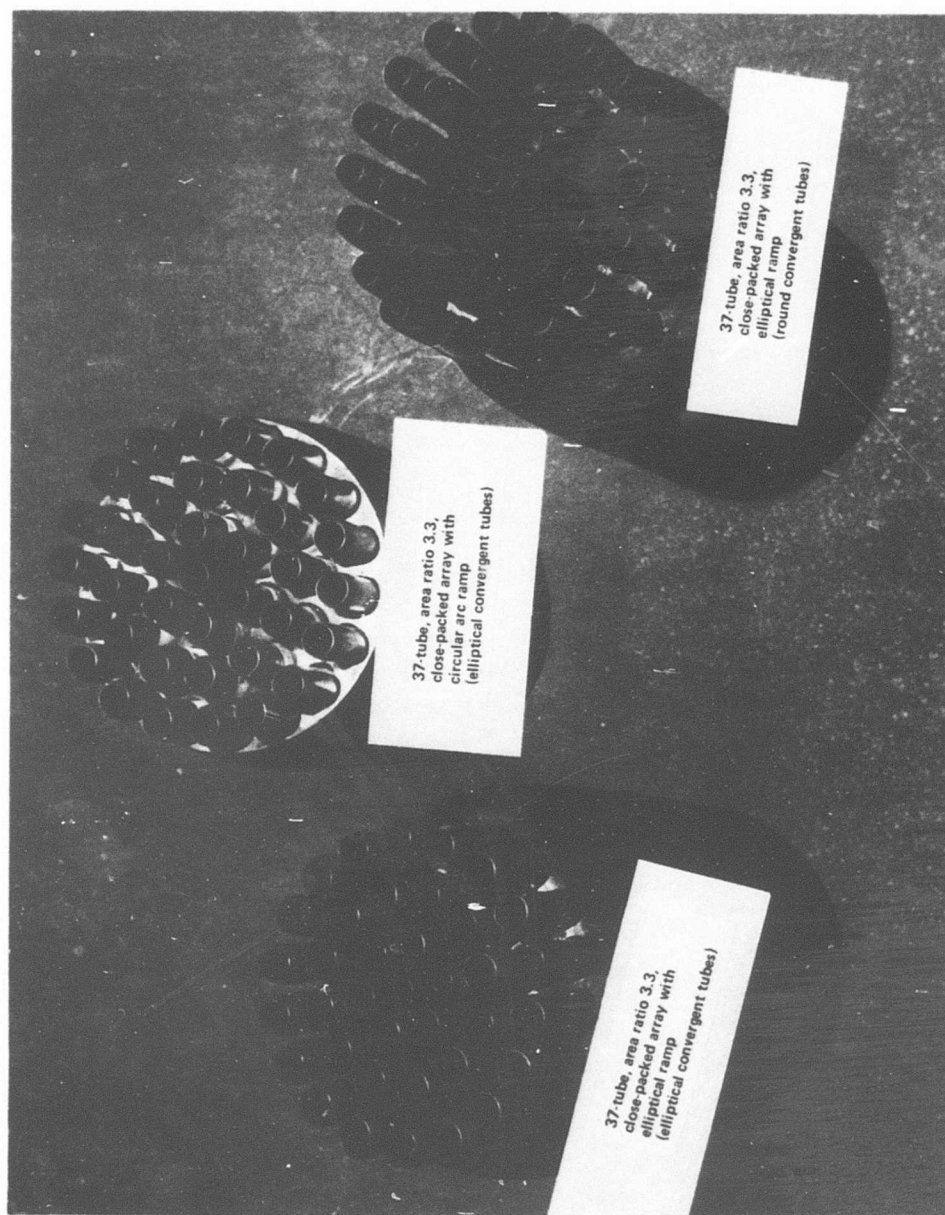
Figure 37.—Comparison of 37-Tube, Area Ratio 3.3 Nozzles

77

Figure 38.—37-Tube, Area Ratio 3.3, Close-Packed Arrays With Various Ramps and Tube Shapes

37-tube, AR-3.3, close-packed array w/elliptical ramp (round convergent tubes)

37-tube, AR 3.3, close-packed array w/circular arc ramp (elliptical tubes)

37-tube, AR-3.3, close-packed array w/elliptical ramp (elliptical tubes)

Material: 0.75-in.-diam, 0.020-wall, 321 CRES tubing (37)

Tube length = 6.0 in. (exit plane to tube holder plate)
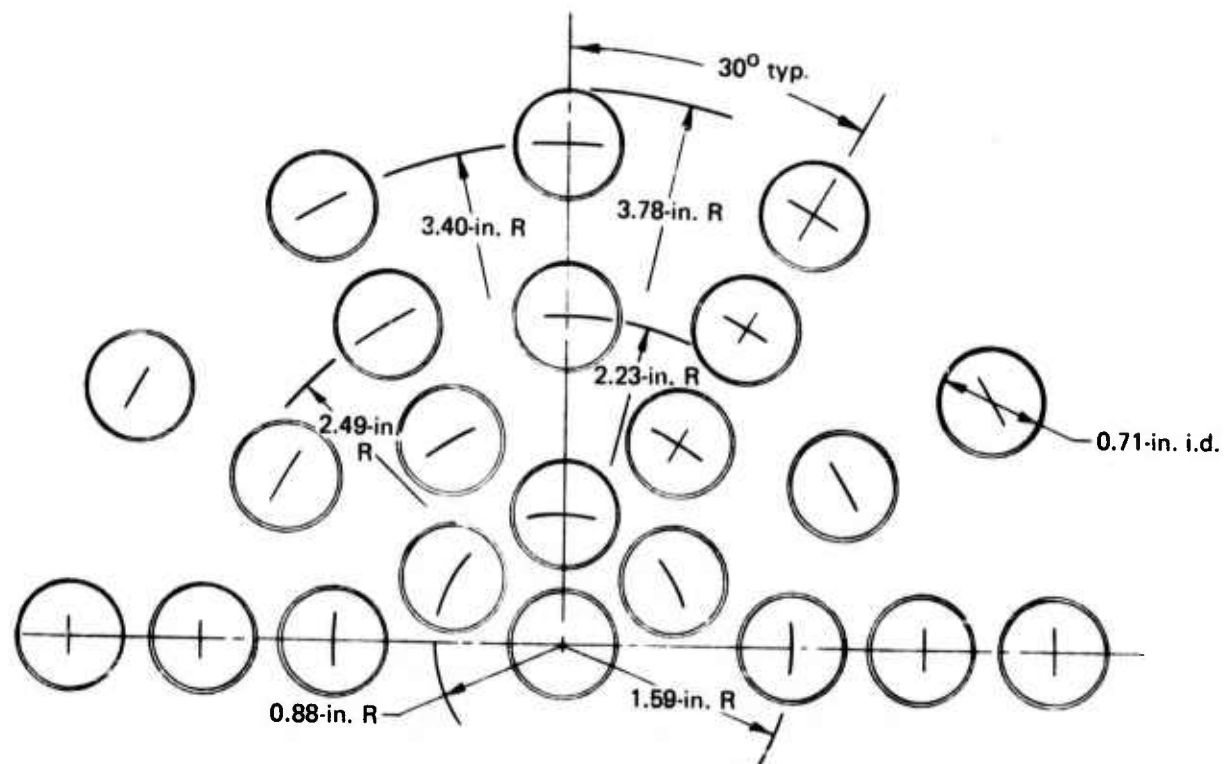
Figure 39.—37-Tube, Area Ratio 3.3, Radial Array With Round Non-Convergent Tubes
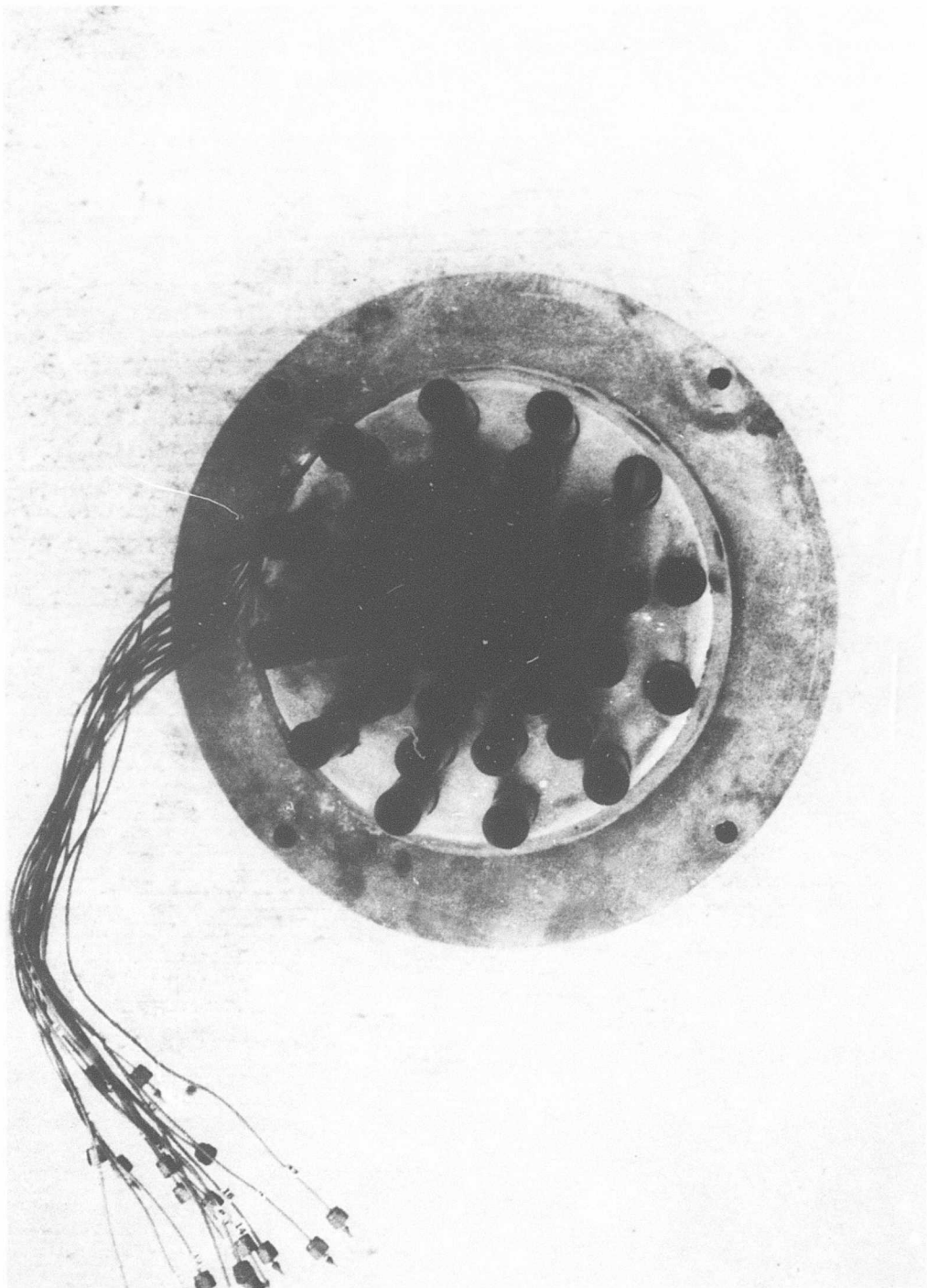
Figure 40.—37-Tube, Area Ratio 3.3, Radial Array With Round Non-Convergent Tubes
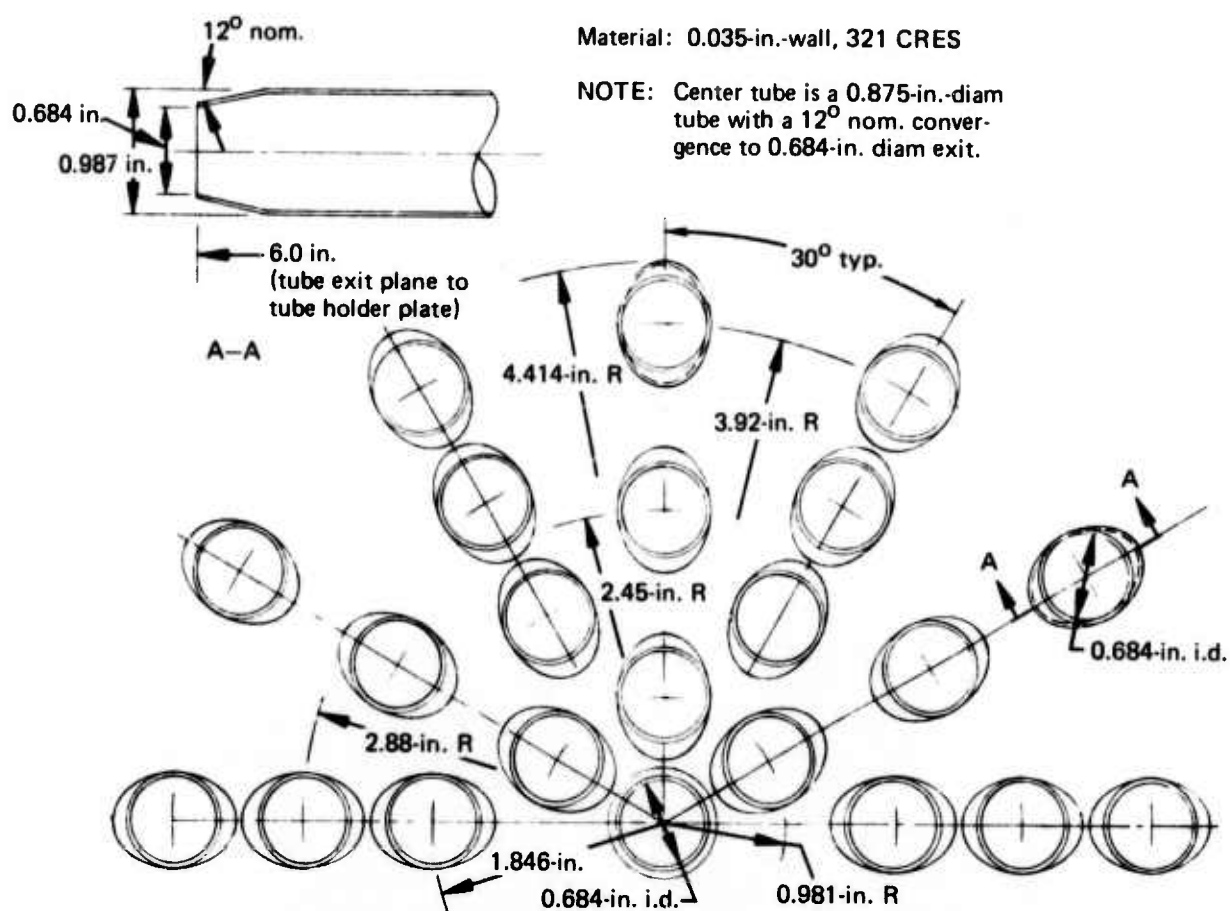
Figure 41.—37-Tube, Area Ratio 4.5, Radial Array With Elliptical Convergent Tubes

81
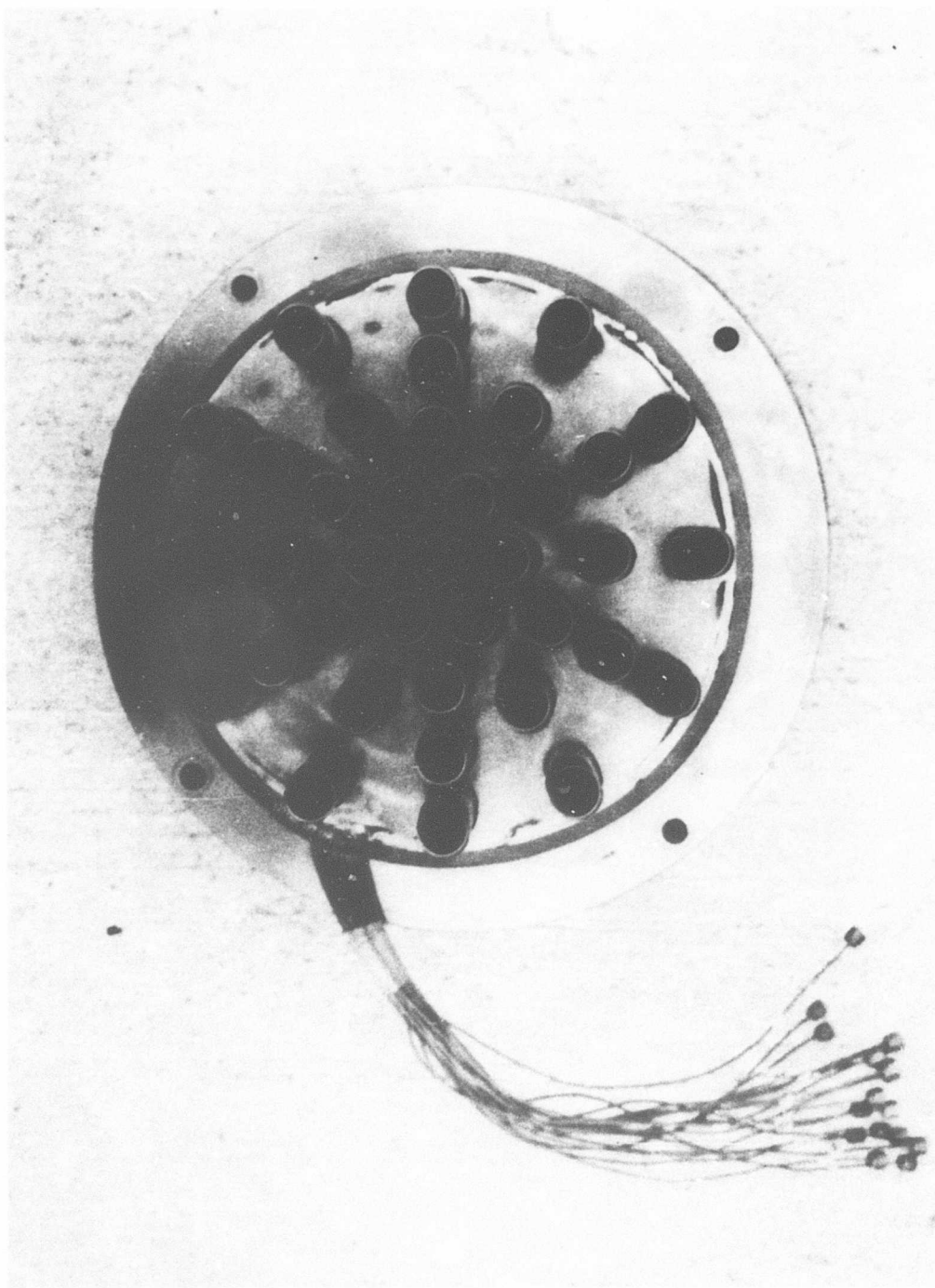
Figure 42.—37-Tube, Area Ratio 4.5, Radial Array With Elliptical Convergent Tubes
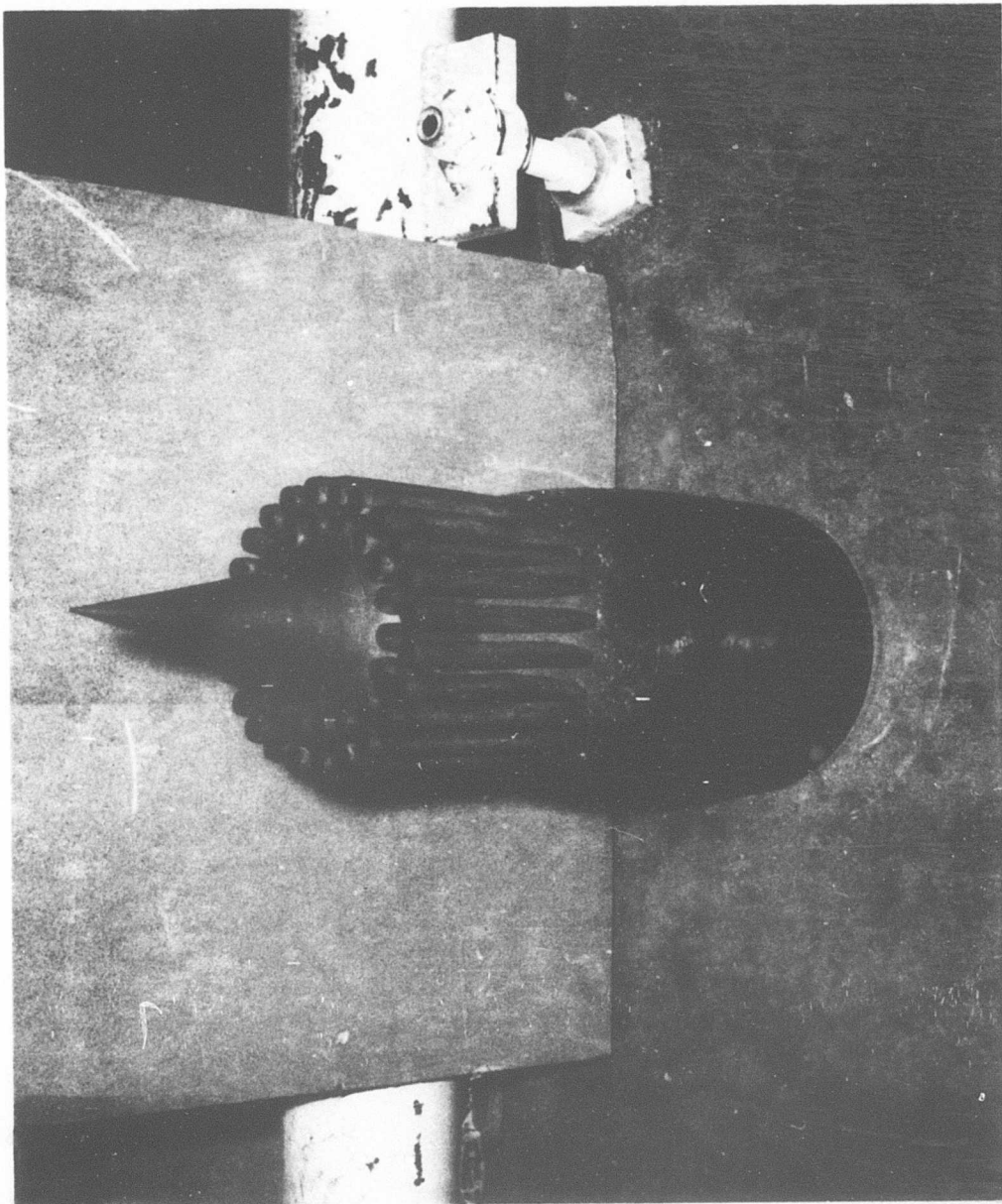
Figure 43.—42-Tube Annular Plug Nozzle
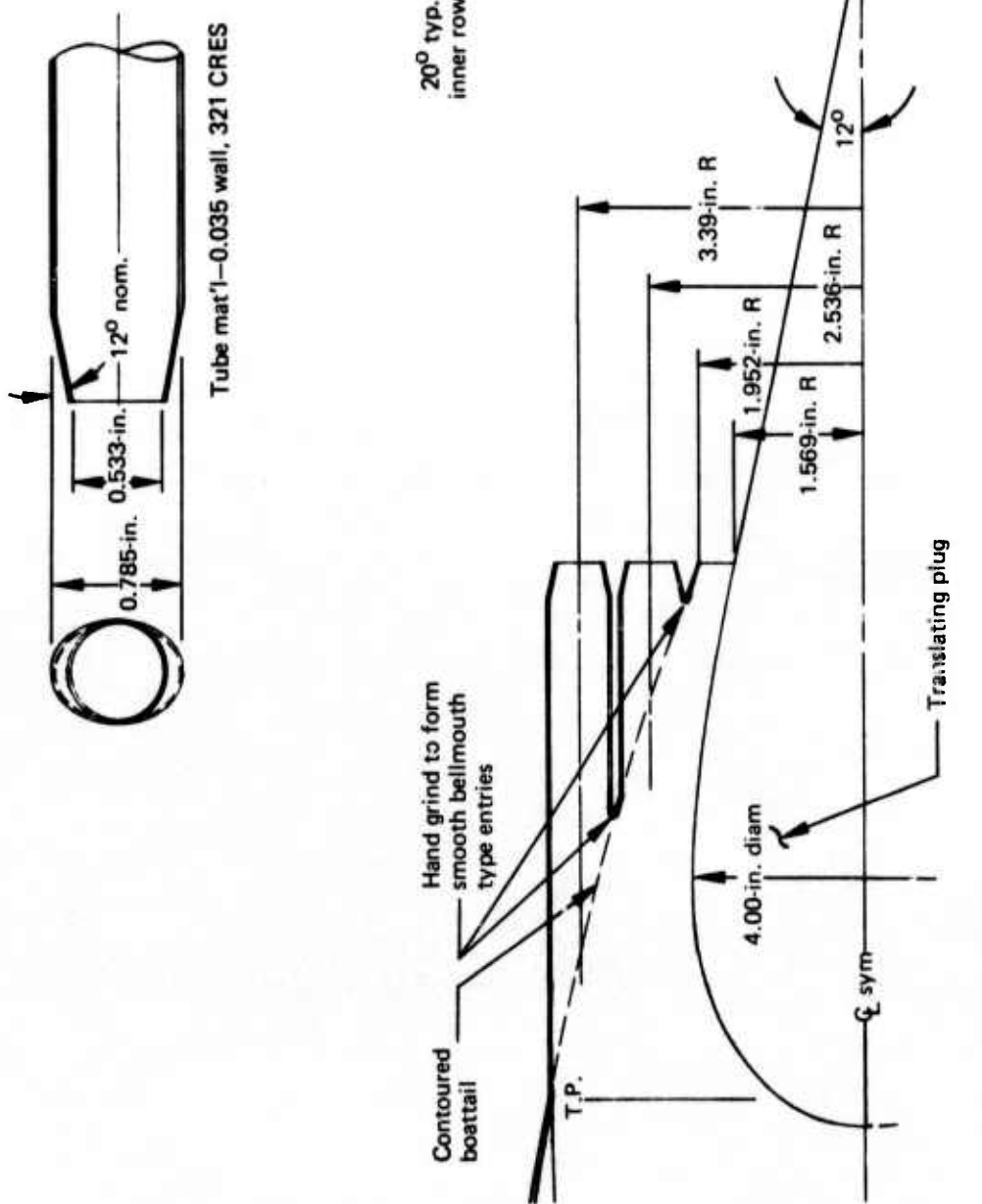
Figure 44.—42-Tube Annular Plug Nozzle

Comparison of 61-Tube Close-Packed
and 42-Tube Close-Packed with Annulus Suppressors

Area ratio = 3.3 $A_p = 13.59 \text{ in}^2$

42 tubes
with annulus   61 tubes

0.383 in.

12° Conical plug
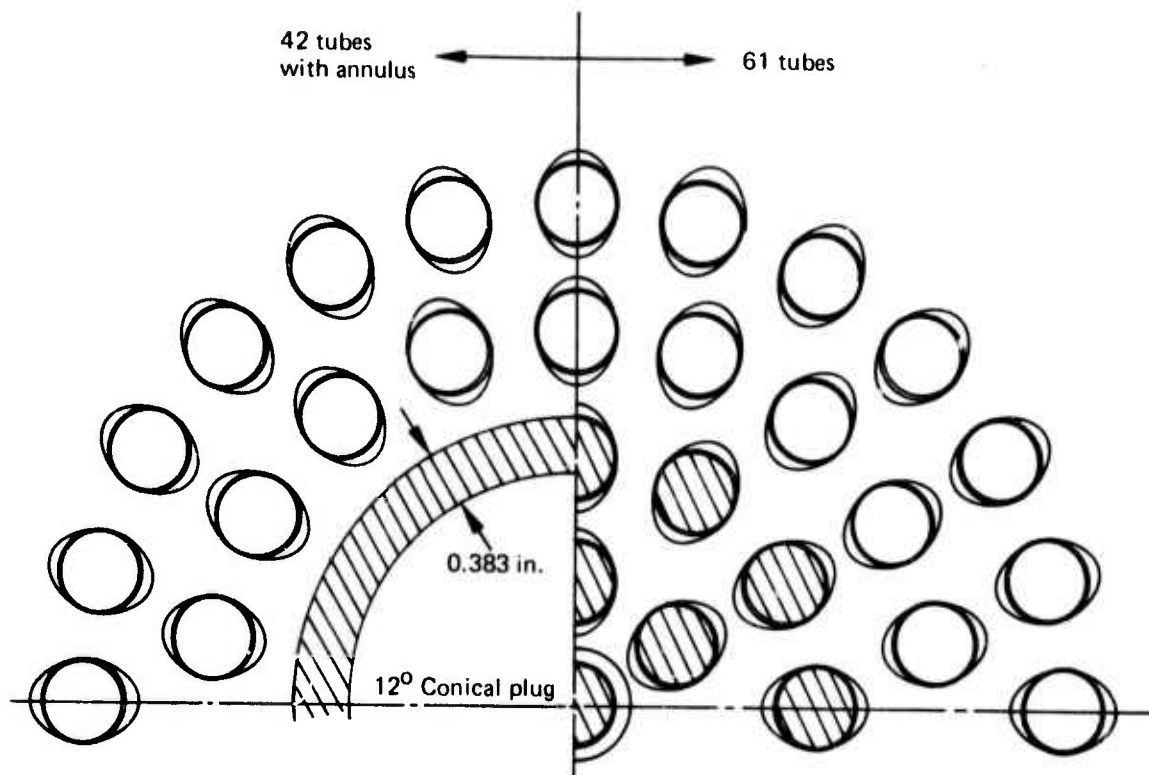
Figure 45.—Comparison: 61-Tube (AR-3.3) Suppressor and 42-Tube Annular Plug
         Nozzle (AR-3.3)
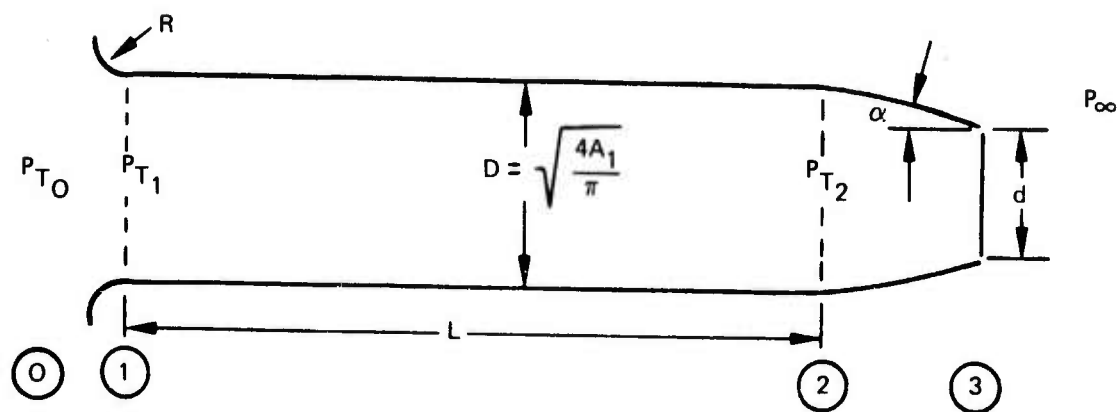
Figure 46.—Schematic of Single Tube
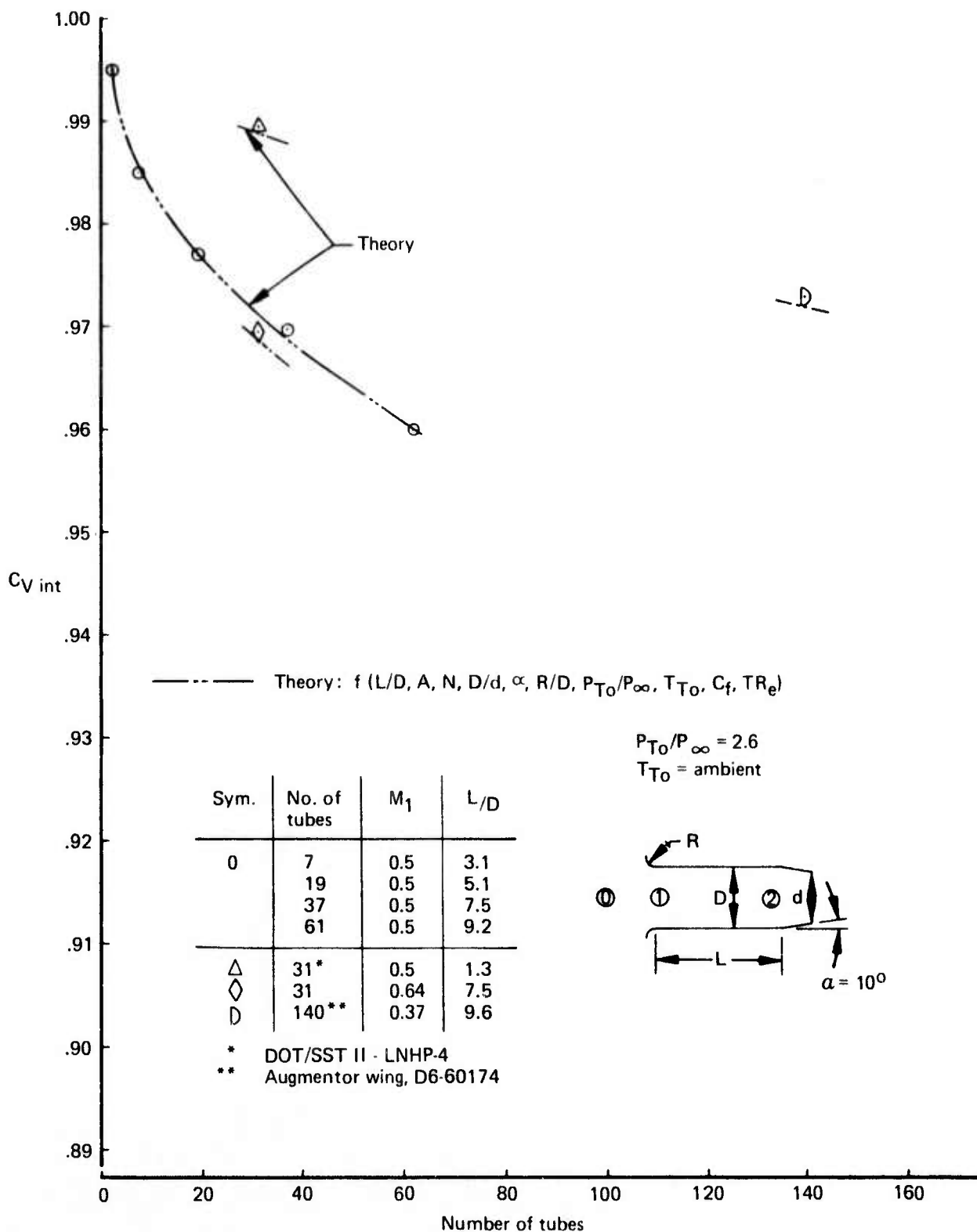
Figure 47.—Internal Velocity Coefficient For Various Tubular Convergent Nozzles--Comparison of Data and Theory
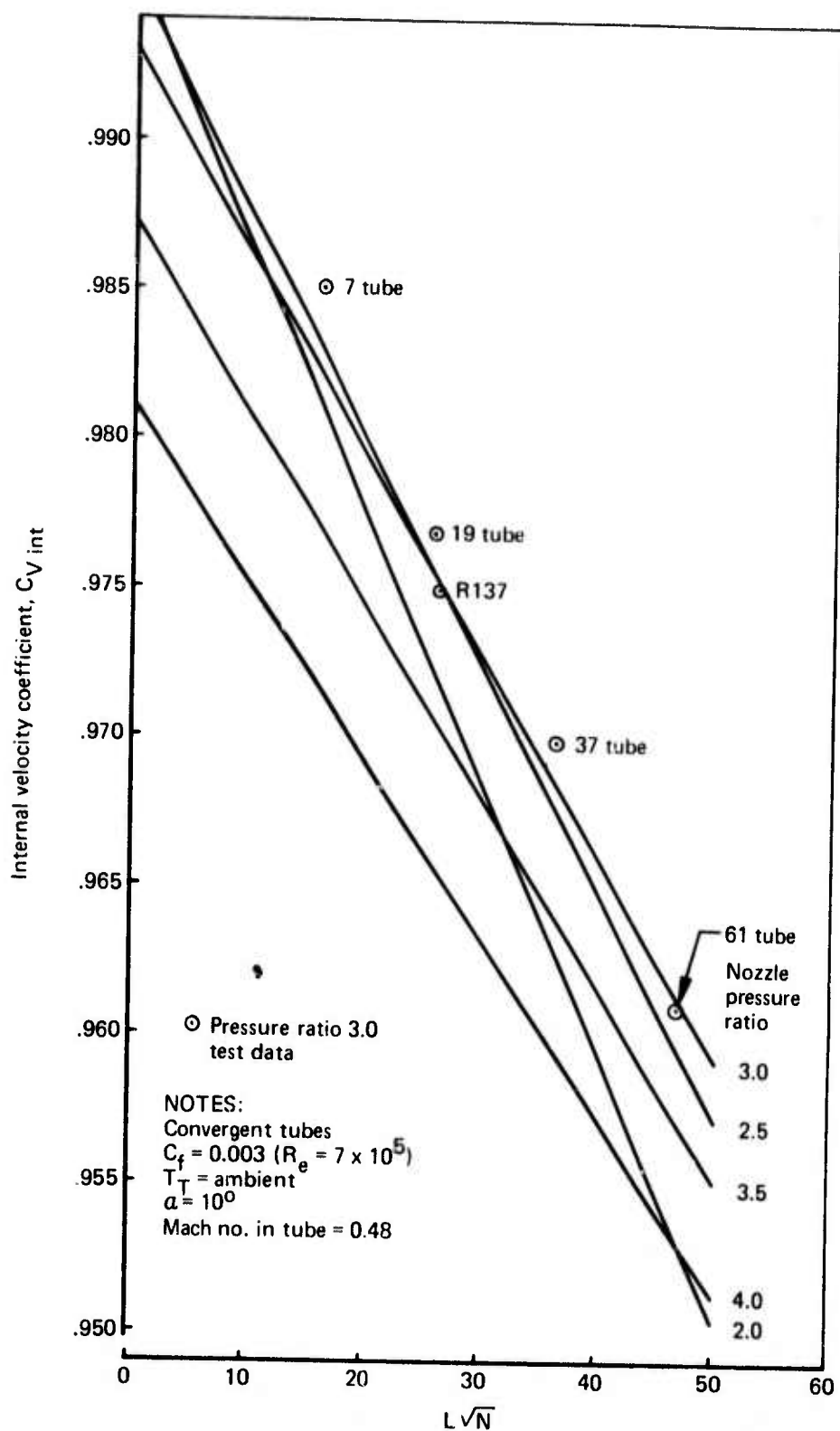
Figure 48.—$C_{V\ int}$ as a Function of Tube Length, Tube Number, and Pressure Ratio
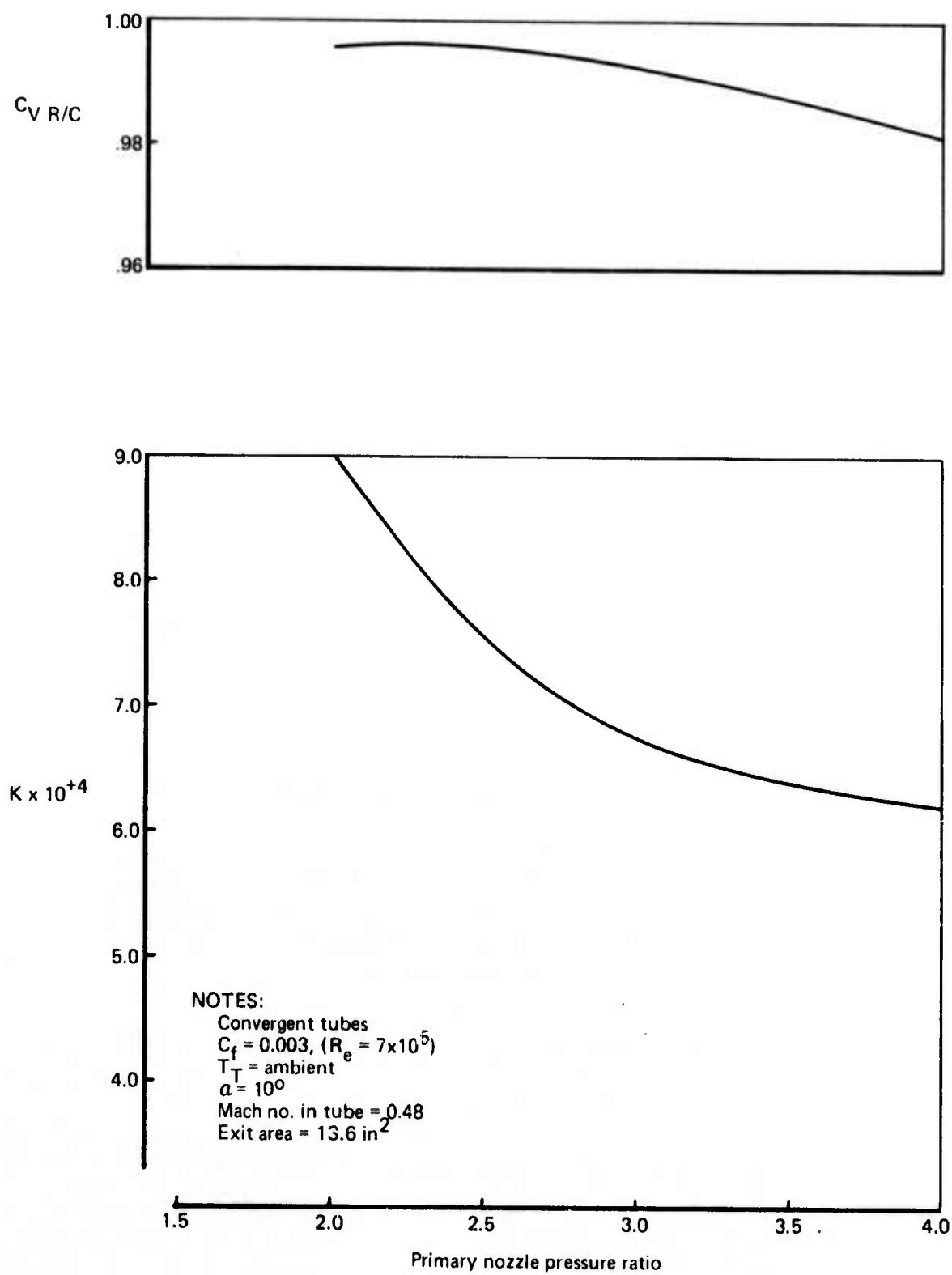
Figure 49.—Parameters in Performance Equation $C_{V \, int} = C_{V \, R/C} - K \, L \sqrt{N}$

NOTES:
  Convergent tubes
  $C_f = 0.003$, $(R_e = 7 \times 10^5)$
  T_T = ambient
  $a = 10^o$
  Mach no. in tube = 0.48
  Exit area = 13.6 in^2
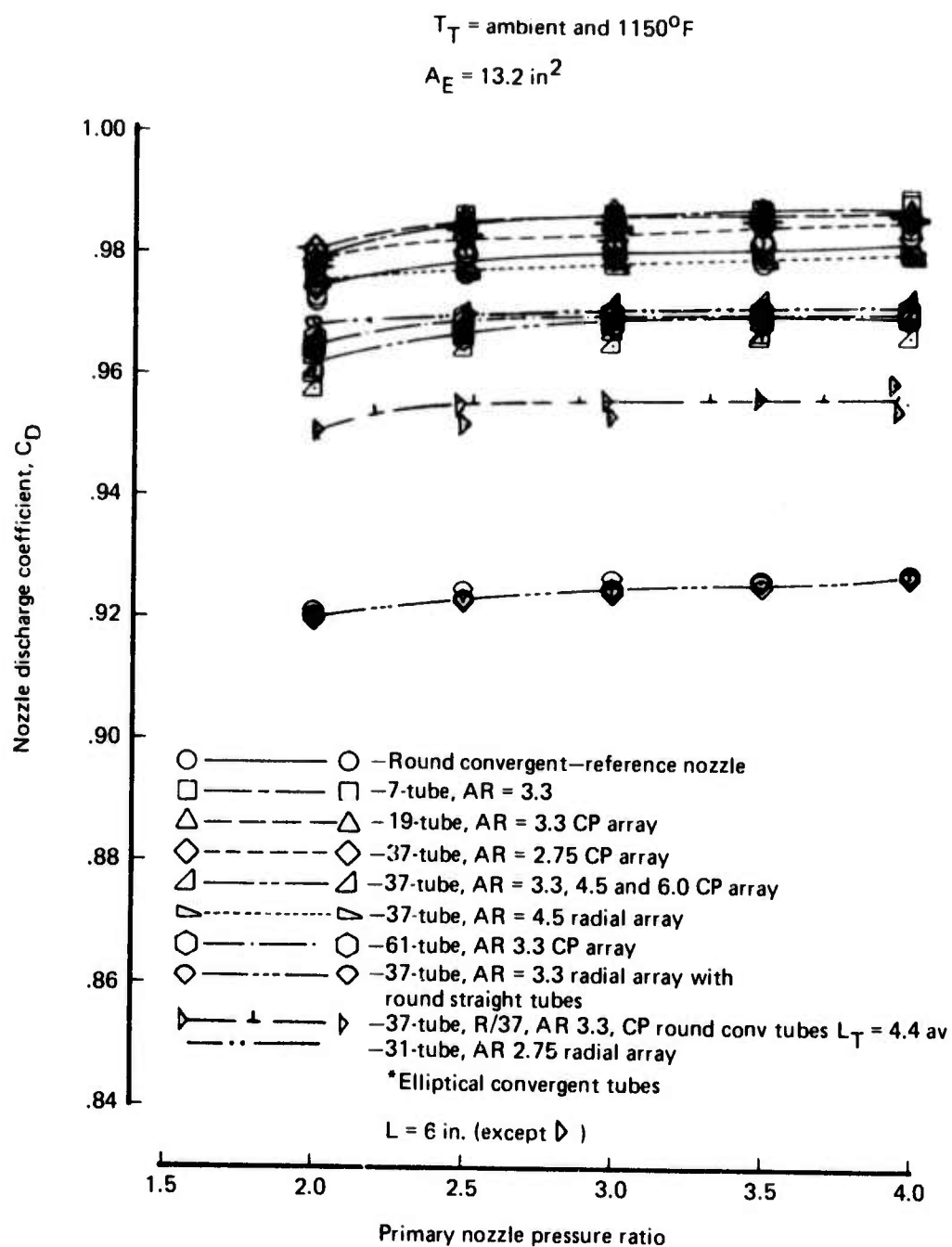
Figure 50.—Discharge Coefficients Ambient and 1150°F
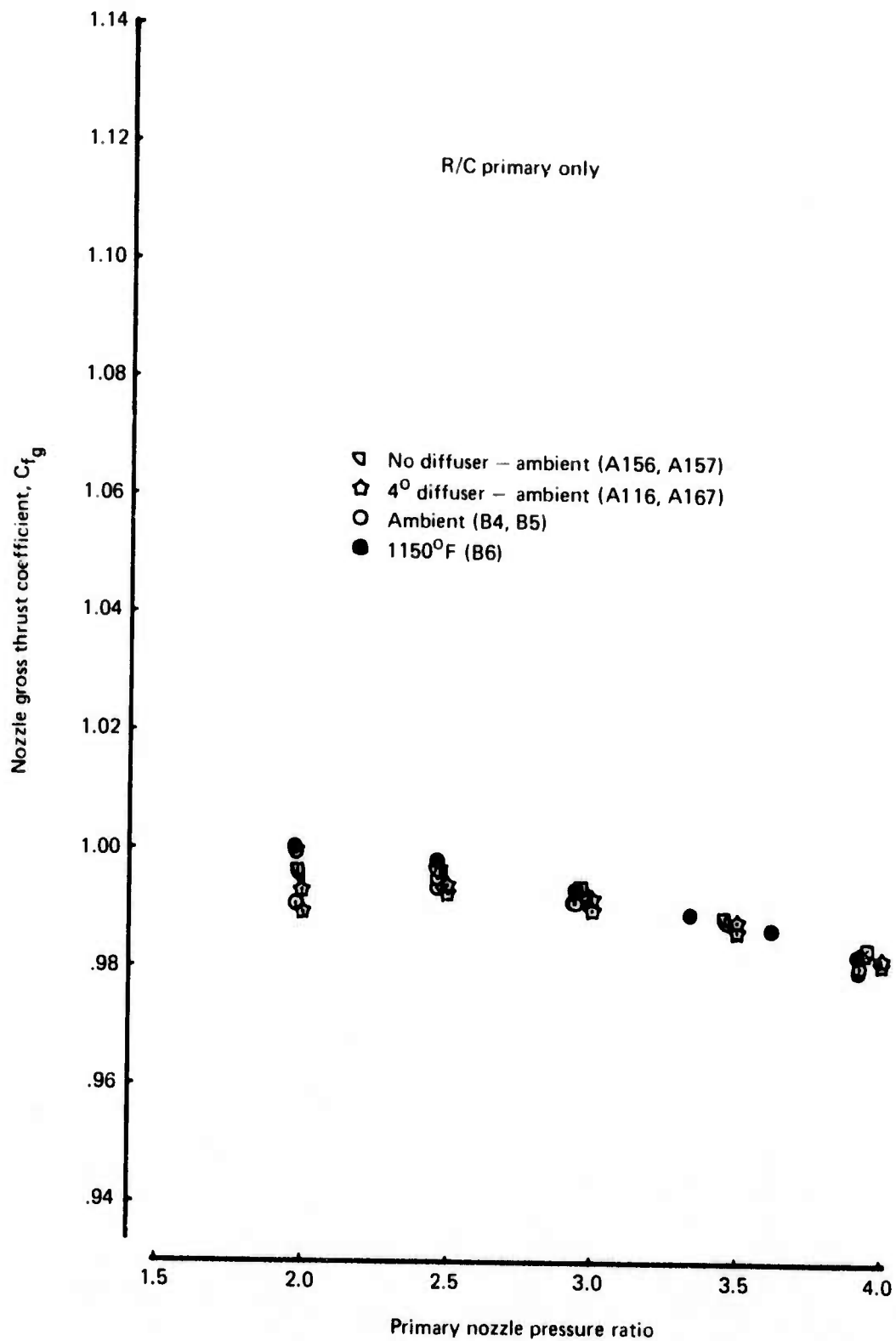
Figure 51.—Gross Thrust Coefficient Versus Pressure Ratio for R/C Nozzle
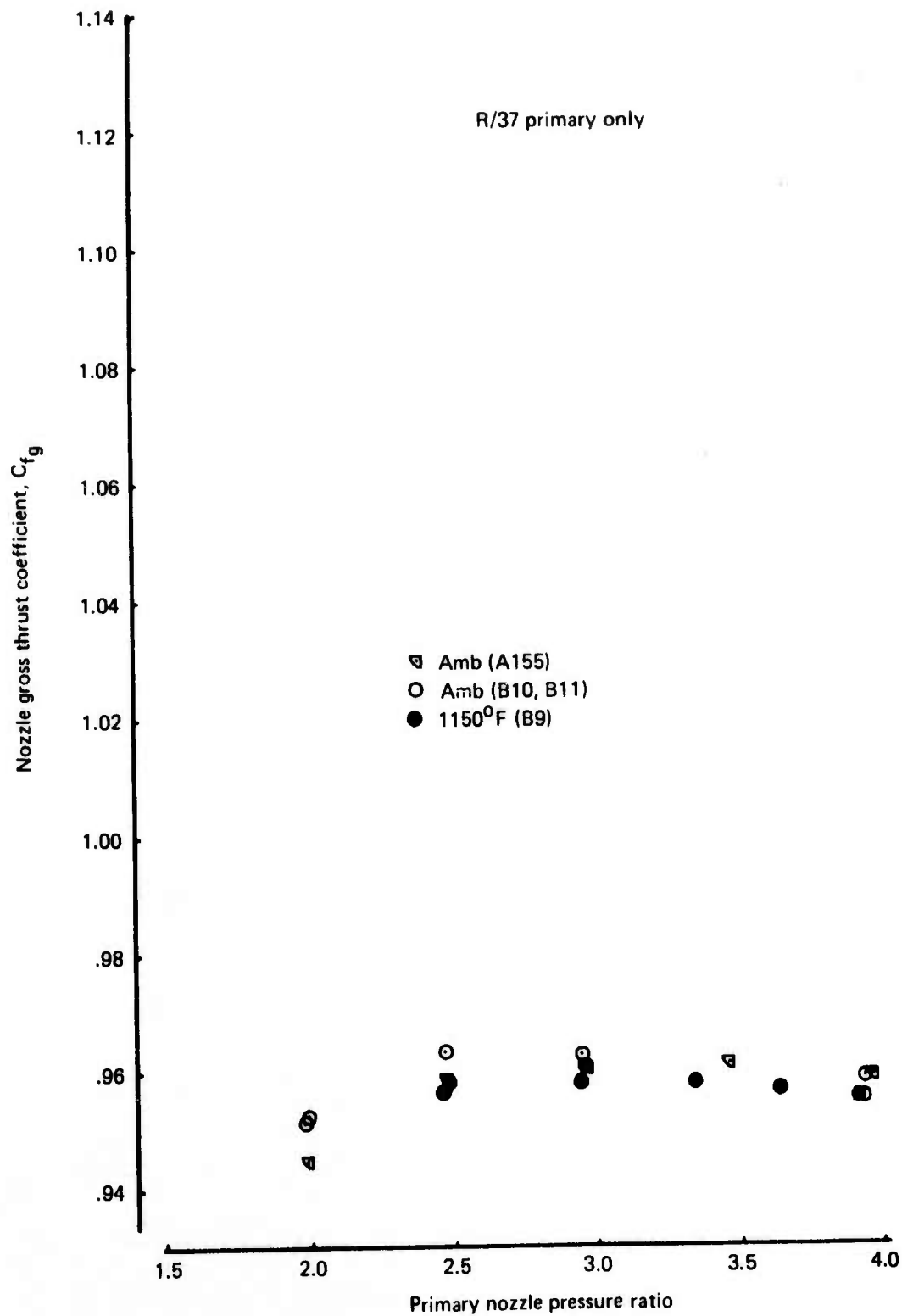
Figure 52.—Gross Thrust Coefficient Versus Pressure Ratio for R/37 Nozzle
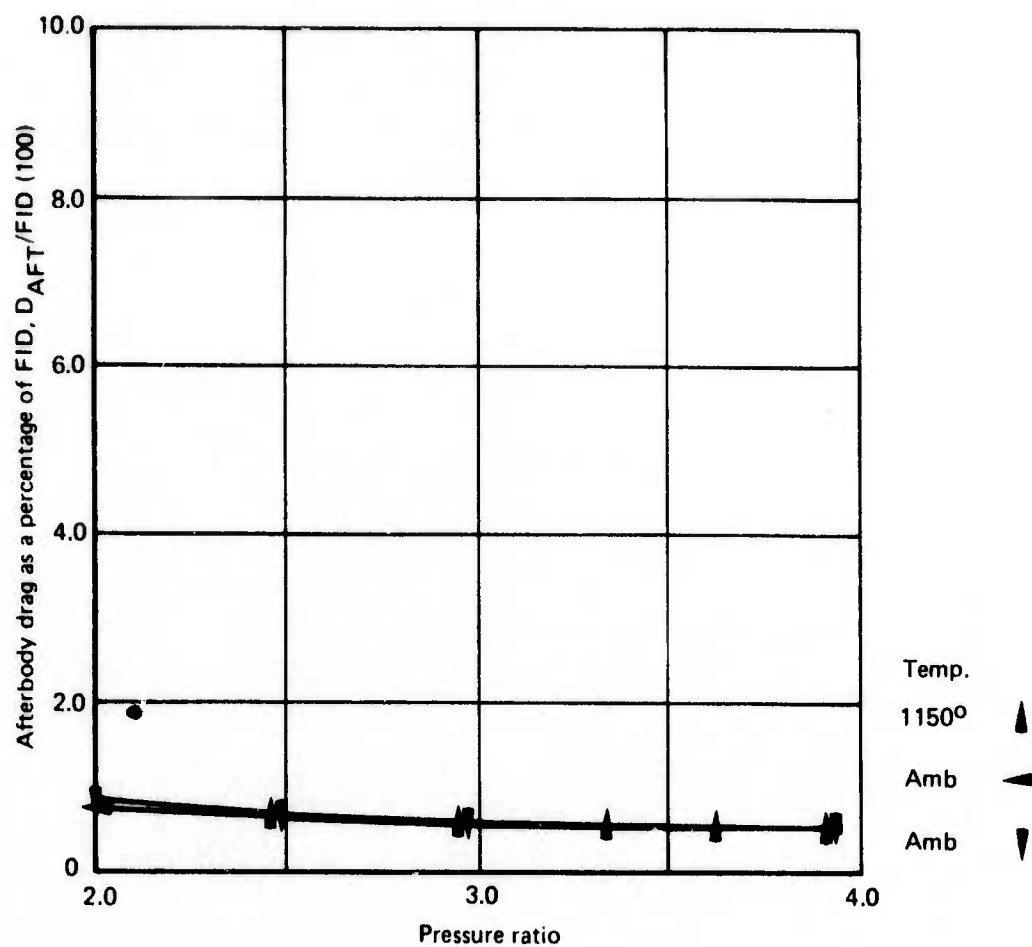
Figure 53.—Afterbody Drag as a Percentage of FID for (R/37) 37-Tube, Area Ratio 3.3, Close-Packed Array (Round Convergent Tubes)

93

Figure 54.—C_{f_g} Versus Tube Length and Pressure Ratio—7-Tube Nozzle

94

Afterbody drag as a percentage of FID, D_{AFT}/FID (100)

10.0

8.0

6.0

4.0

2.0

$\dfrac{L_T}{D_{eq}}$	Temp.	
0.75	1150°	◄
0.75	Amb	▼
0.75	Amb	►
0.50	Amb	□
0.50	Amb	♦
0.25	Amb	+
0.25	Amb	△

2.0   3.0   4.0
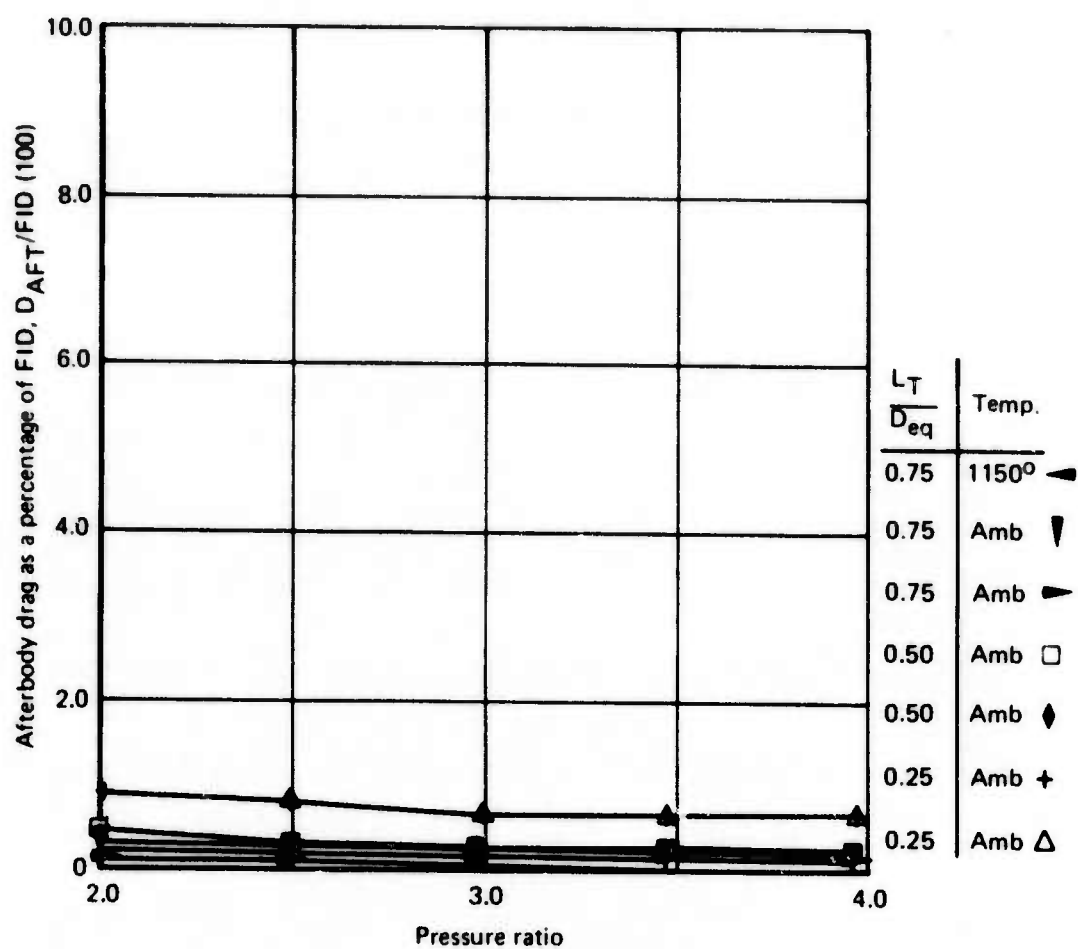
Pressure ratio

Figure 55.—Afterbody Drag as a Percentage of FID for 7-Tube, Area Ratio 3.3 Suppressor

95

19 Tubes, Area Ratio 3.3 Primary
Close-Packed Array
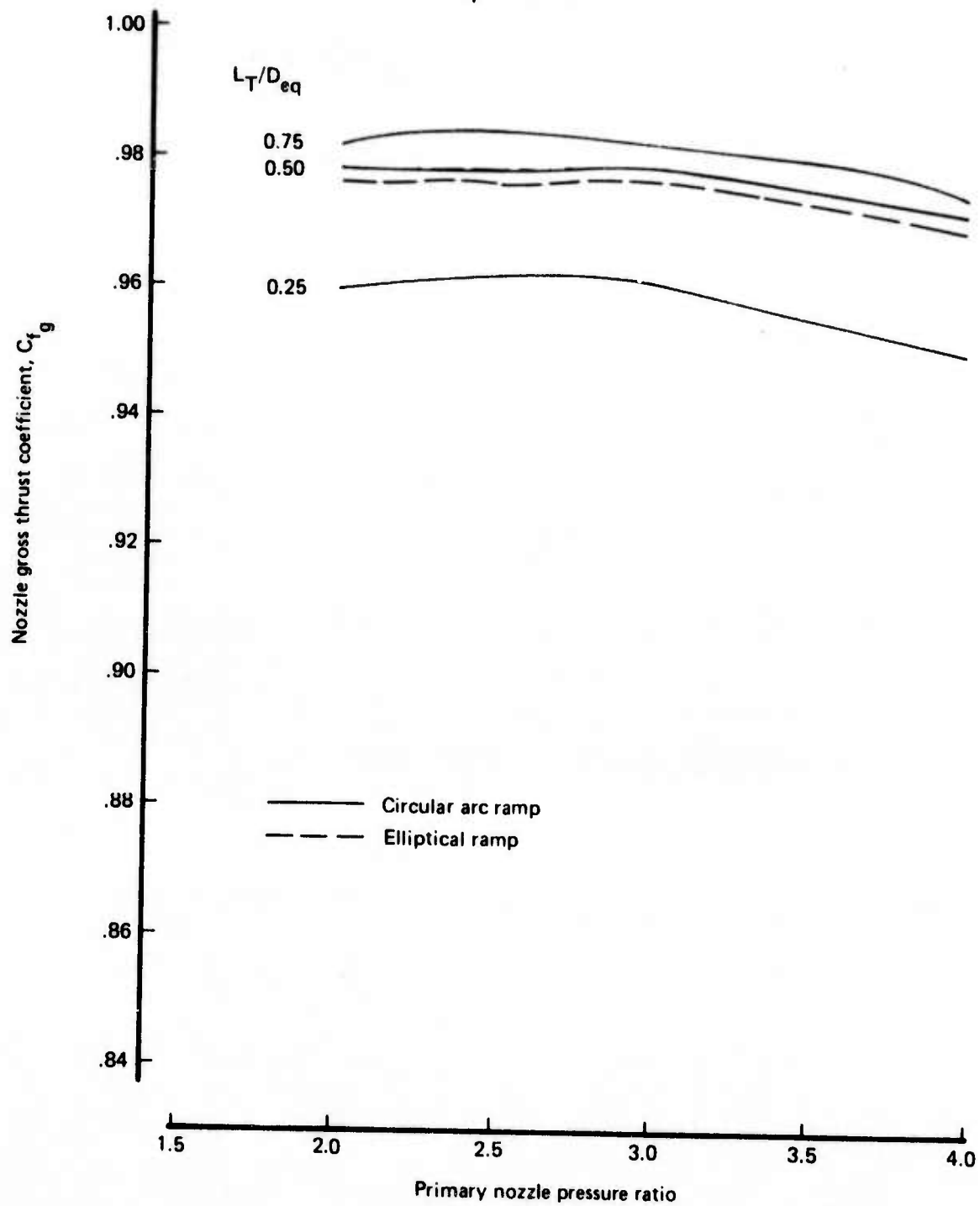
Figure 56.—C_{f_g} Versus Tube Length and Pressure Ratio—19 Tubes

96
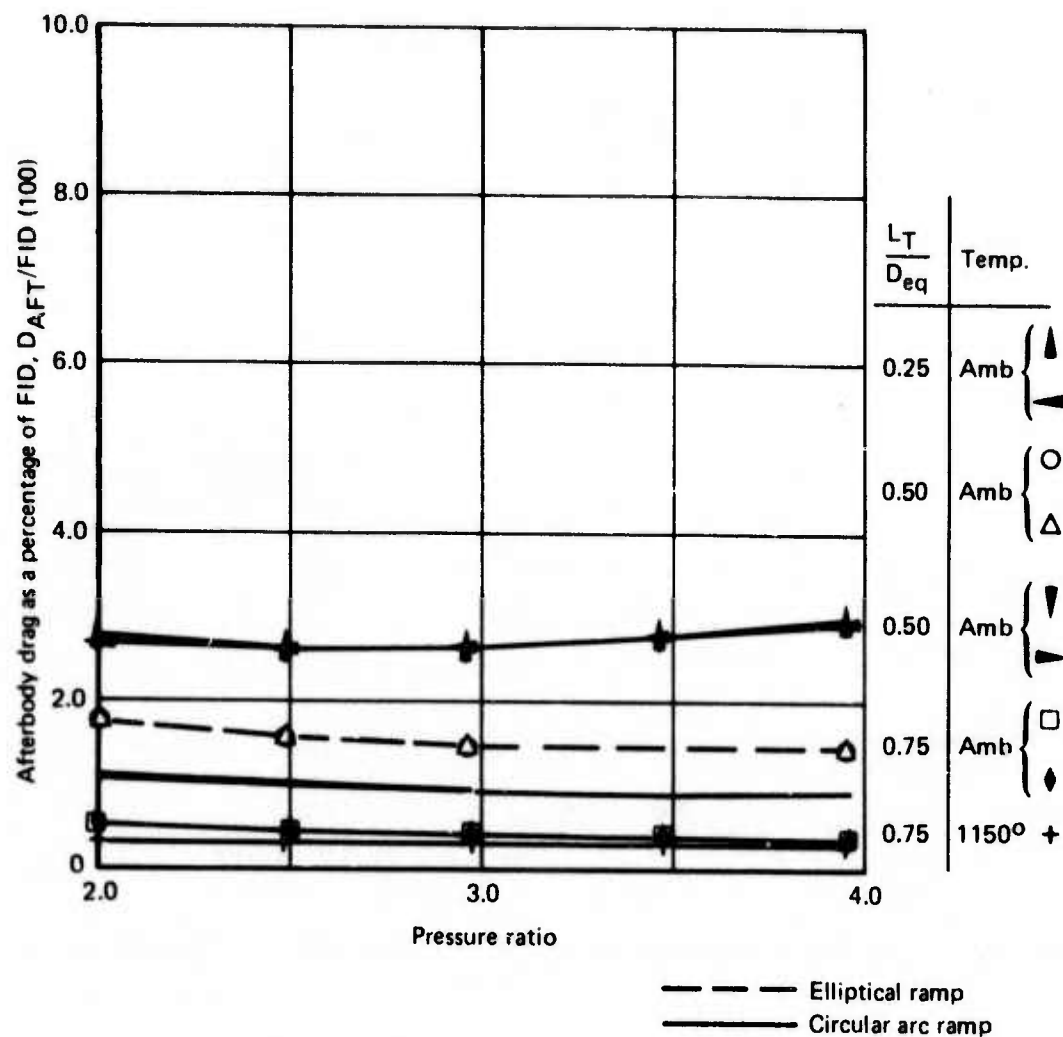
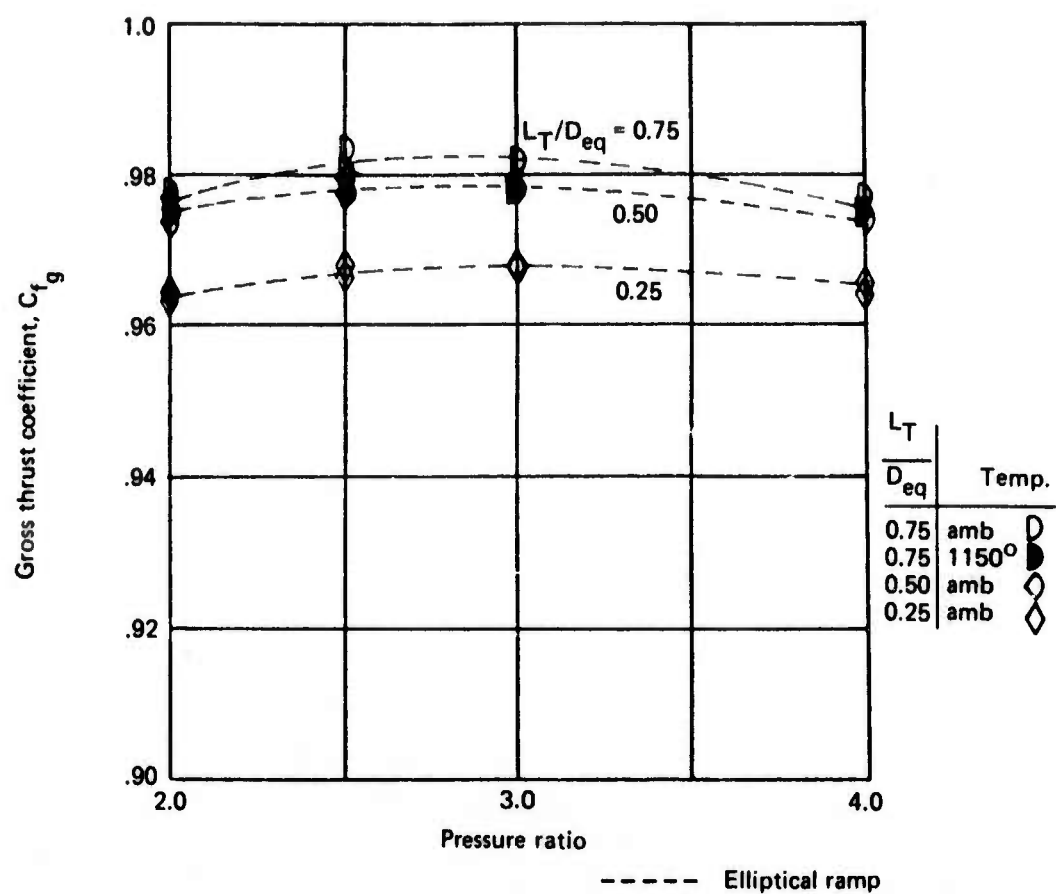Figure 57.—Afterbody Drag as a Percentage of FID for 19-Tube, Area Ratio 3.3, Close-Packed Array

97
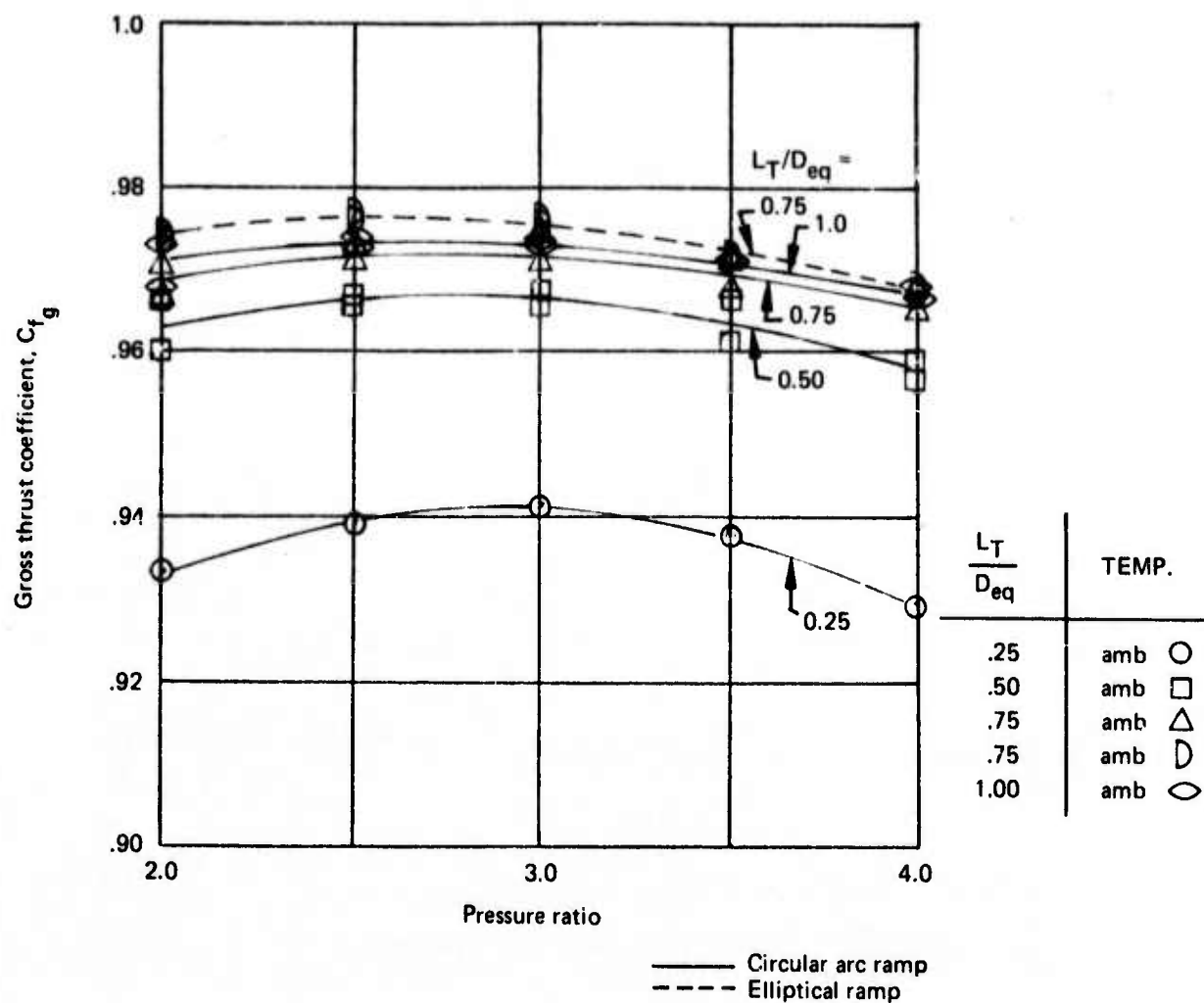
Figure 58.—Gross Thrust Coefficient for the 37-Tube, Area Ratio 3.3, Close-Packed Array
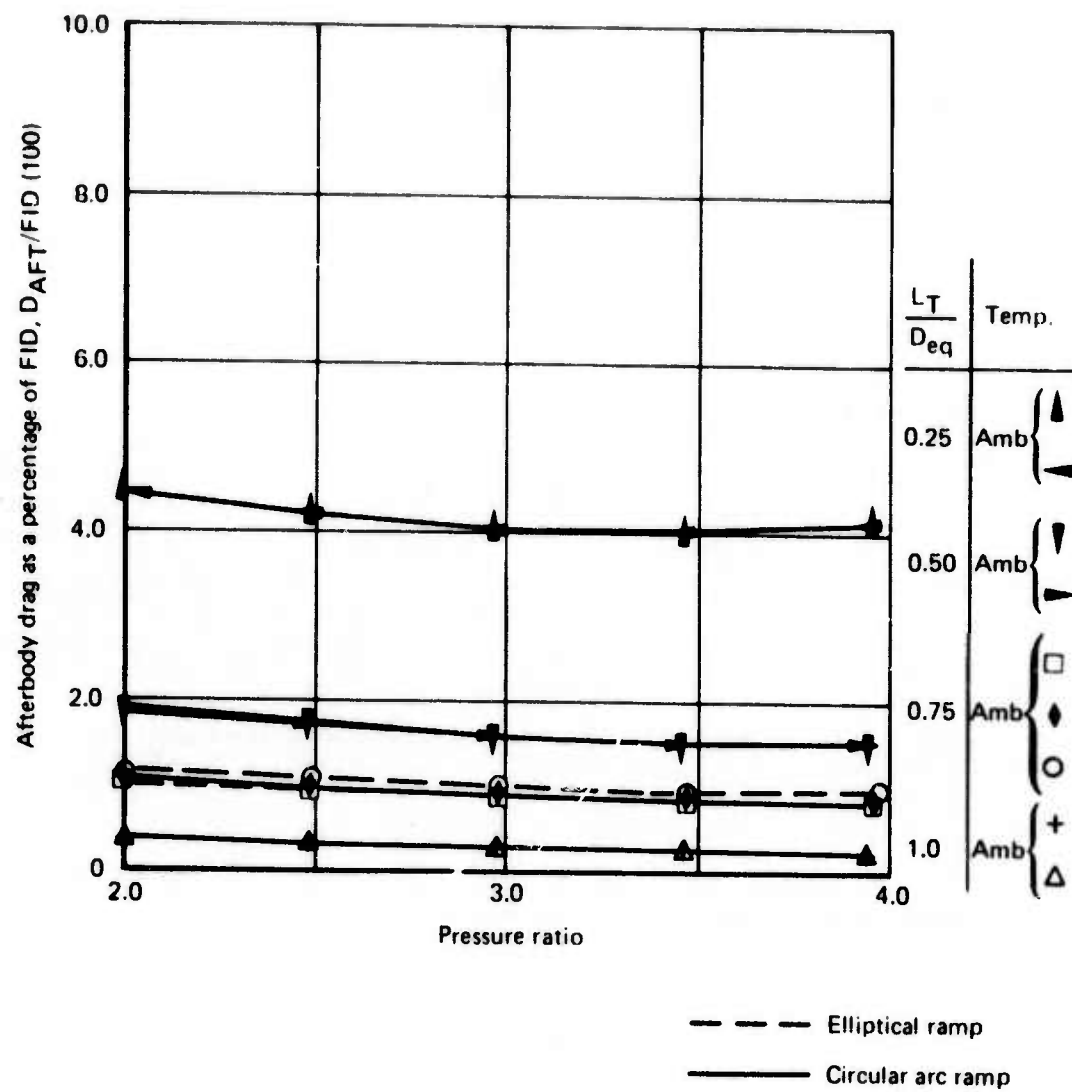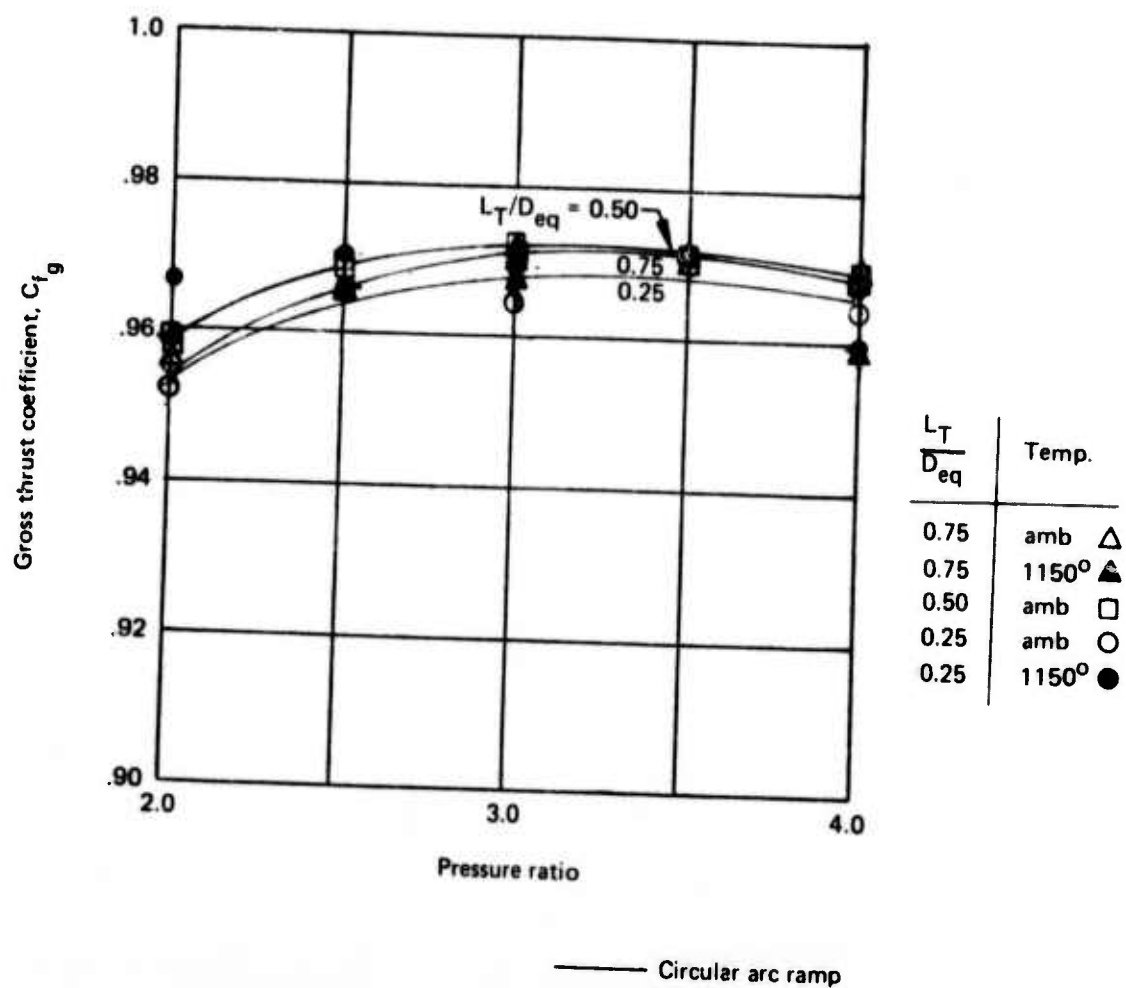
Figure 59.—Afterbody Drag as a Percentage of FID for 37-Tube, Area Ratio 3.3, Close-Packed Array
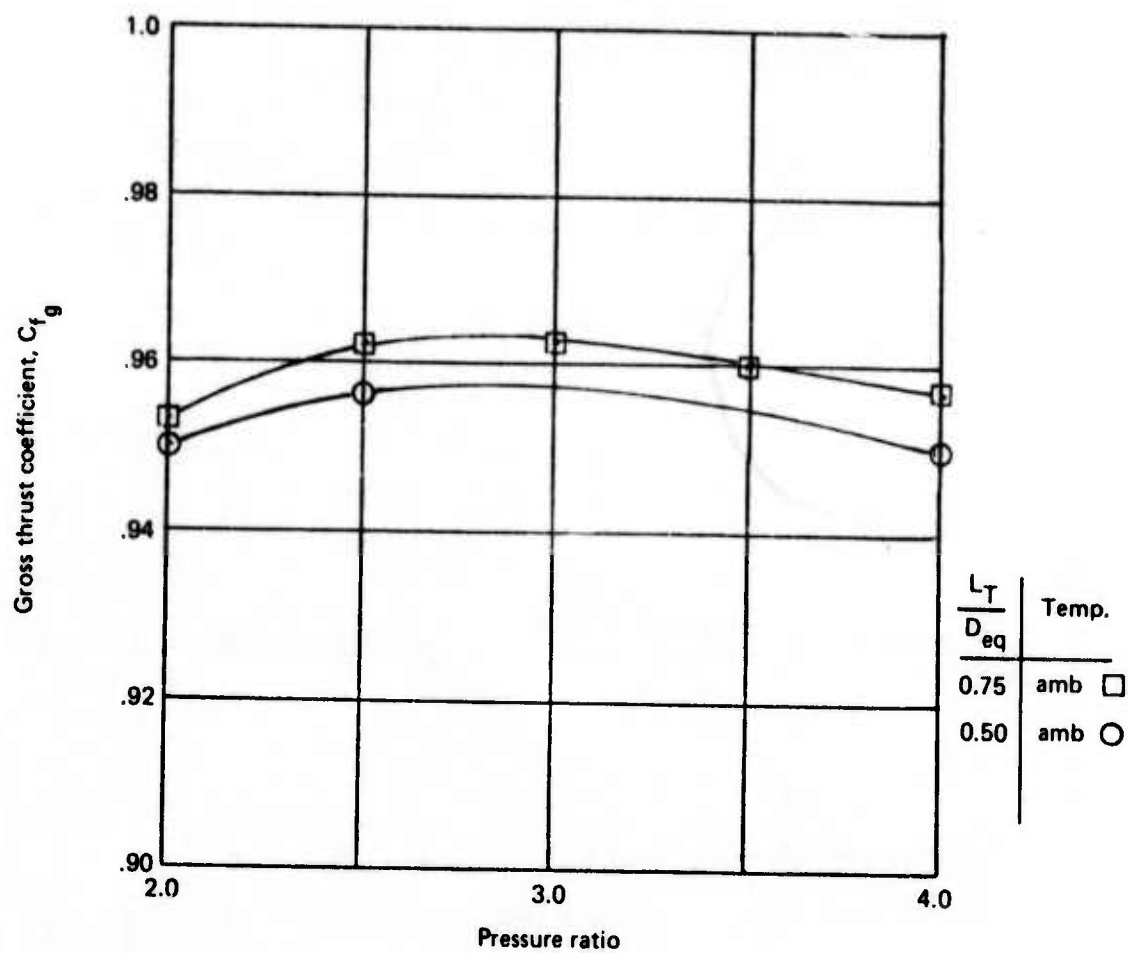
Figure 60.—Gross Thrust Coefficient for the 37-Tube, Area Ratio 3.3, Close-Packed Array With Round Convergent Tubes and Elliptical Ramp

100
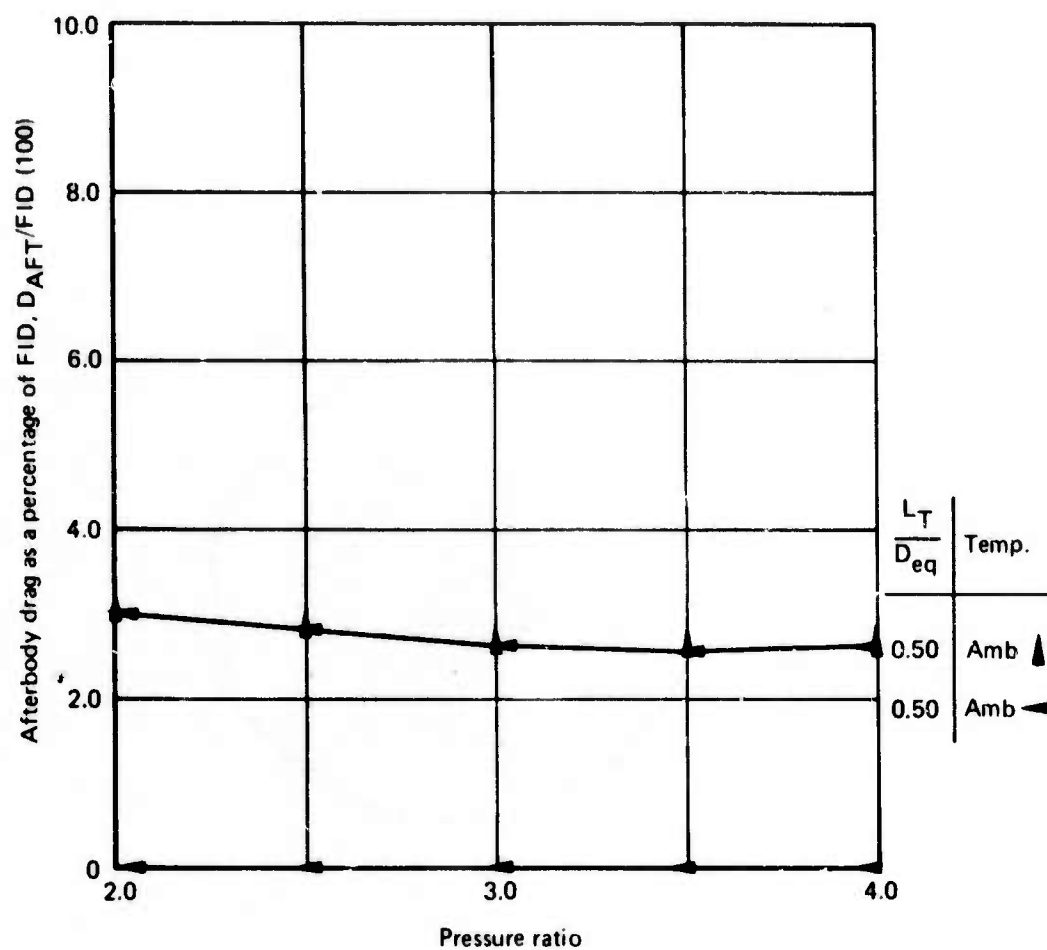
Figure 61.—Afterbody Drag as a Percentage of FID for 37-Tube, Area Ratio 3.3, Close-Packed Array Elliptical Ramp and Round Convergent Tubes
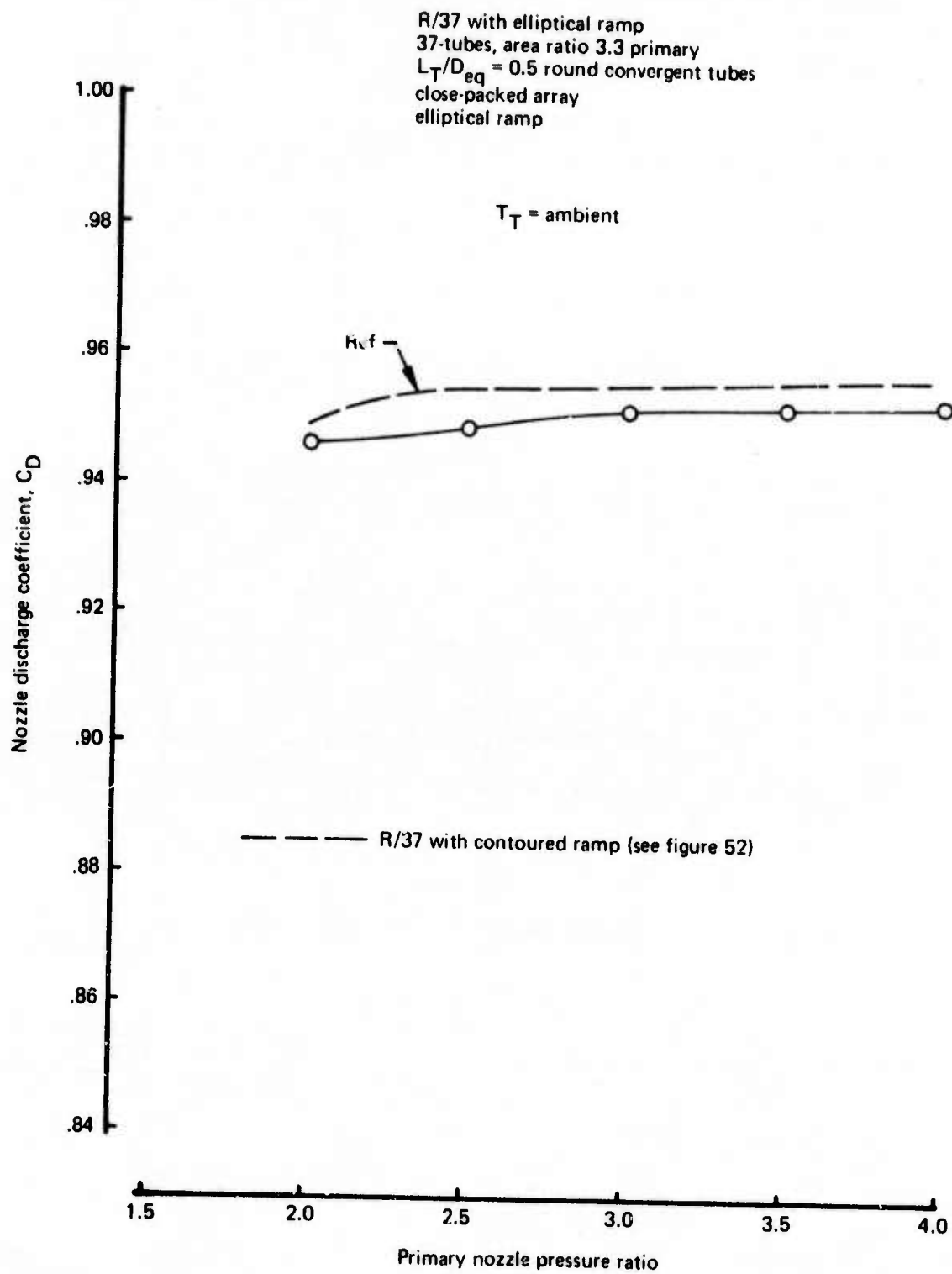
Figure 62.—Discharge Coefficient for R/37 Fitted With Elliptical Ramp

102
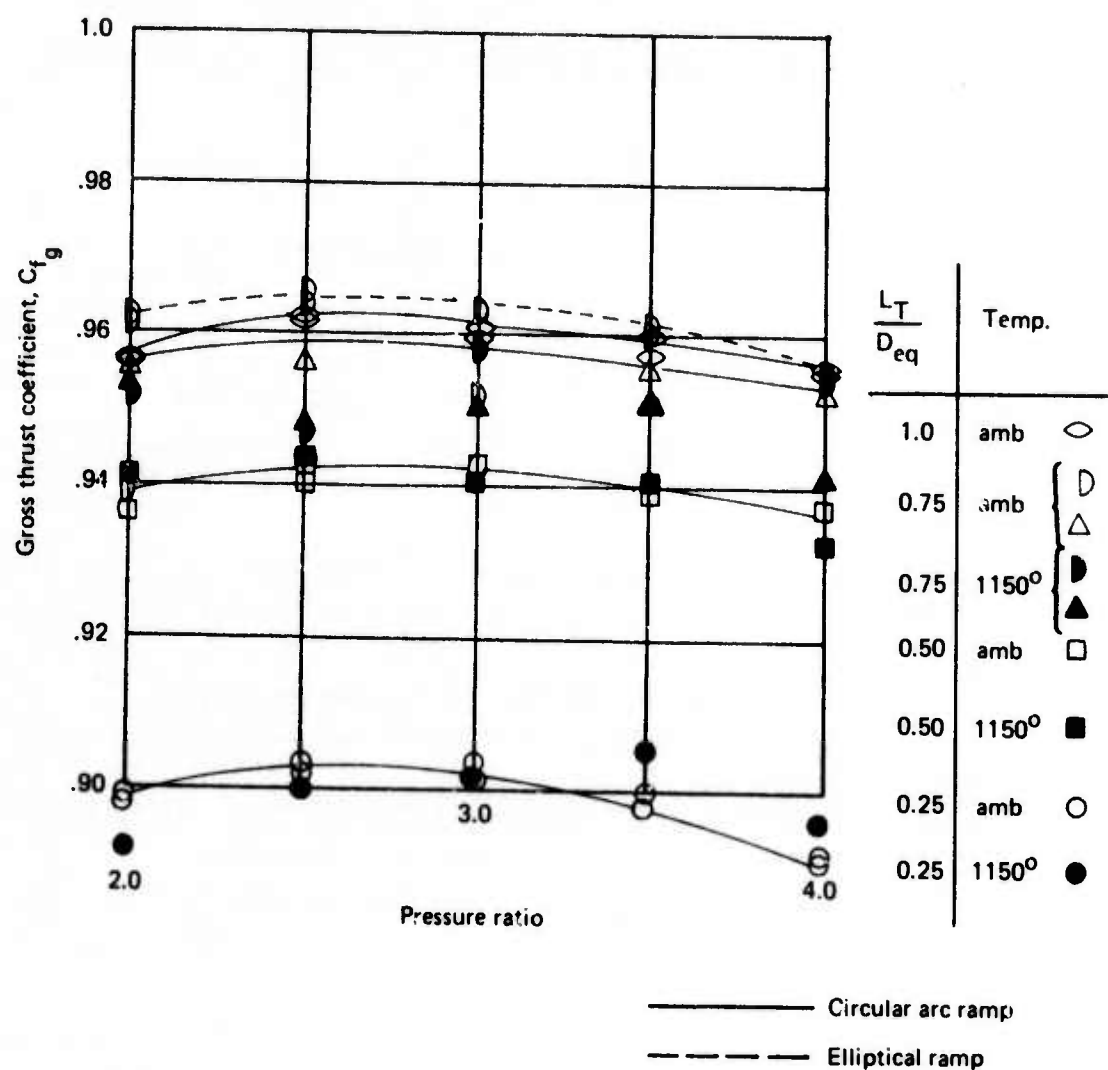
Figure 63.—Gross Thrust Coefficient for the 61-Tube, Area Ratio 3.3, Close-Packed Array

103
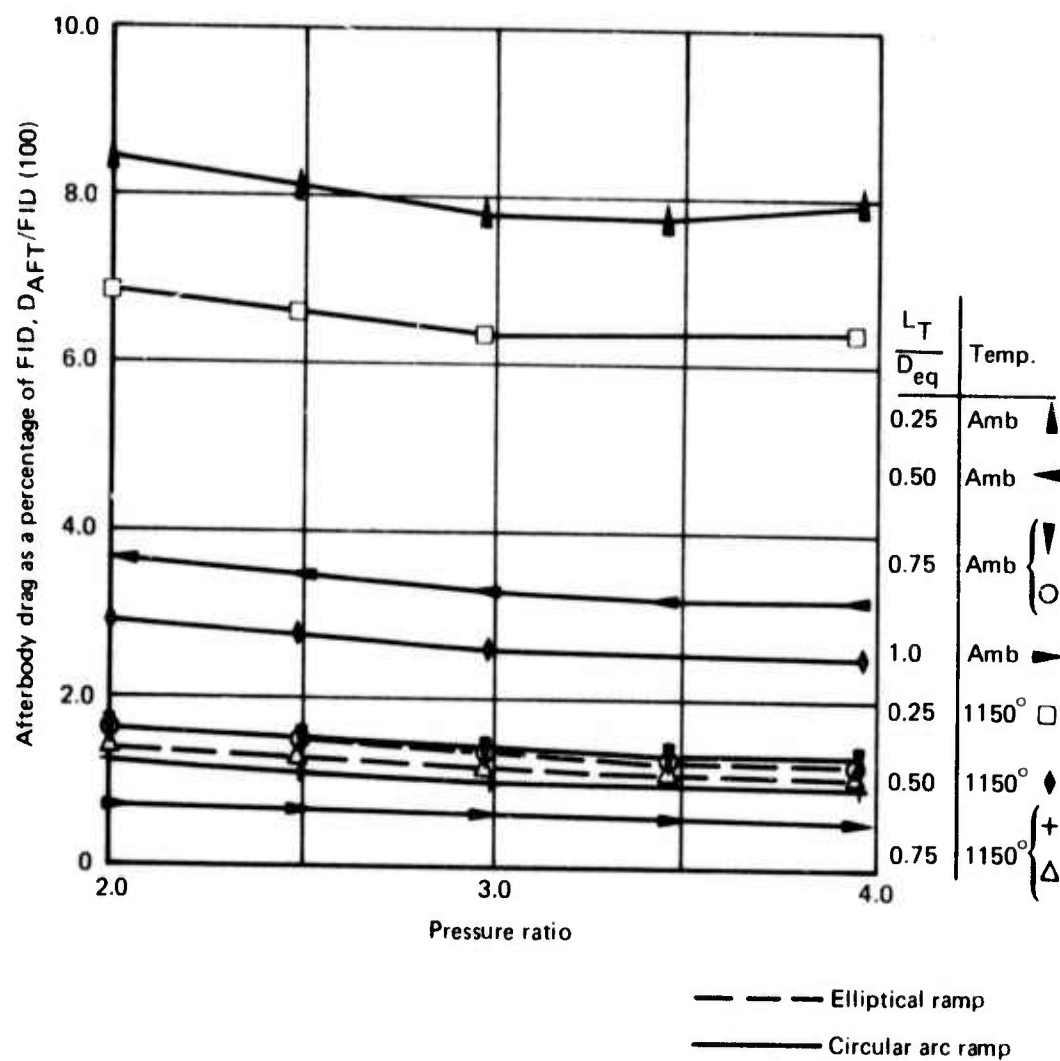
Figure 64.—Afterbody Drag as a Percentage of FID for 61-Tube, Area Ratio 3.3, Close-Packed Array
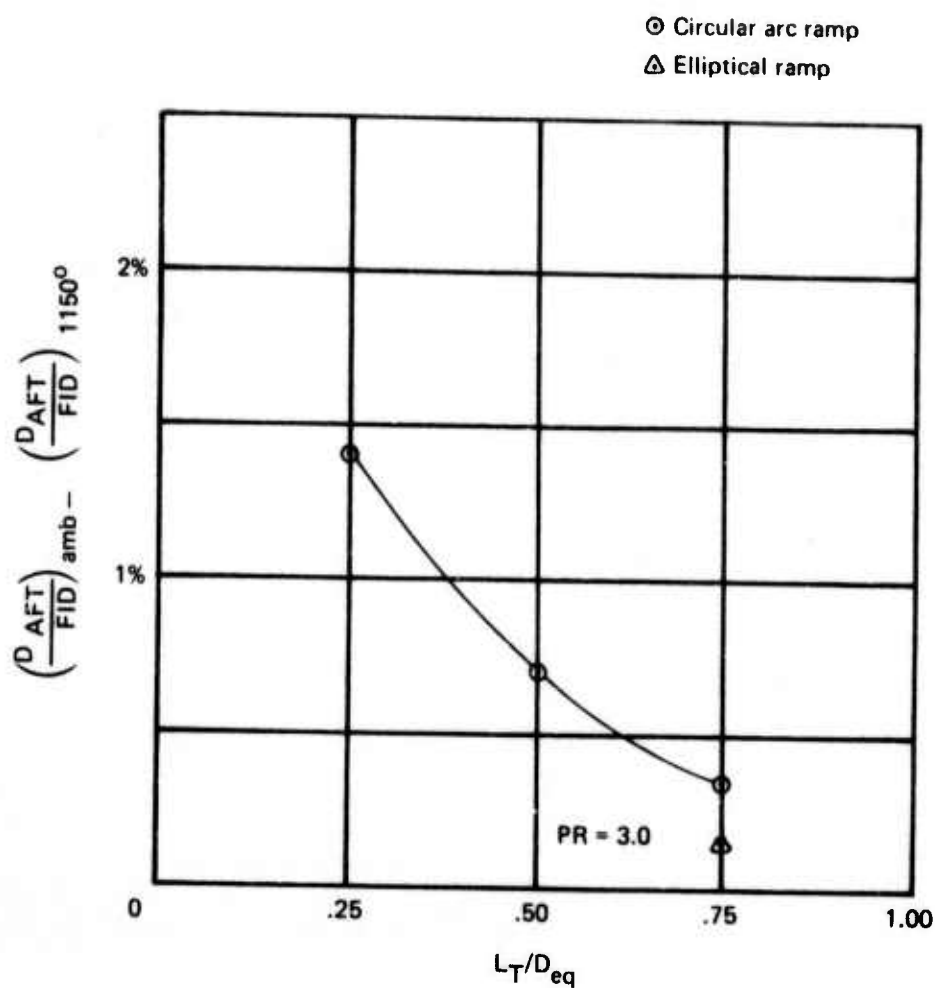
Figure 65.—Effect of Temperature on D_{AFT}/FID for Various Tube Lengths (61-Tube, Area Ratio 3.3, Close-Packed)

105
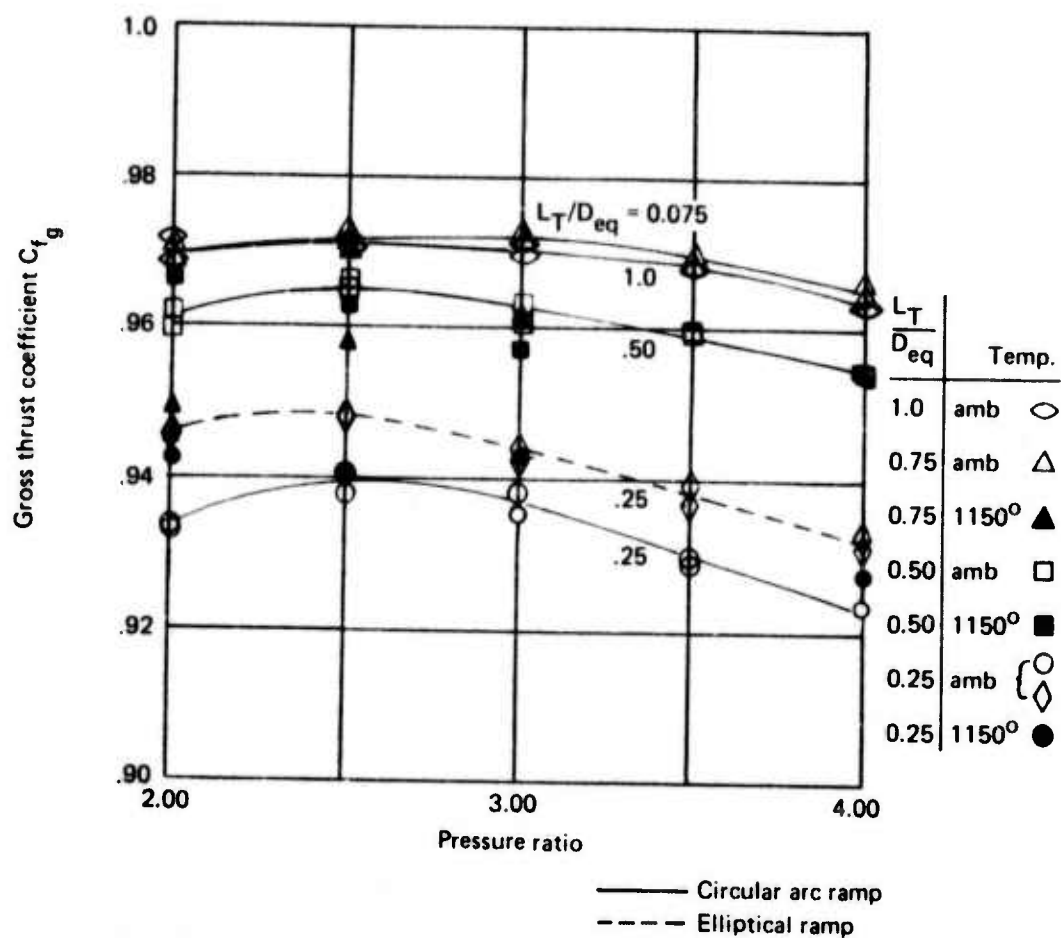
Figure 66.–Gross Thrust Coefficient for the 37-Tube, Area Ratio 2.75, Close-Packed Array
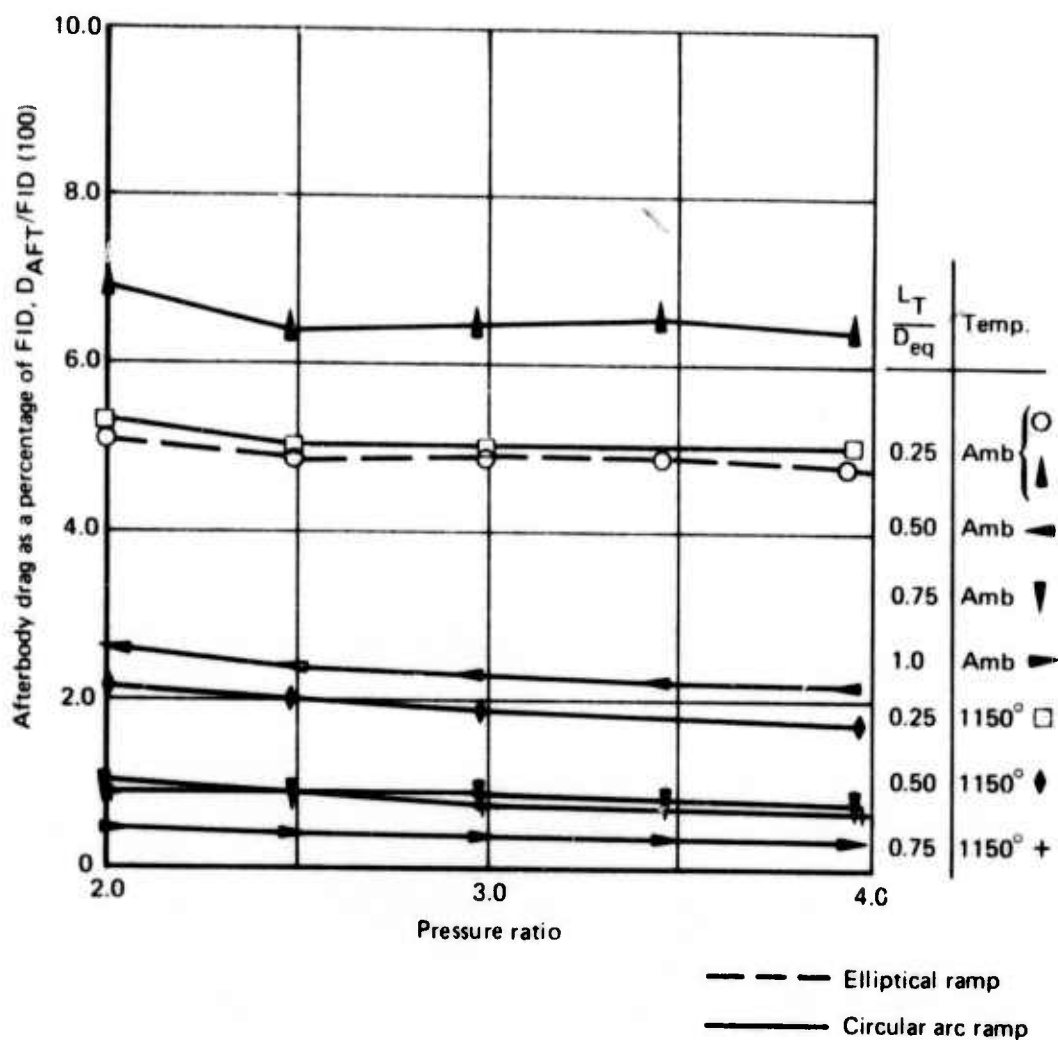
Figure 67.—Afterbody Drag as a Percentage of FID for 37-Tube, Area Ratio 2.75, Close-Packed Array
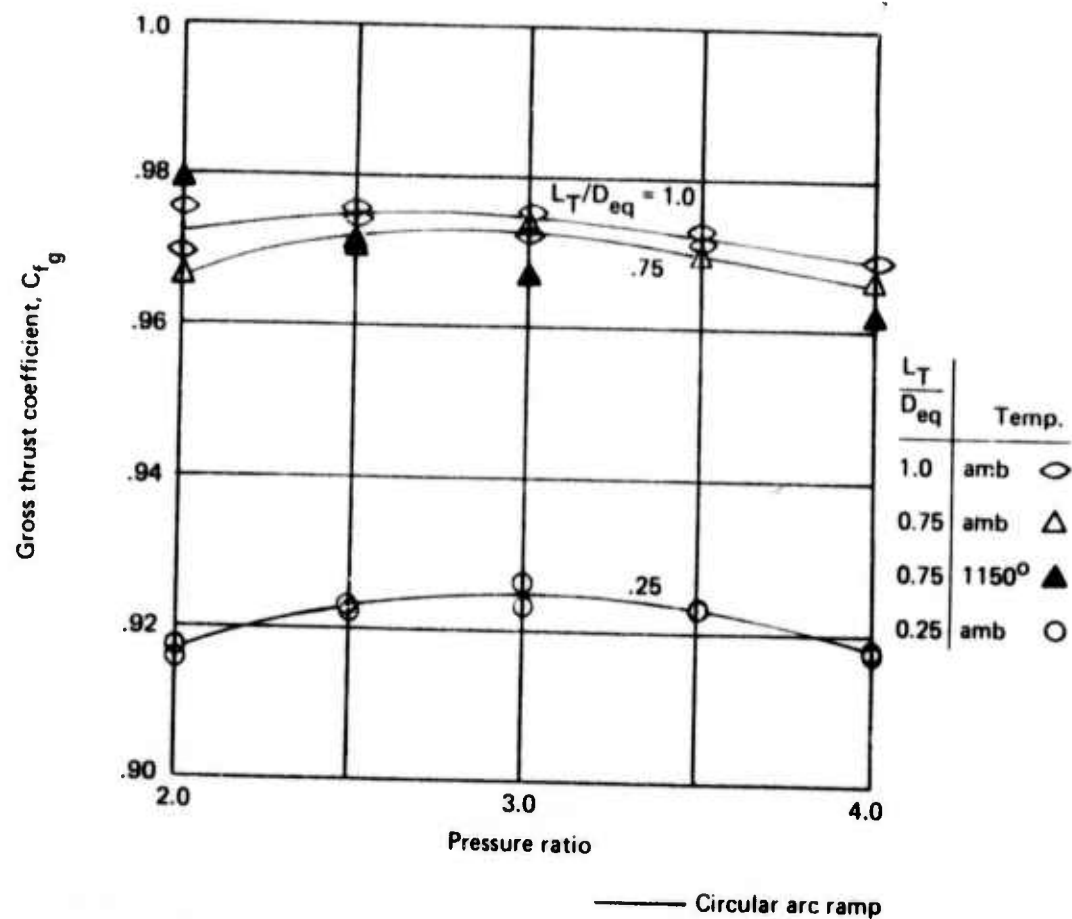
Figure 68.—Gross Thrust Coefficient for the 37-Tube, Area Ratio 4.5, Close-Packed Array
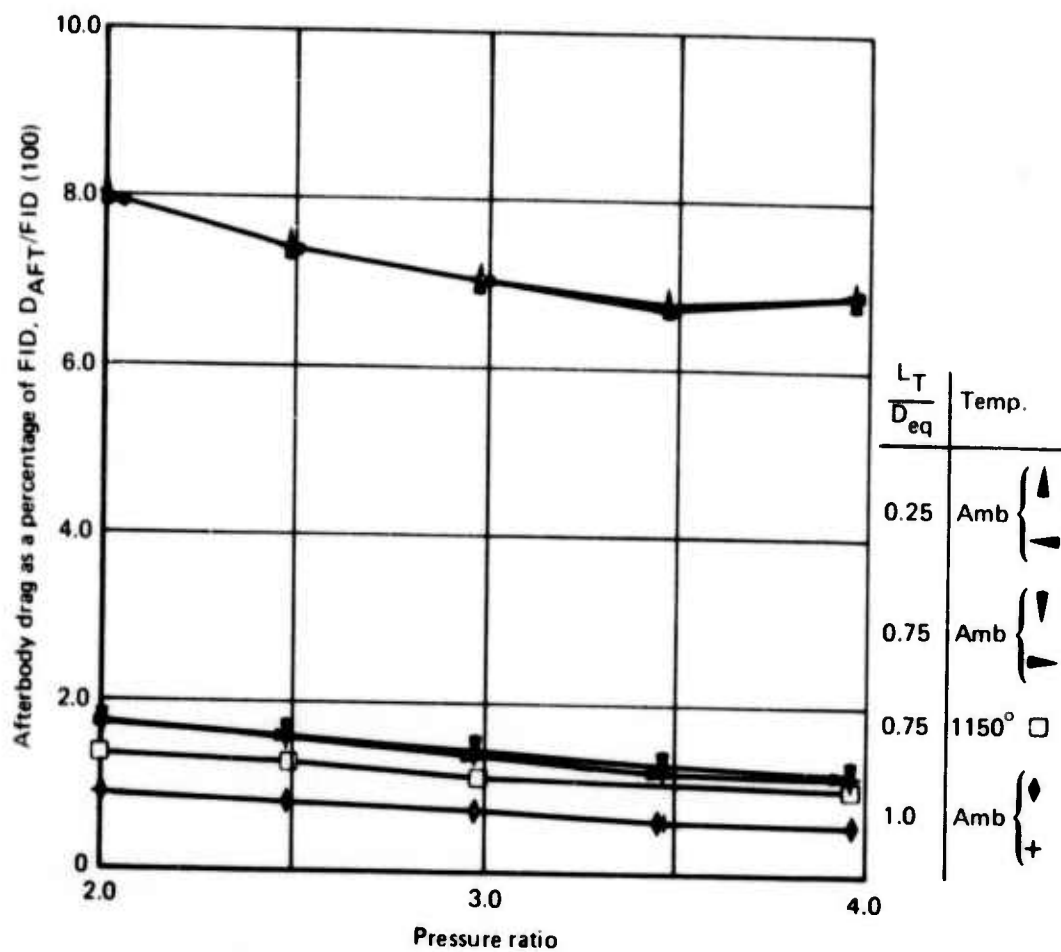
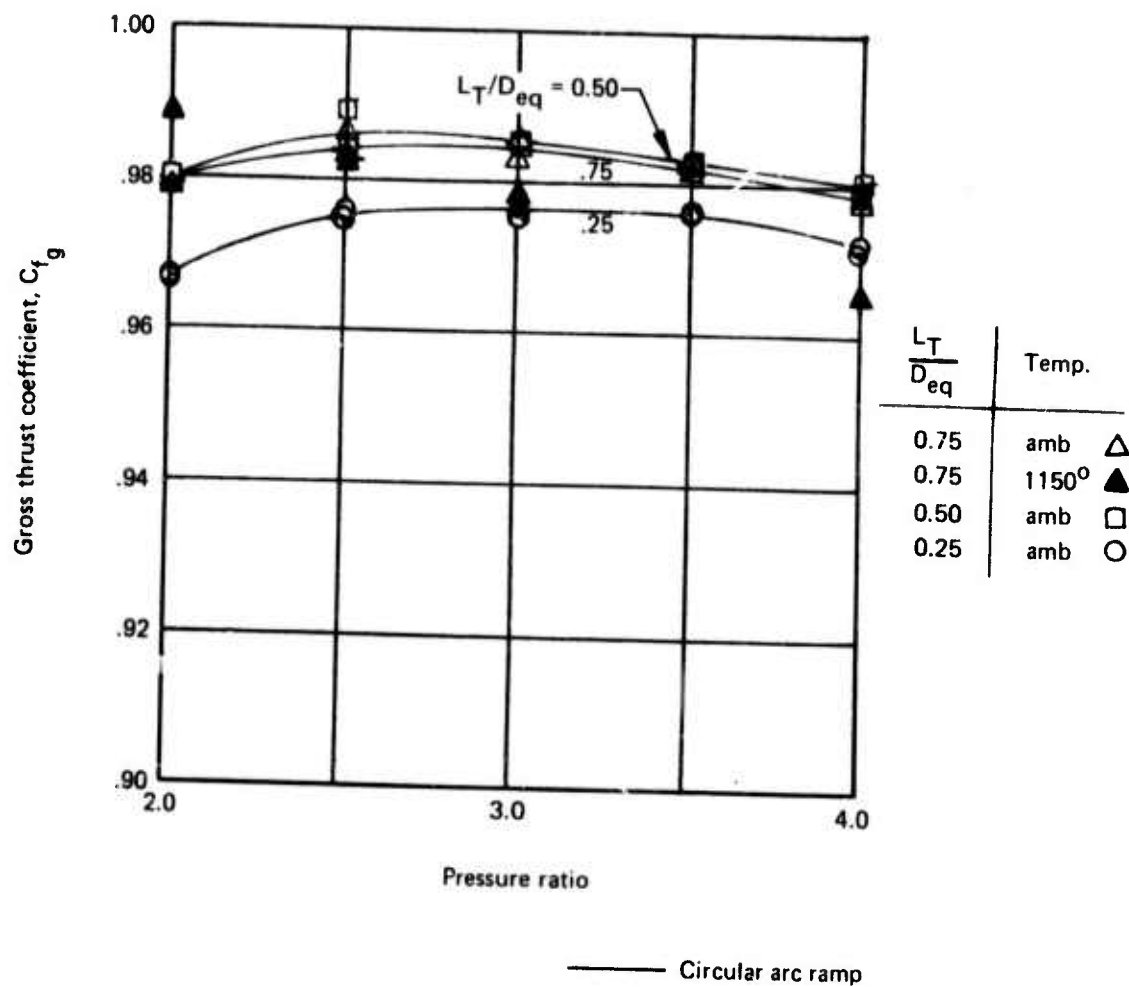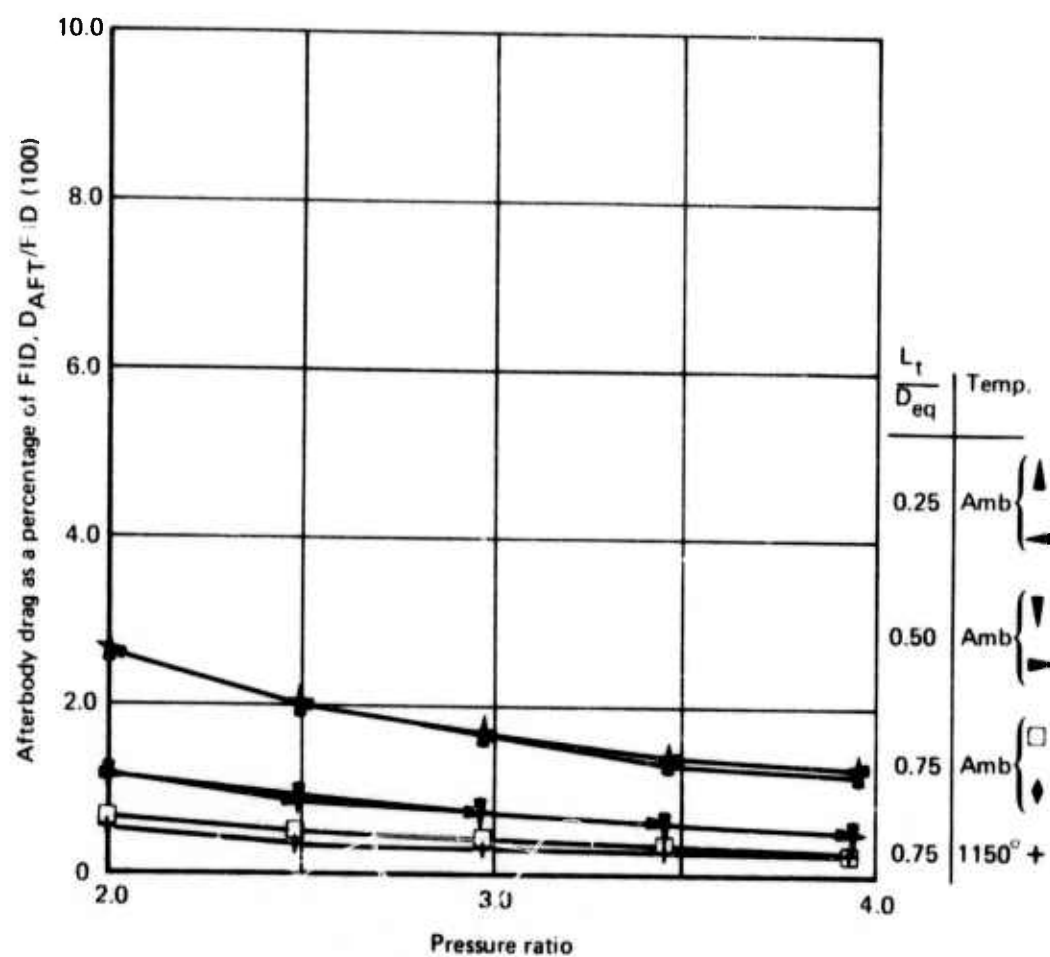Figure 69.—Afterbody Drag as a Percentage of FID for 37-Tube, Area Ratio 4.5, Close-Packed Array Circular Arc Ramp
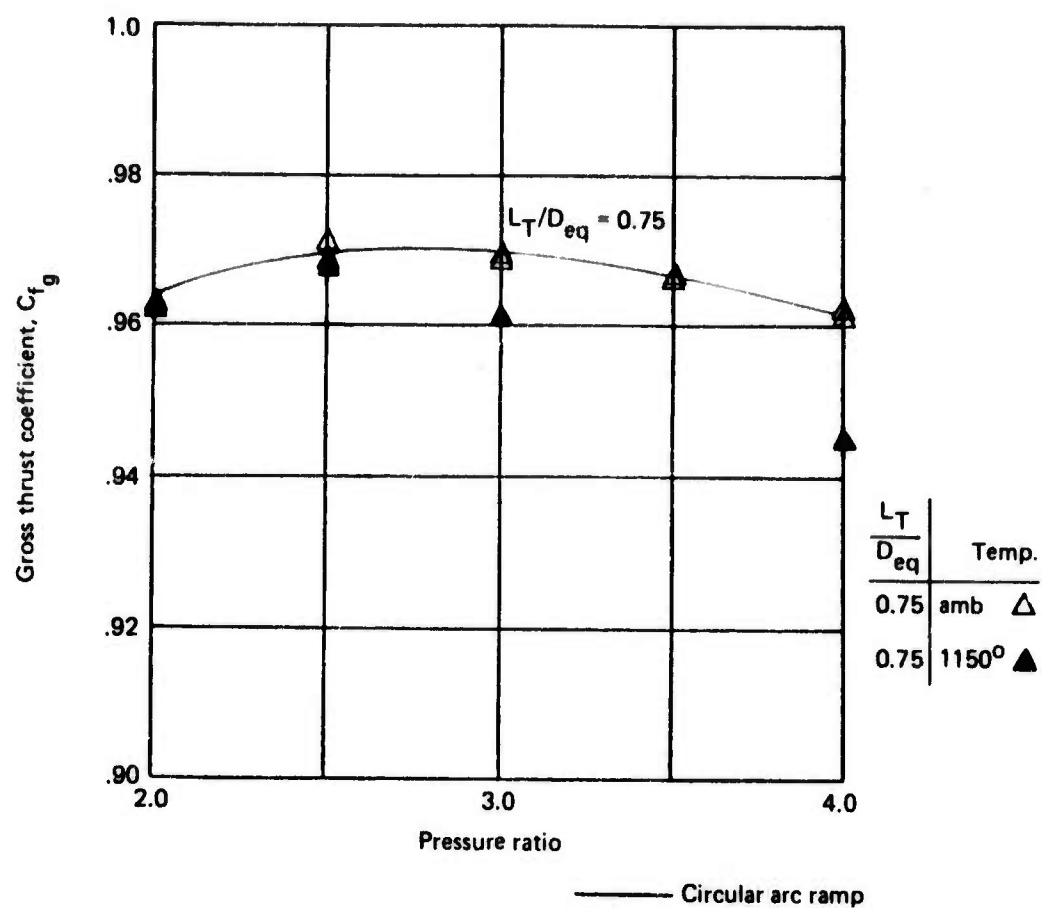
Figure 70.—Gross Thrust Coefficient for the 37-Tube, Area Ratio 6.0, Close-Packed Array With Circular Arc Ramp

110
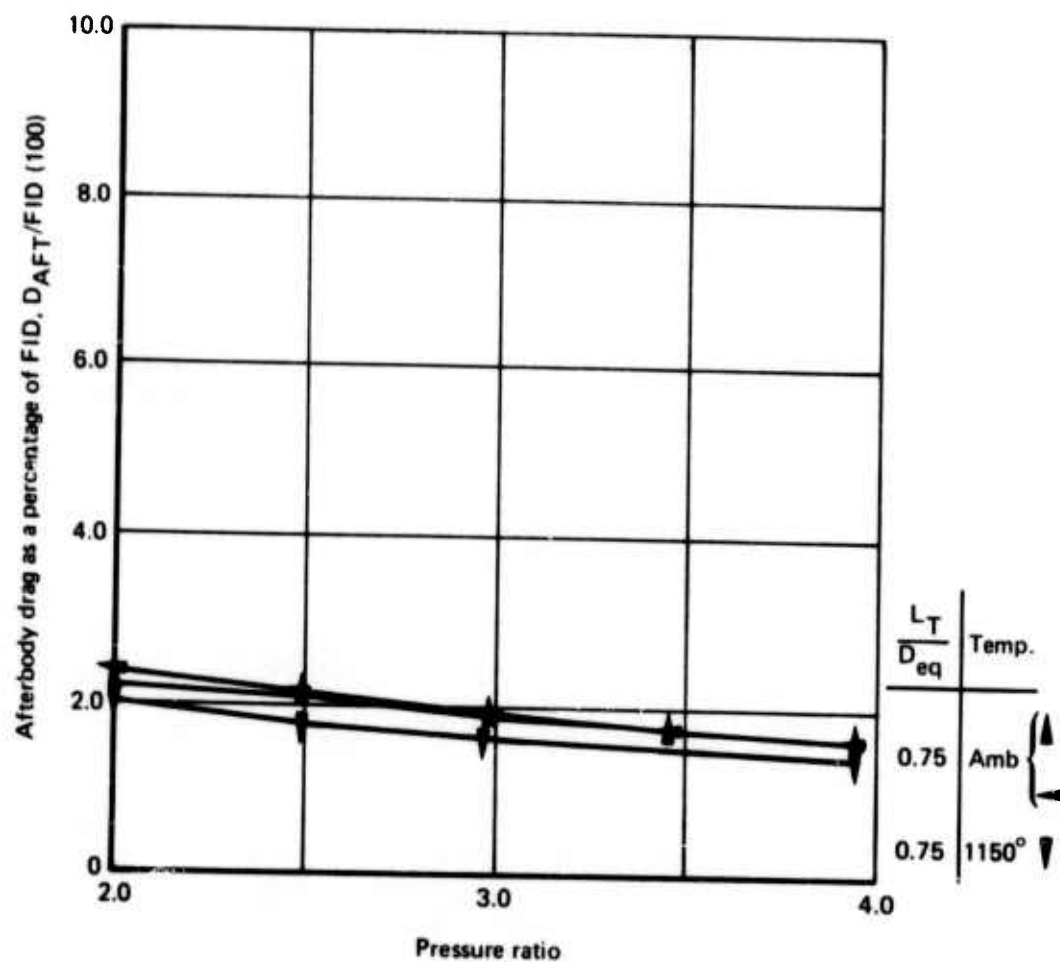
Figure 71.—Afterbody Drag as a Percentage of FID for 37-Tube, Area Ratio 6.0, Close-Packed Array Circular Arc Ramp

1.0

.98

.96

.94

.92

.90

Gross thrust coefficient, C_{f_g}

$L_T/D_{eq} = 0.75$

0.50

0.25

$\dfrac{L_T}{D_{eq}}$	Temp.	
0.75	amb	
0.75	1150°	
0.50	amb	
0.25	amb	

2.0   3.0   4.0

Pressure ratio

- - - - - Elliptical ramp

Figure 72.–Gross Thrust Coefficient for the 31-Tube, Area Ratio 2.75, Radial Array

112
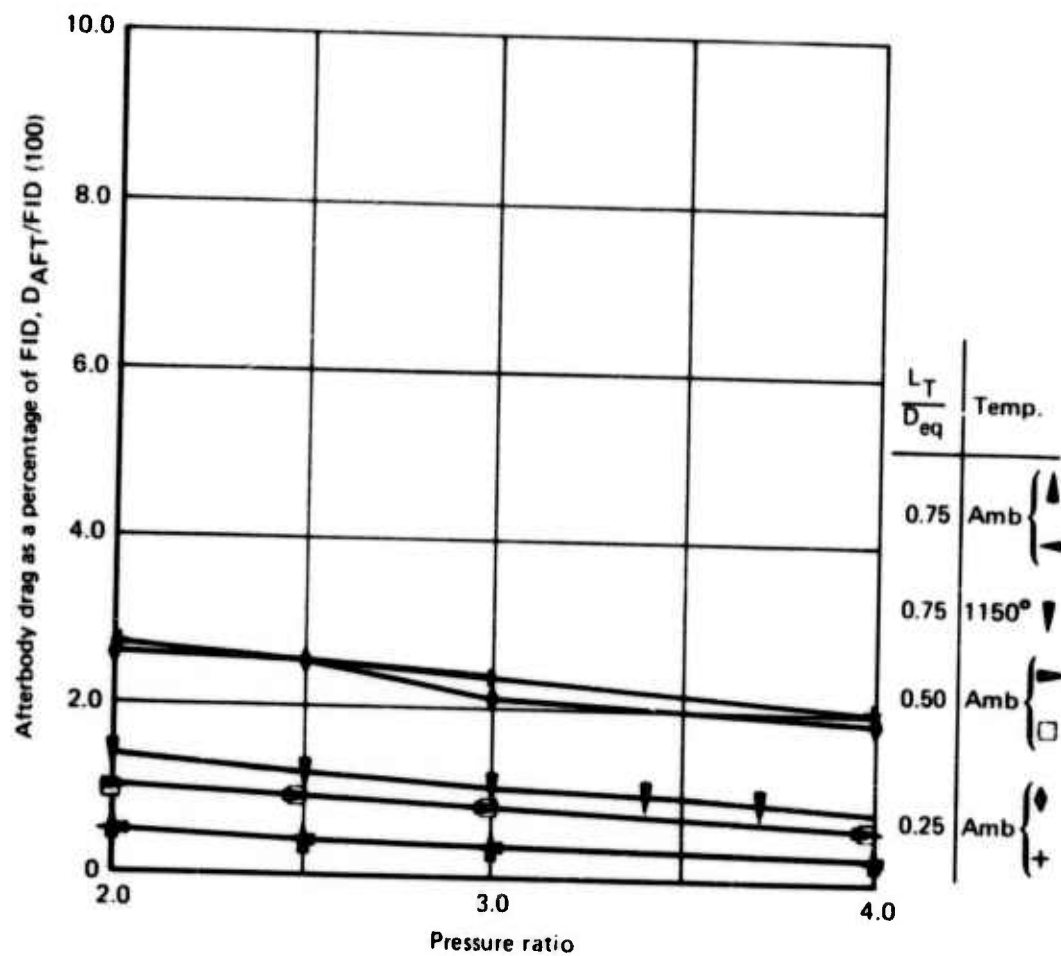
Figure 73.—Afterbody Drag as a Percentage of FID for 31-Tube, Area Ratio 2.75, Radial Array Elliptical Ramp

Figure 74.—Gross Thrust Coefficient for the 37-Tube, Area Ratio 3.3, Radial Array

114
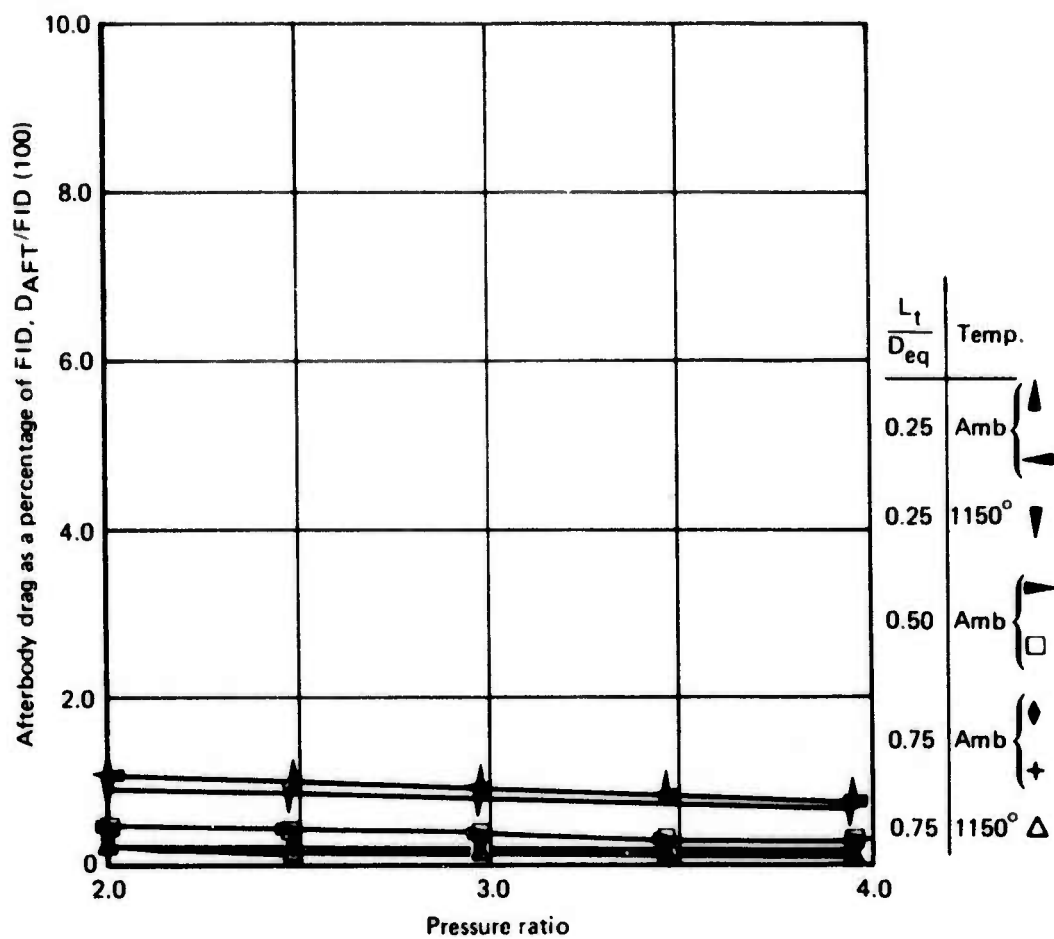
Figure 75.--Afterbody Drag as a Percentage of FID for 37-Tube Area Ratio
3.3 Radial Array With Round Non-Converging Tubes and
Circular Arc Ramp

115
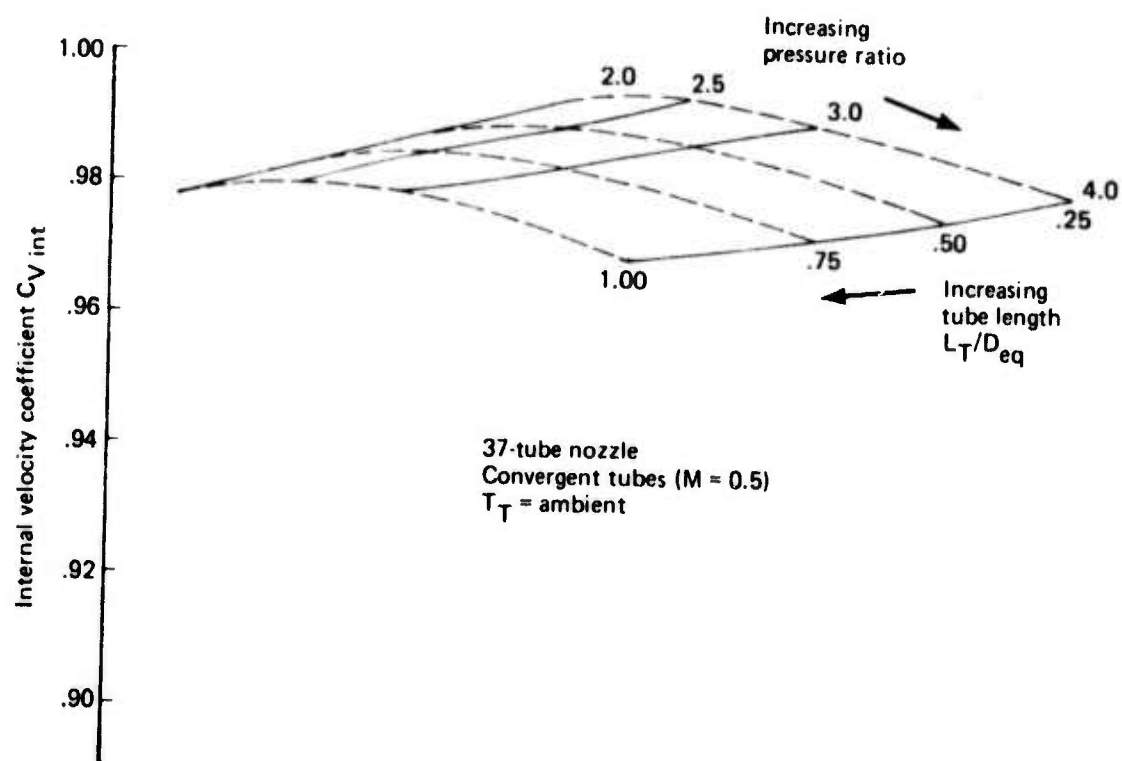
Figure 76.—Internal Velocity Coefficient Versus Pressure Ratio and Tube Length for 37-Tube Nozzles With Elliptical Convergent Tubes (M = 0.5)
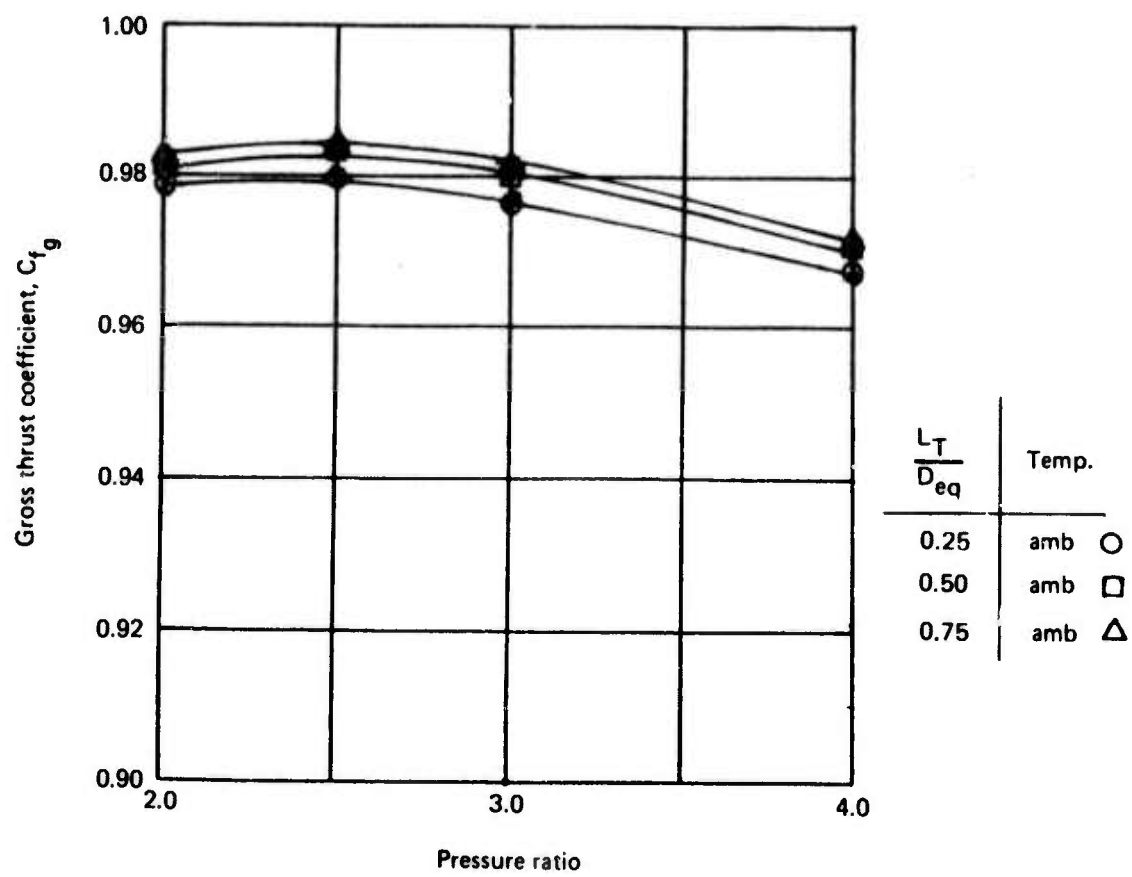
Figure 77.—Gross Thrust Coefficient for the 37-Tube, Area Ratio 3.3, Radial Array Circular Arc Ramp and Elliptical Convergent Tubes (Constructed)

117

Figure 78.—Gross Thrust Coefficient for the 37-Tube, Area Ratio 4.5, Radial Array

Figure 79.—Afterbody Drag as a Percentage of FID for 37-Tube Area Ratio 4.5, Radial Array Circular Arc Ramp
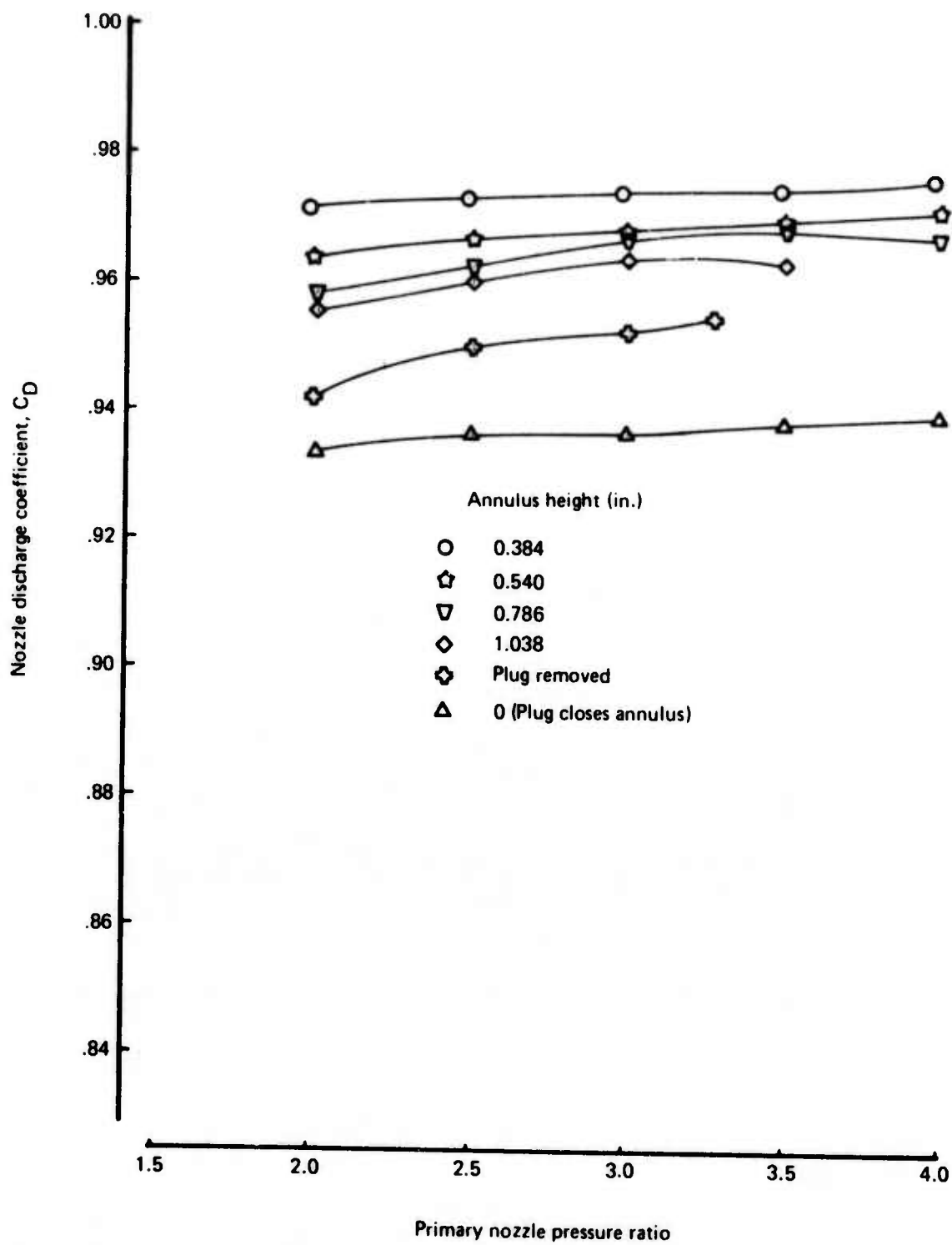
Figure 80.—Discharge Coefficient for 42-Tube Annular-Plug Nozzle for Various Annulus Heights

42-Tube, Area Ratio 3.3 Primary
No Ejector
T_T - ambient

Annulus height:
⬙ plug removed
◇ 1.038
▽ 0.786
⬠ 0.540
○ 0.384 (AR=3.3)
△ 0

— — — 61 3-in. tubes—AR=3.3 (L_T/D_{eq} = 0.75)
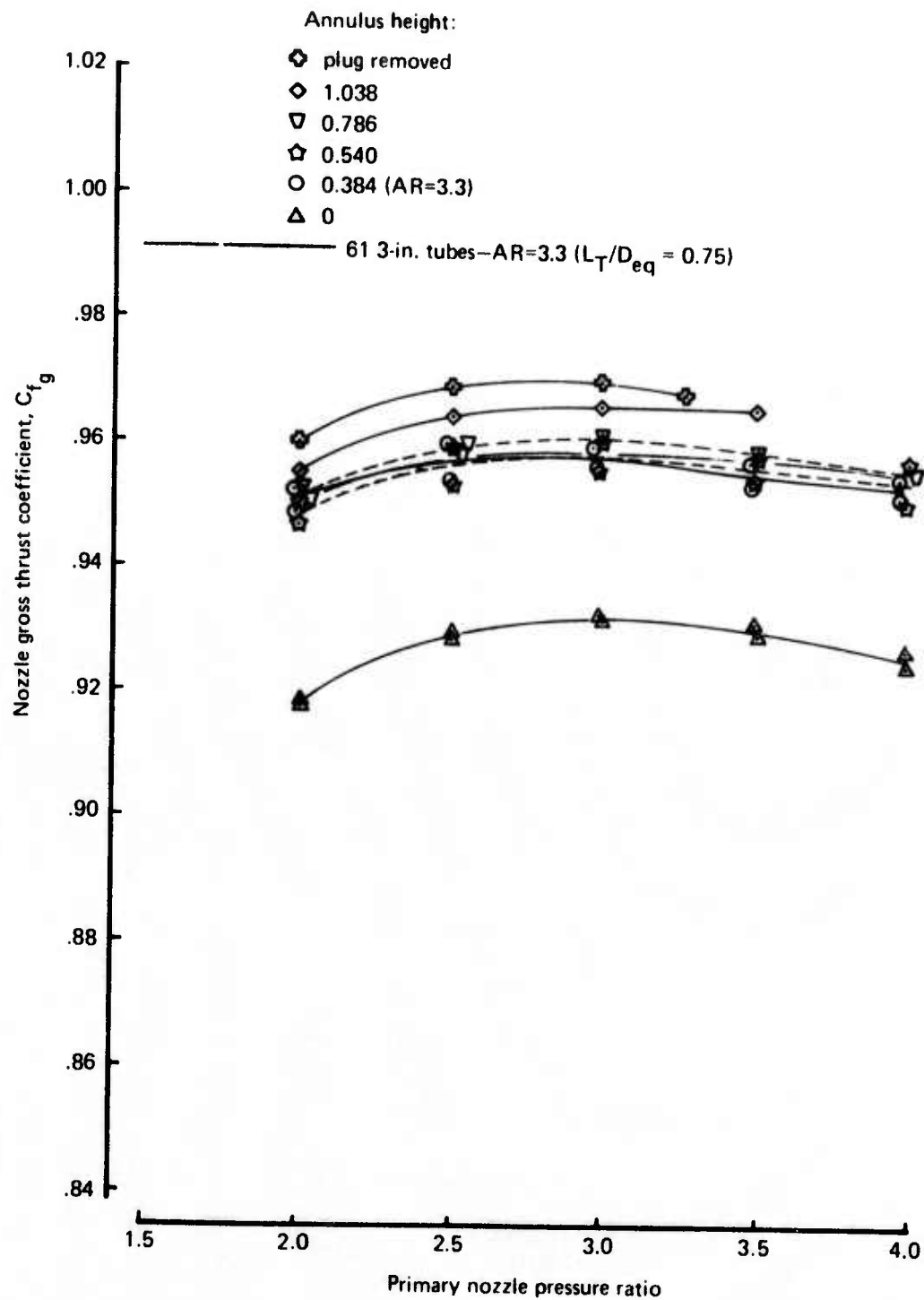
Figure 81.—C_{f_g} 42-Tube Annular Plug Nozzle—Various Annulus Heights (Ambient)

121
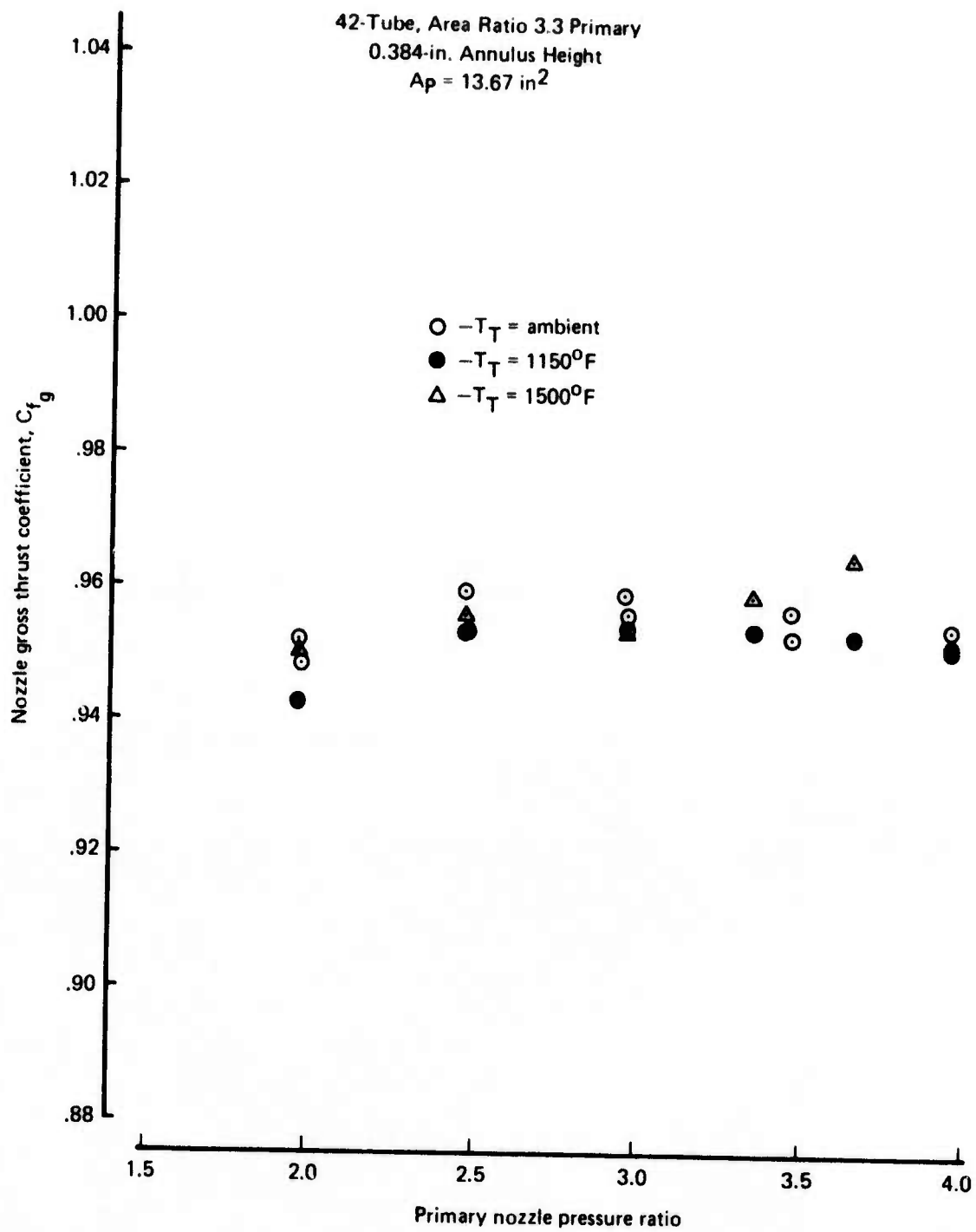
Figure 82.—C_{f_g} 42-Tube, Annular-Plug Nozzle (AR=3.3) Ambient and 1150°F

Nozzle gross thrust coefficient, C_{f_g}

1.00

.98

7 Tubes

37-Tube radial array

19 Tubes

Ⓐ

Ⓐ

Ⓐ

$L_T/D_{eq} = 1.0$

$L_T/D_{eq} = 0.75$

.96

$L_T/D_{eq} = 0.50$

37 Tubes

Increasing tube number →

.94

Ⓐ

$L_T/D_{eq} = 0.25$

61 Tubes

Increasing tube length ↑

.92

.90

CONSTANTS:

——— Close-packed arrays

- Nozzle area ratio = 3.3
- Nozzle pressure ratio = 3.0
- T_T = ambient
- $C_f = 0.003$
- Elliptical convergent tubes
- $A_P = 13.6 \text{ in}^2$ ($D_{eq} = 4$ in.)

.88

.86

Ⓐ Examples of differences in performance due to changing only base array (close-packed arrays vs radial arrays; tube number, tube length, and nozzle area ratio fixed)

Area ratio $= \dfrac{\pi R_b^2}{A}$

$L_T/D_{eq} = L_T / \sqrt{\dfrac{4A}{\pi}}$

L_T

R_b

Figure 83.—Effect of Tube Number, Base Array and Tube Length on Suppressor Performance

123

Figure 84.—Effect of Area Ratio, Base Array, and Tube Length on Suppressor Performance
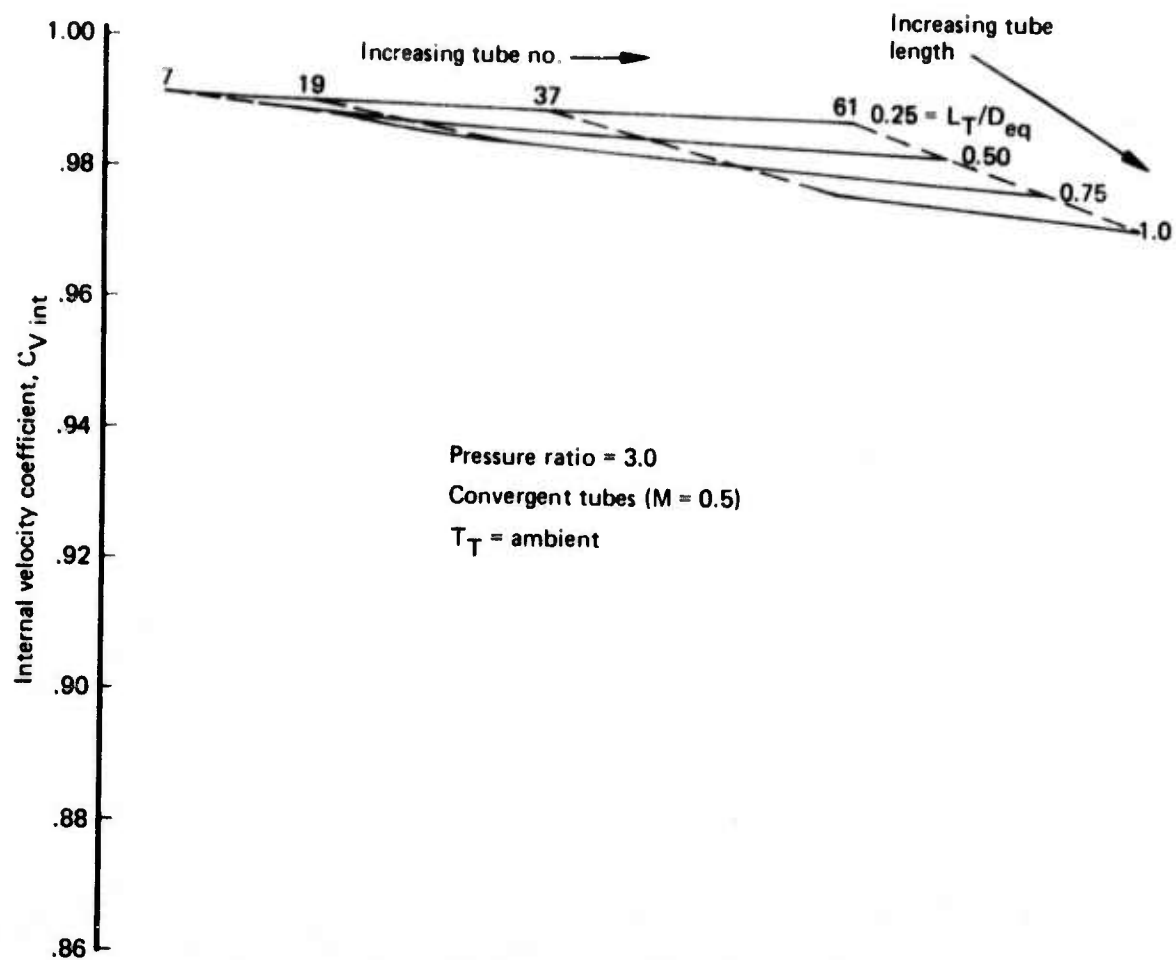
Figure 85.—Effect of Tube Length and Number on Internal Velocity Coefficient Ambient
   Temperature
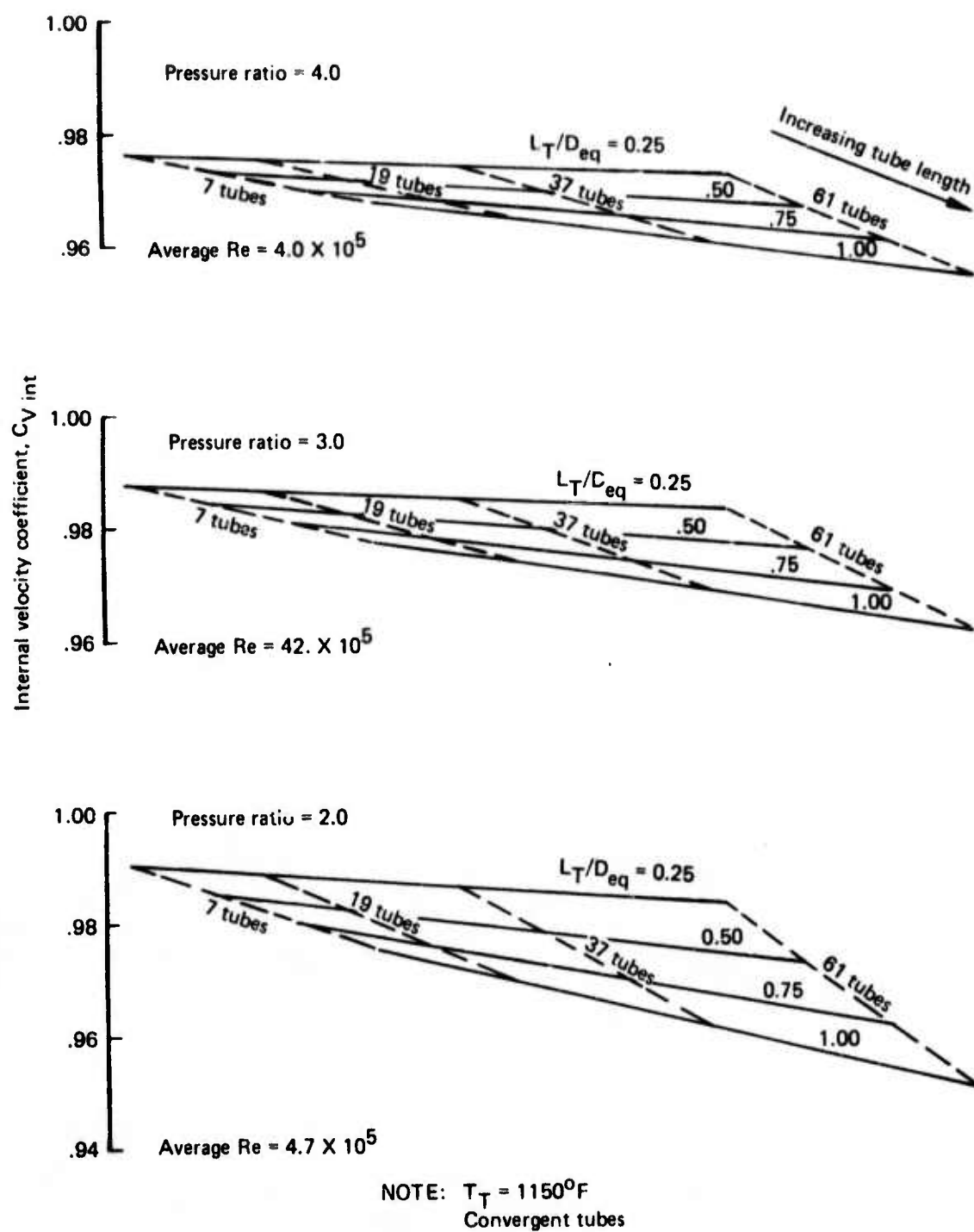
Figure 86.—Effect of Tube Length and Number on Internal Velocity Coefficient at 1150°F
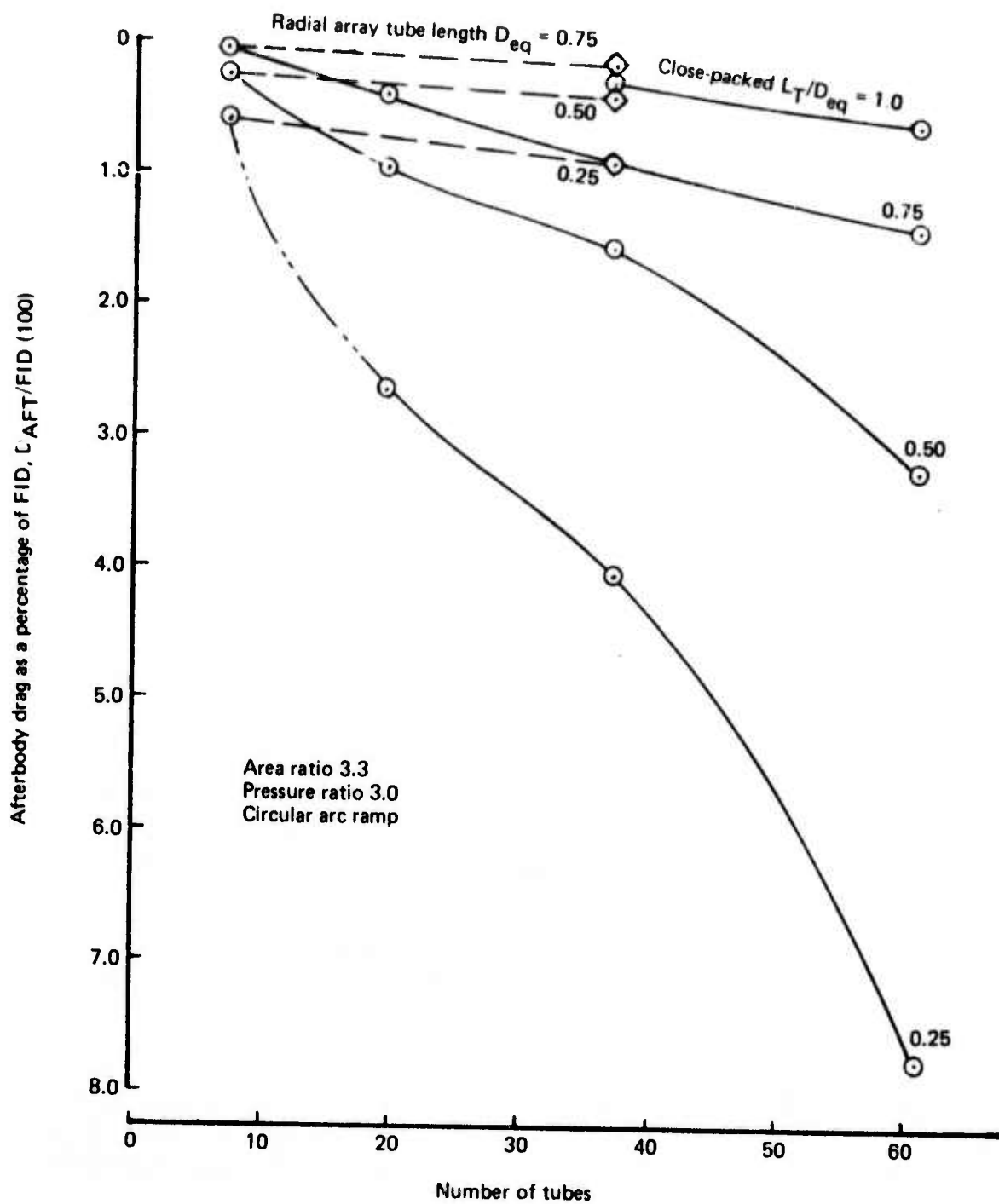
Figure 87.—Afterbody Drag as a Function of Tube Number, Tube Length and Tube Array
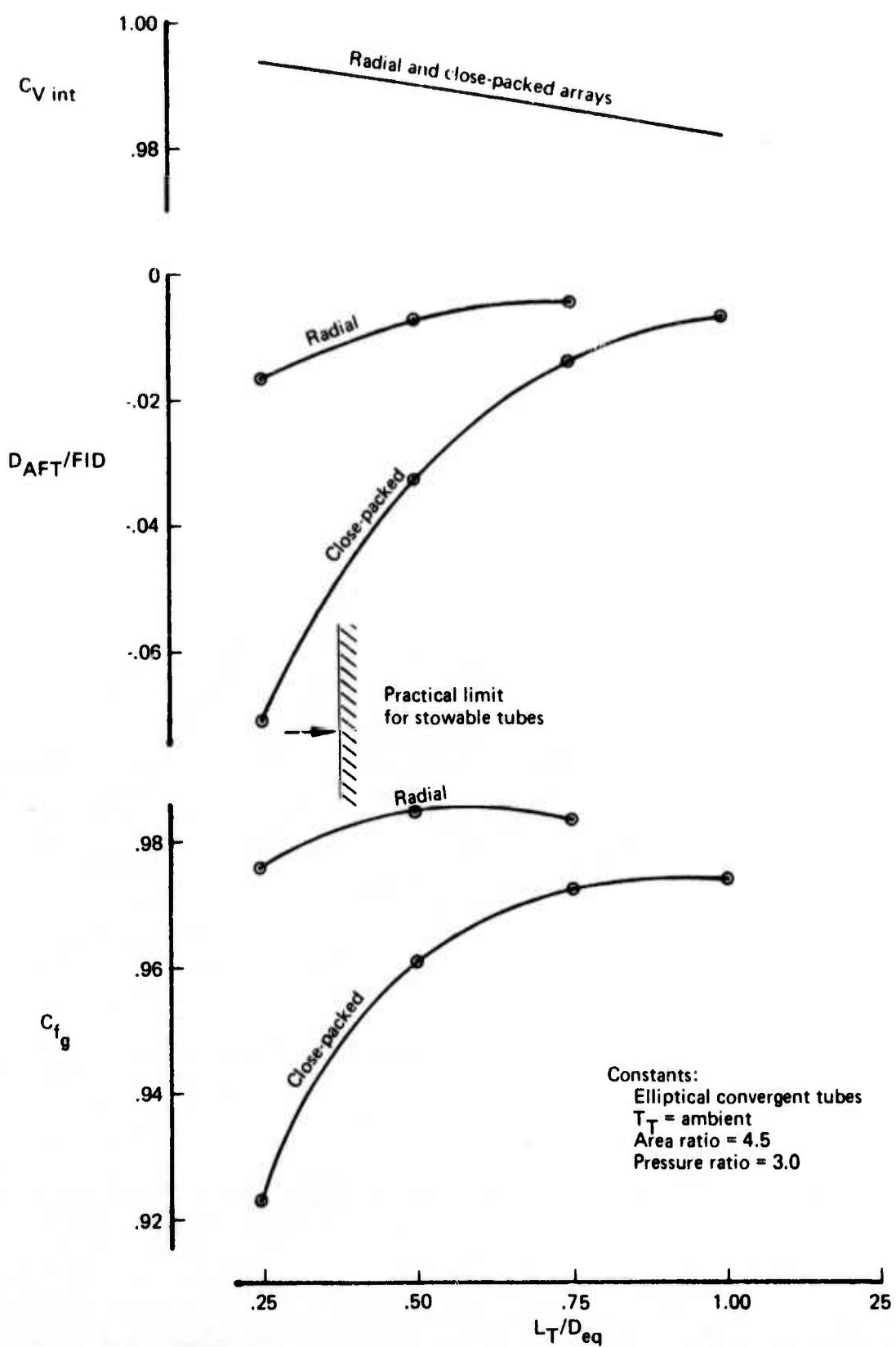
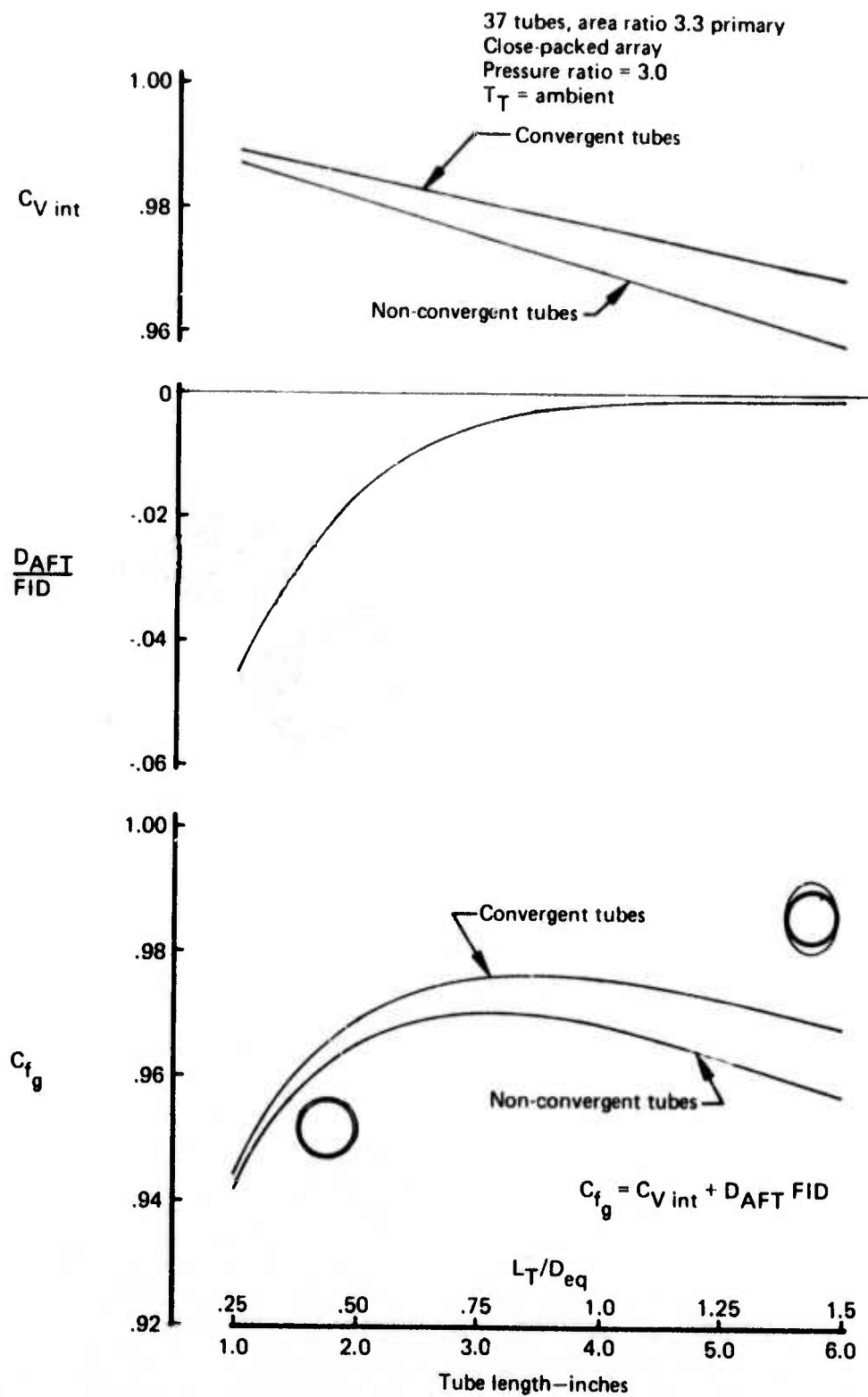Figure 88.—Performance Components for Radial and Close-Packed 37-Tube, Area Ratio 4.5
Arrays

128

Figure 89.—*Effect of Elliptical Convergent Versus Nonconvergent Tubes on Nozzle Performance*

129
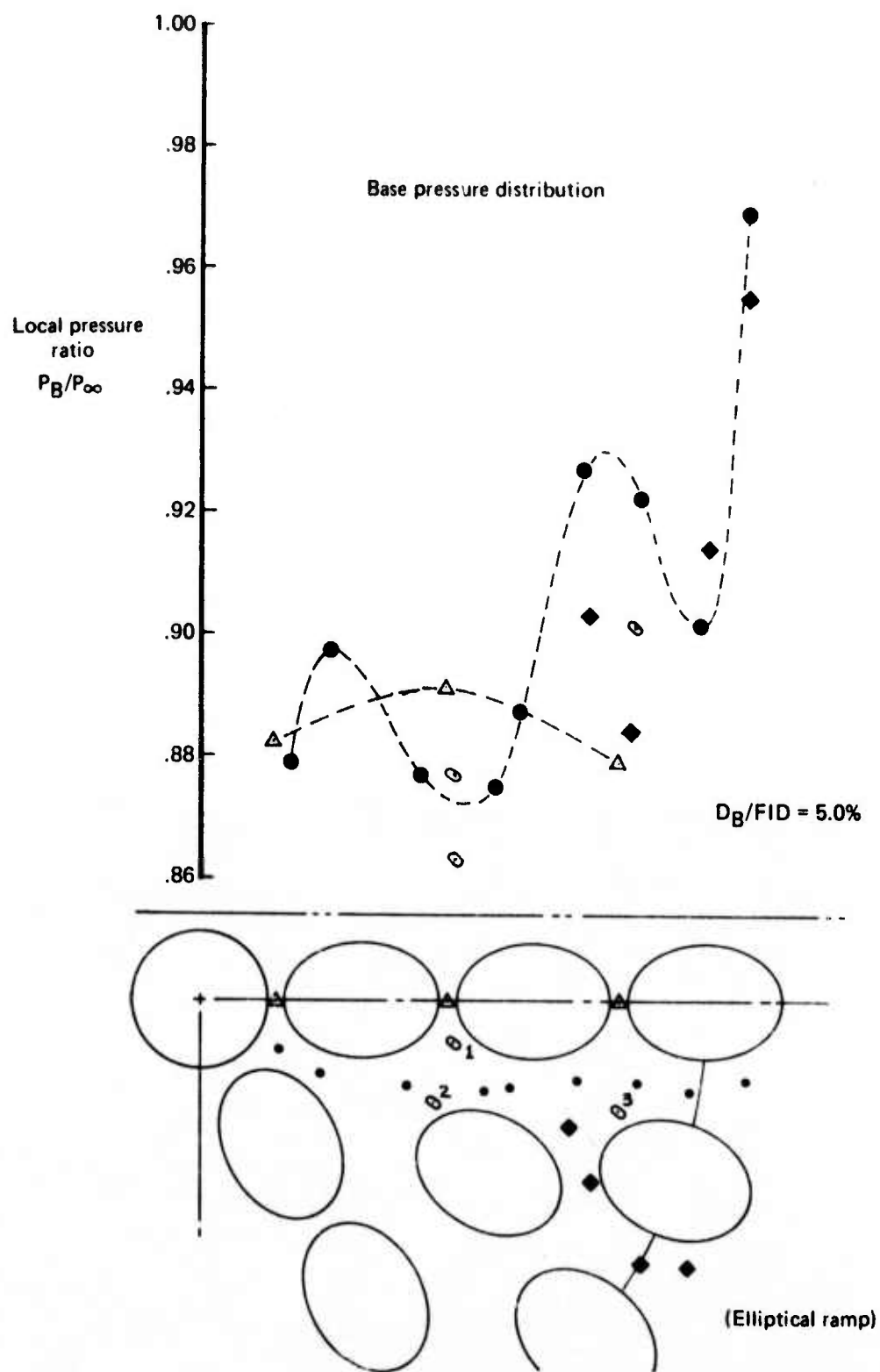
Figure 90.—Base Pressure Distribution 37-Tube, Close-Packed Array, AR = 2.75, L_T/D_{eq} = 0.25, PR = 3.0
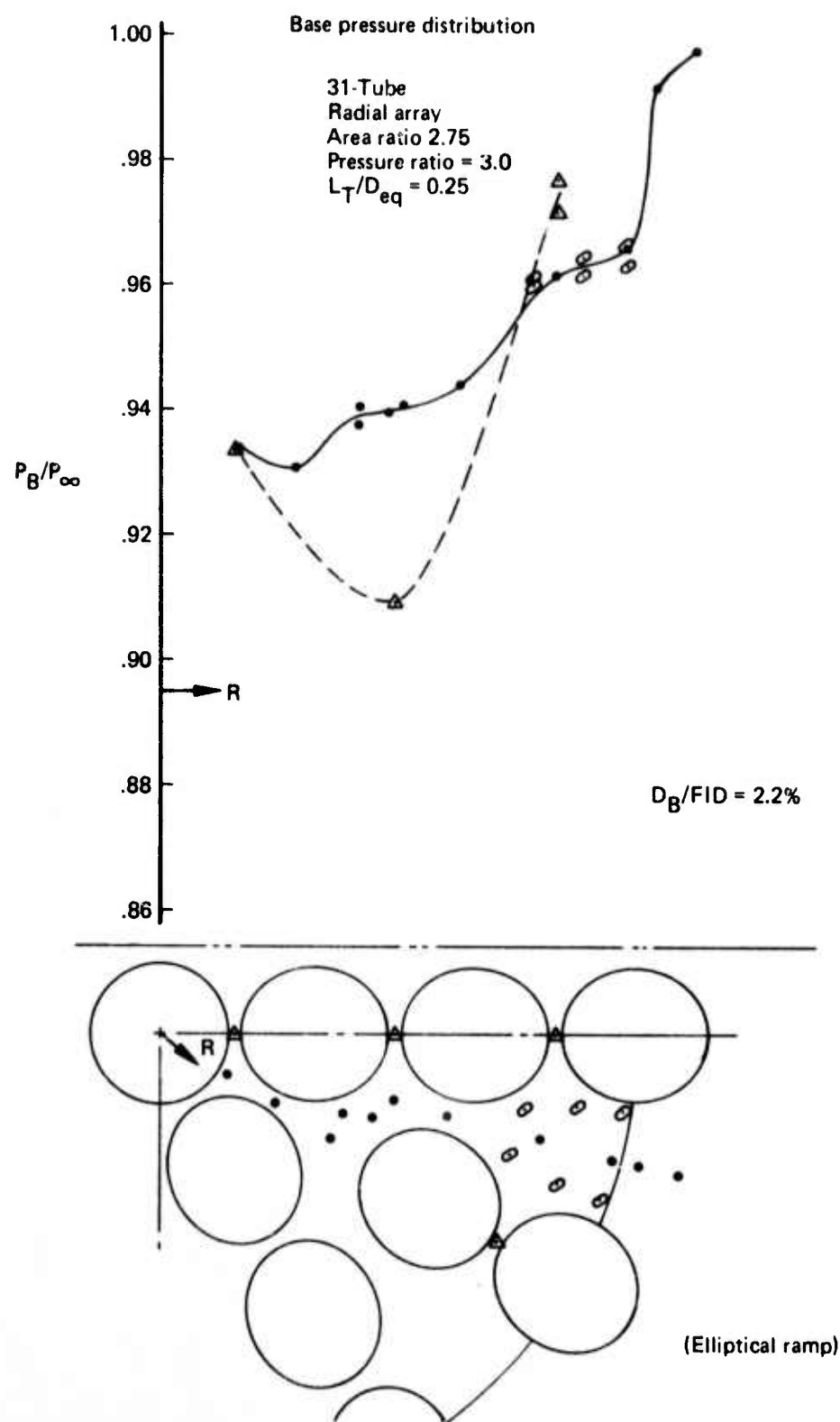
Figure 91.—Base Pressure Distribution 31-Tube Radial Array, AR = 2.75 L_T/D_{eq} = 0.25, PR = 3.0
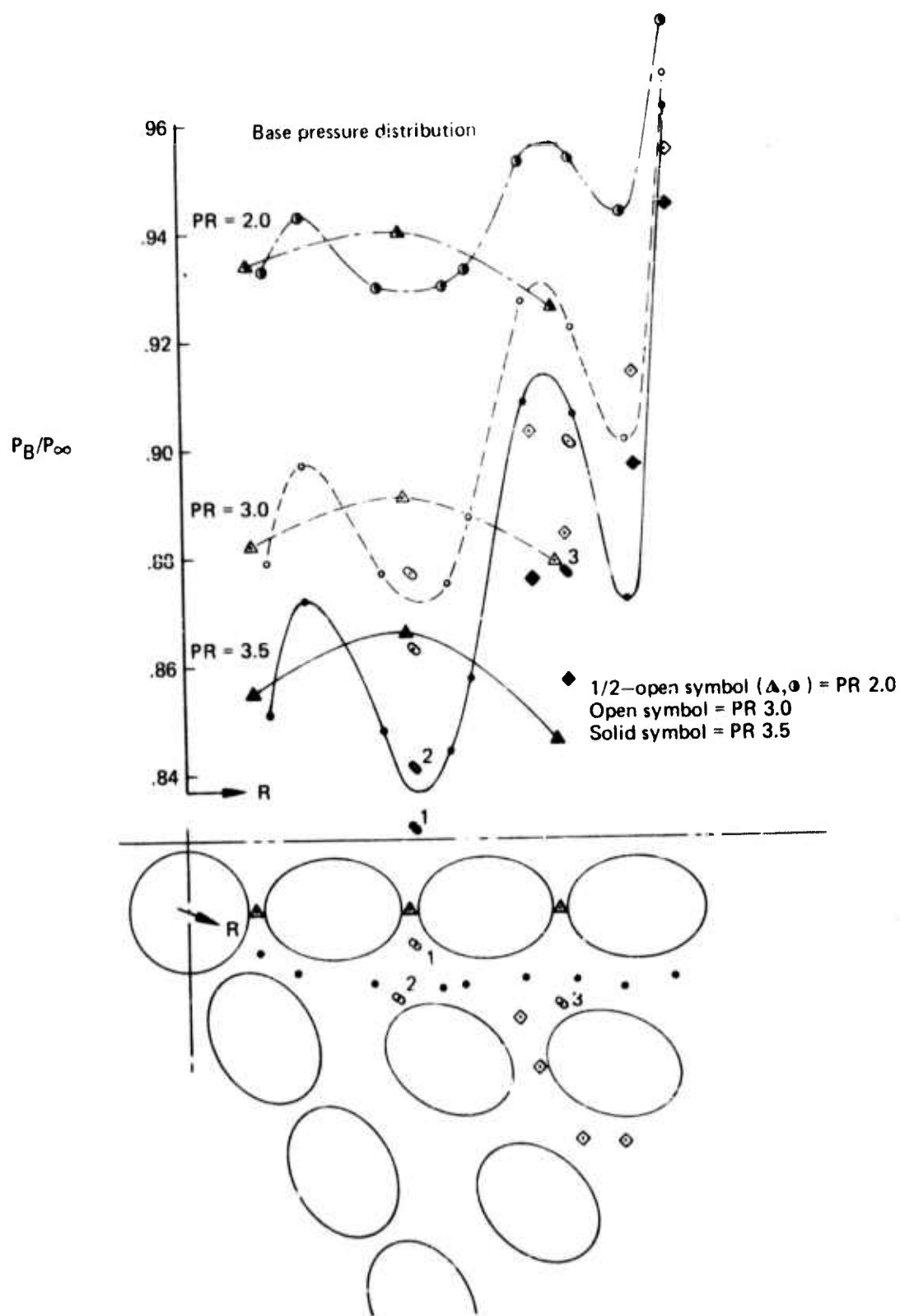
Figure 92.—Effect of Pressure Ratio on Base Pressure Distribution, 37-Tube, Close-Packed Array, AR = 2.75, L_T/D_{eq} = 0.25, PR = 2.0, 3.0, 3.5
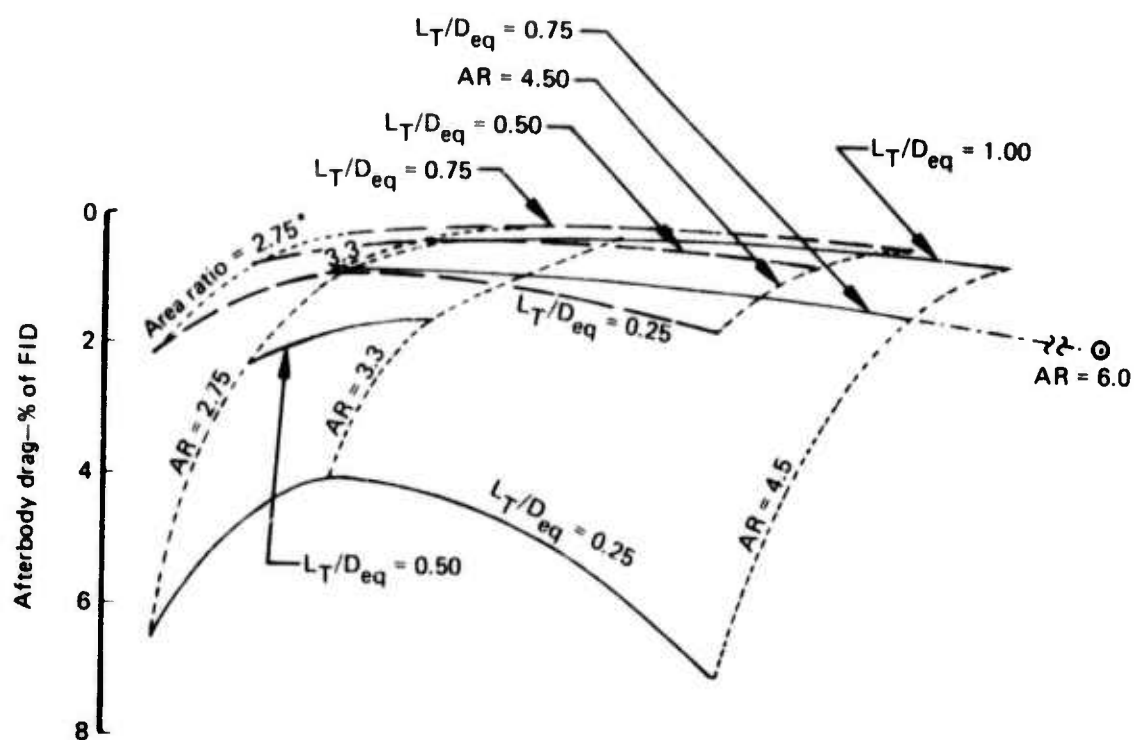
132
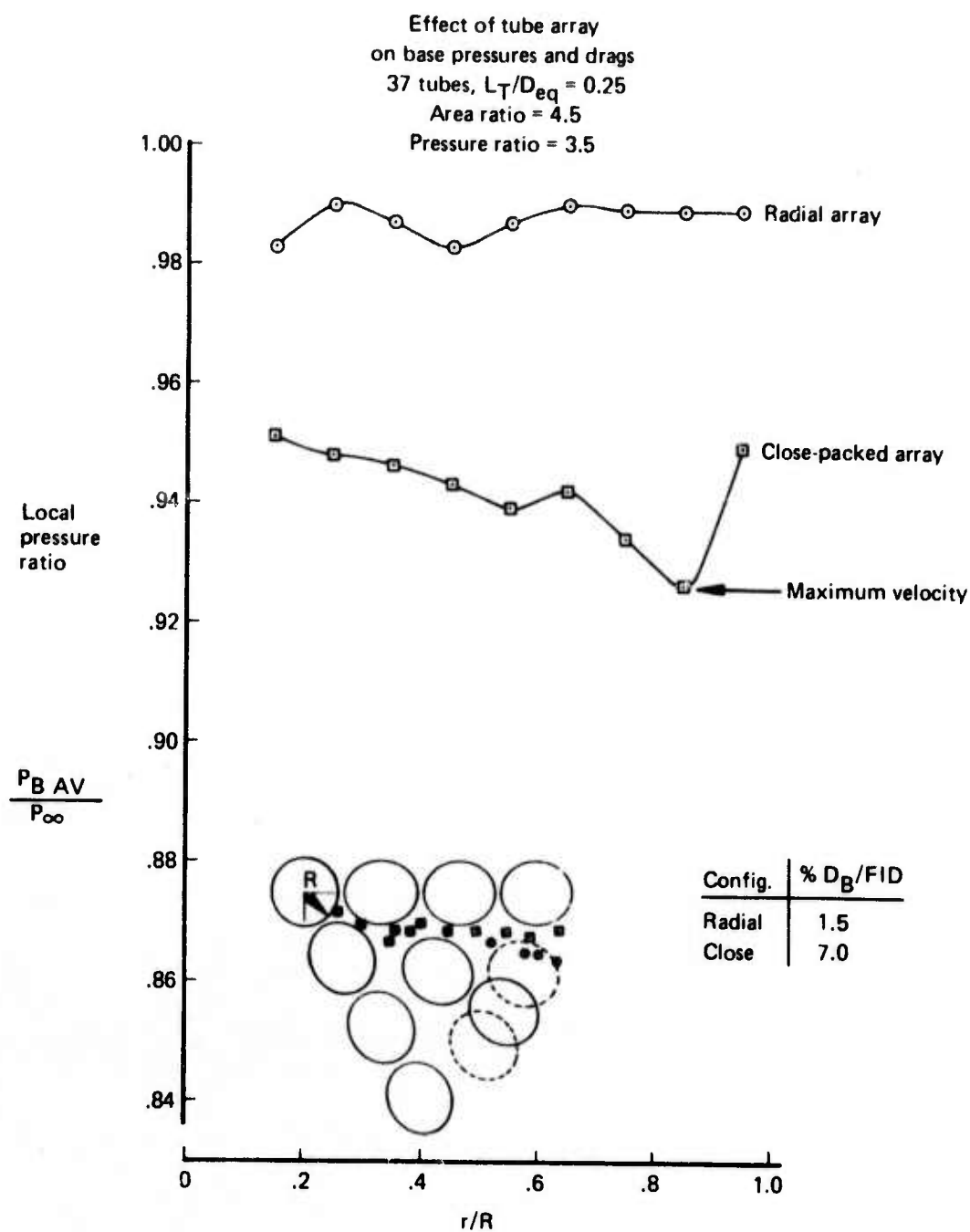
Figure 93.—Effect of Tube Array on Base Pressures and Drag

133

Figure 94.—Effect of Area Ratio and Tube Length on Afterbody Drag as a Percentage of FID

134
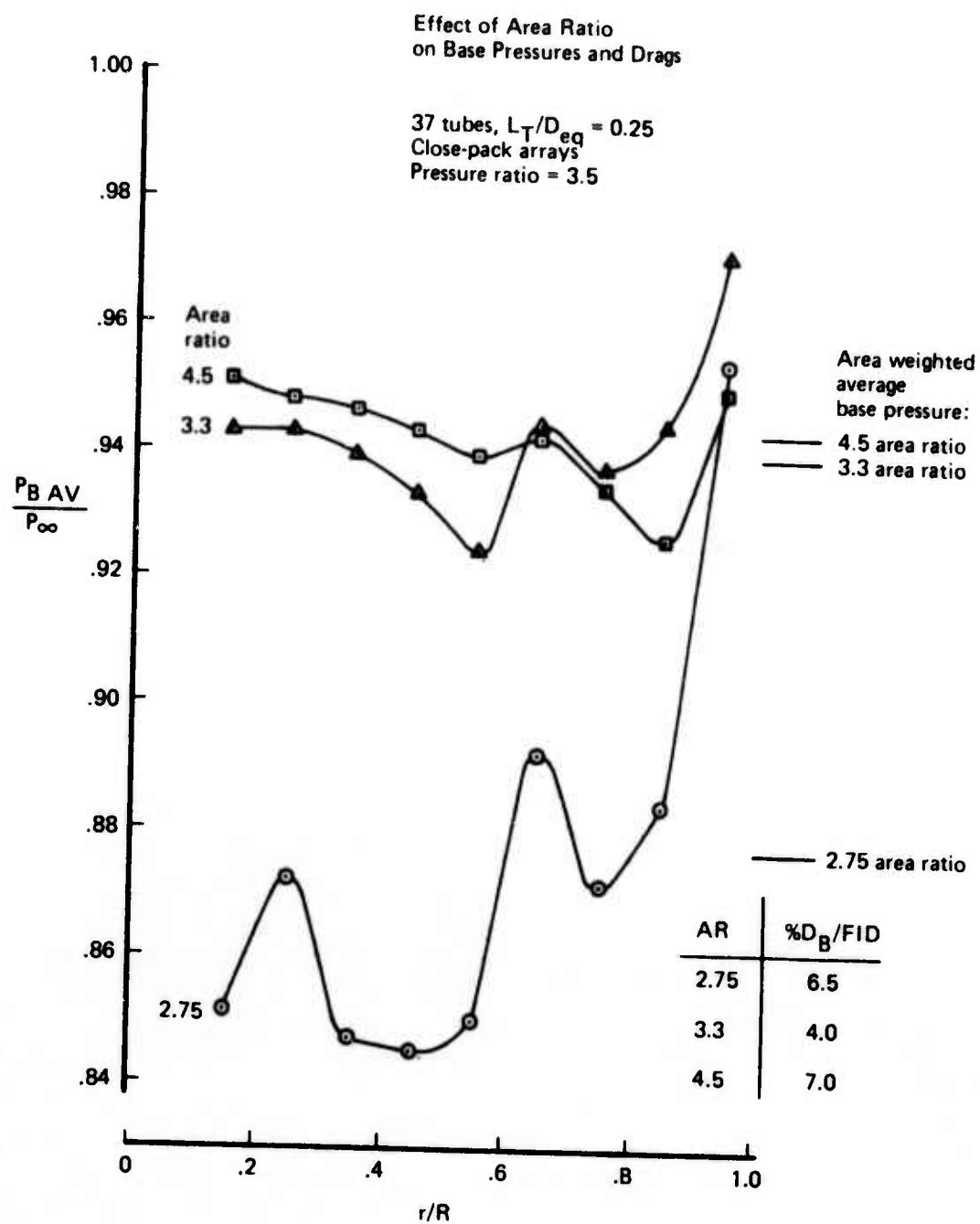
Figure 95.—Effect of Area Ratio on Base Drag and Base Pressures

135

37-tube area ratio = 3.3 close-packed nozzles with elliptical ramps

Gross thrust coefficient

Afterbody drag — % of FID

L_T/D_{eq}

O   Elliptical convergent tubes

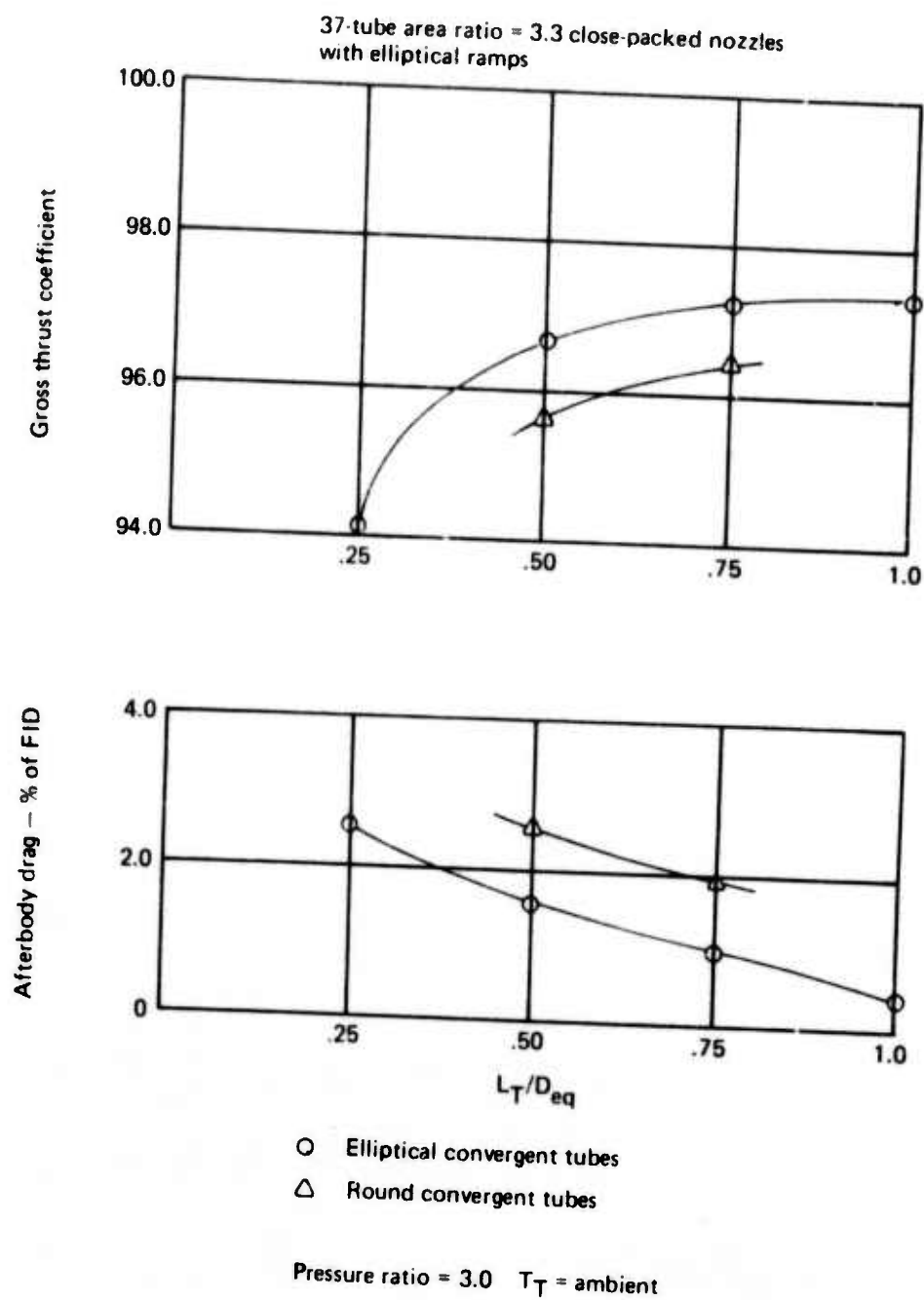△   Round convergent tubes

Pressure ratio = 3.0 T_T = ambient

Figure 96.—Effect of Tube Shape on Gross Thrust Coefficient and Afterbody Drag/FID
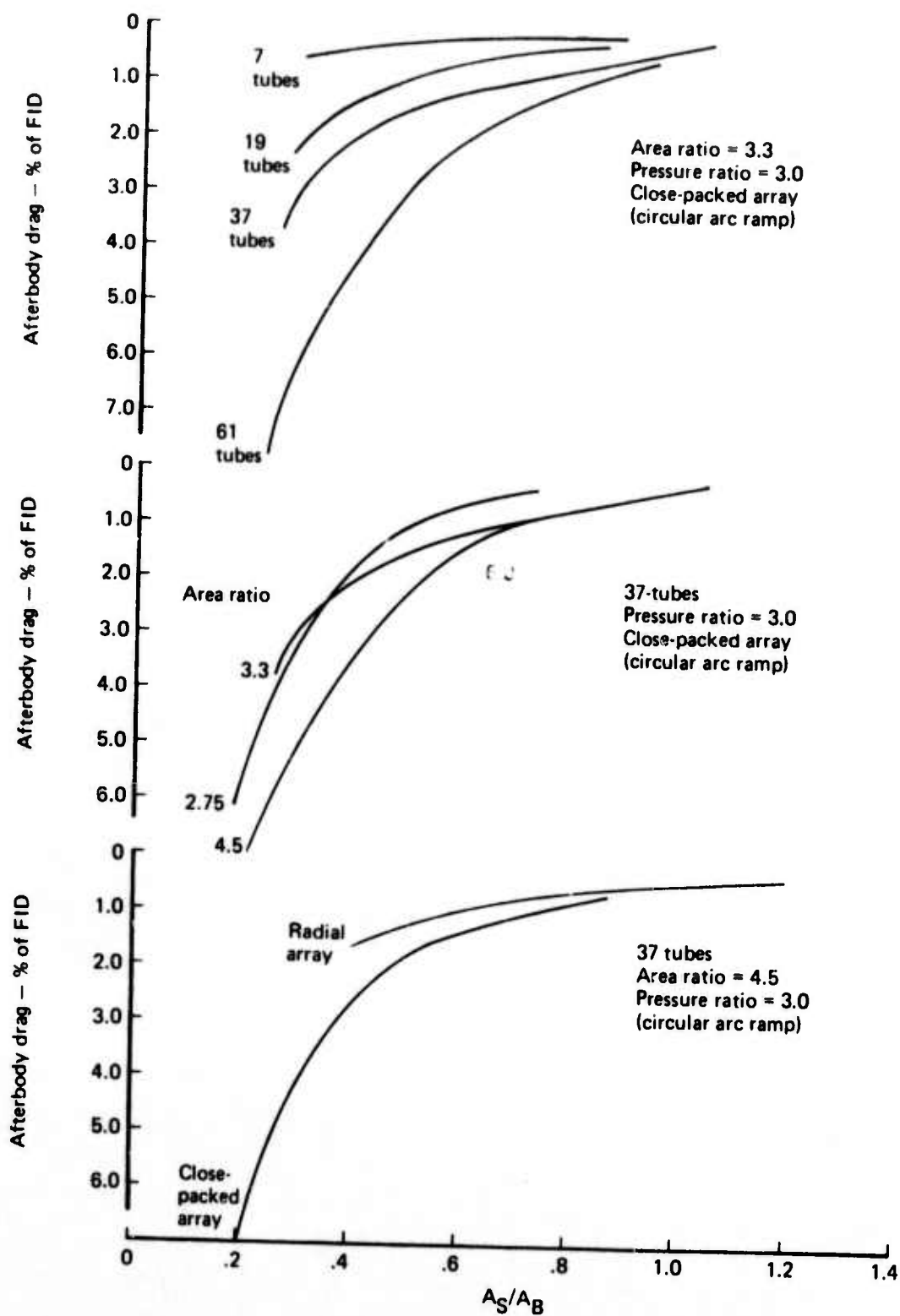
136

Figure 97.—Afterbody Drag/FID Versus Physical Ventilation Parameter (AS/AB) for Various Tube Number, Area Ratios, and Arrays
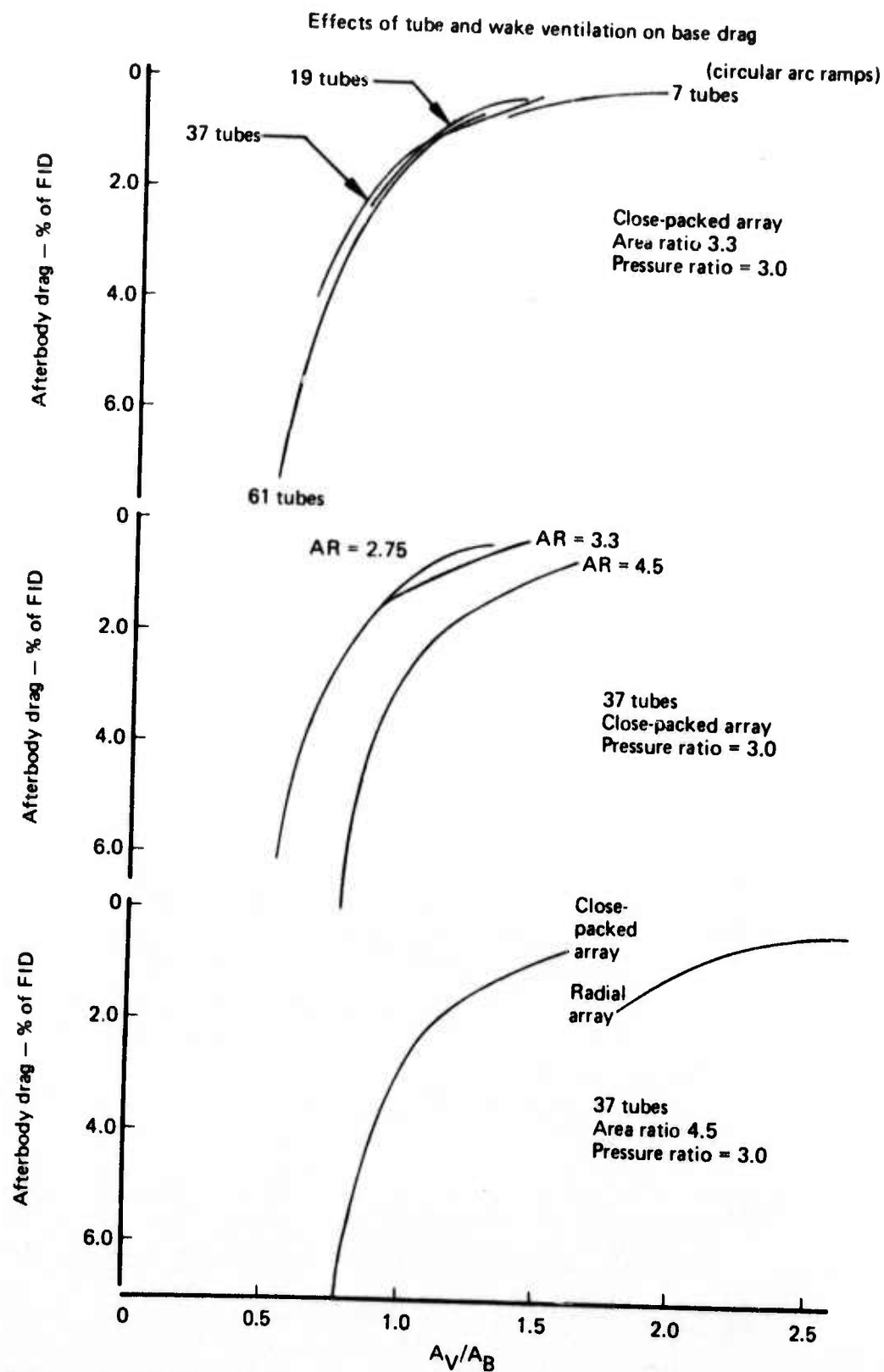
137

Figure 98.—Afterbody Drag/FID Versus Ventilation Parameter Including Jet Wake (AV/AB) for Various Numbers of Tubes, Area Ratios, and Arrays
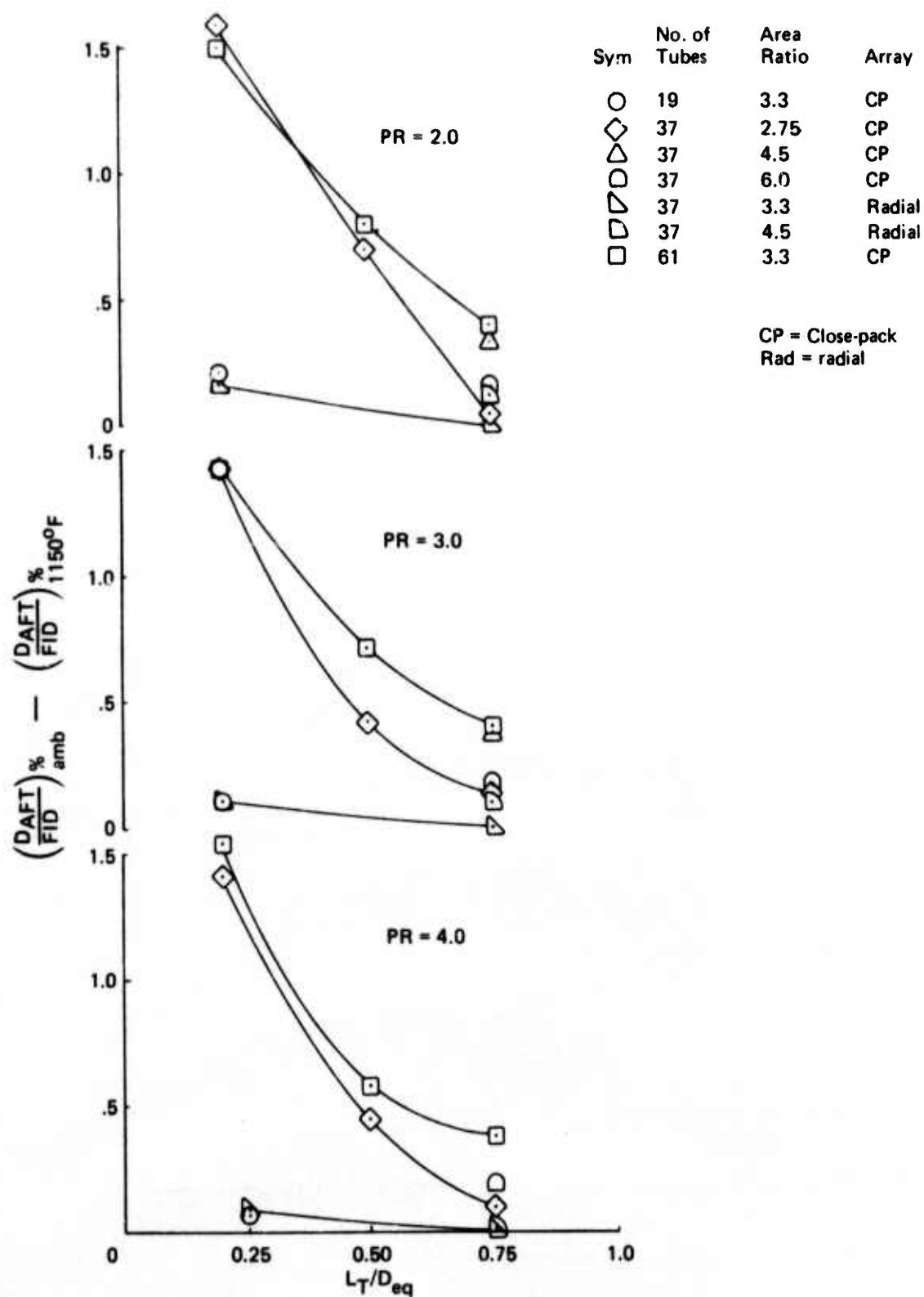
138

Figure 99.—Temperature Induced Changes in Afterbody Drag as a Percentage of FID
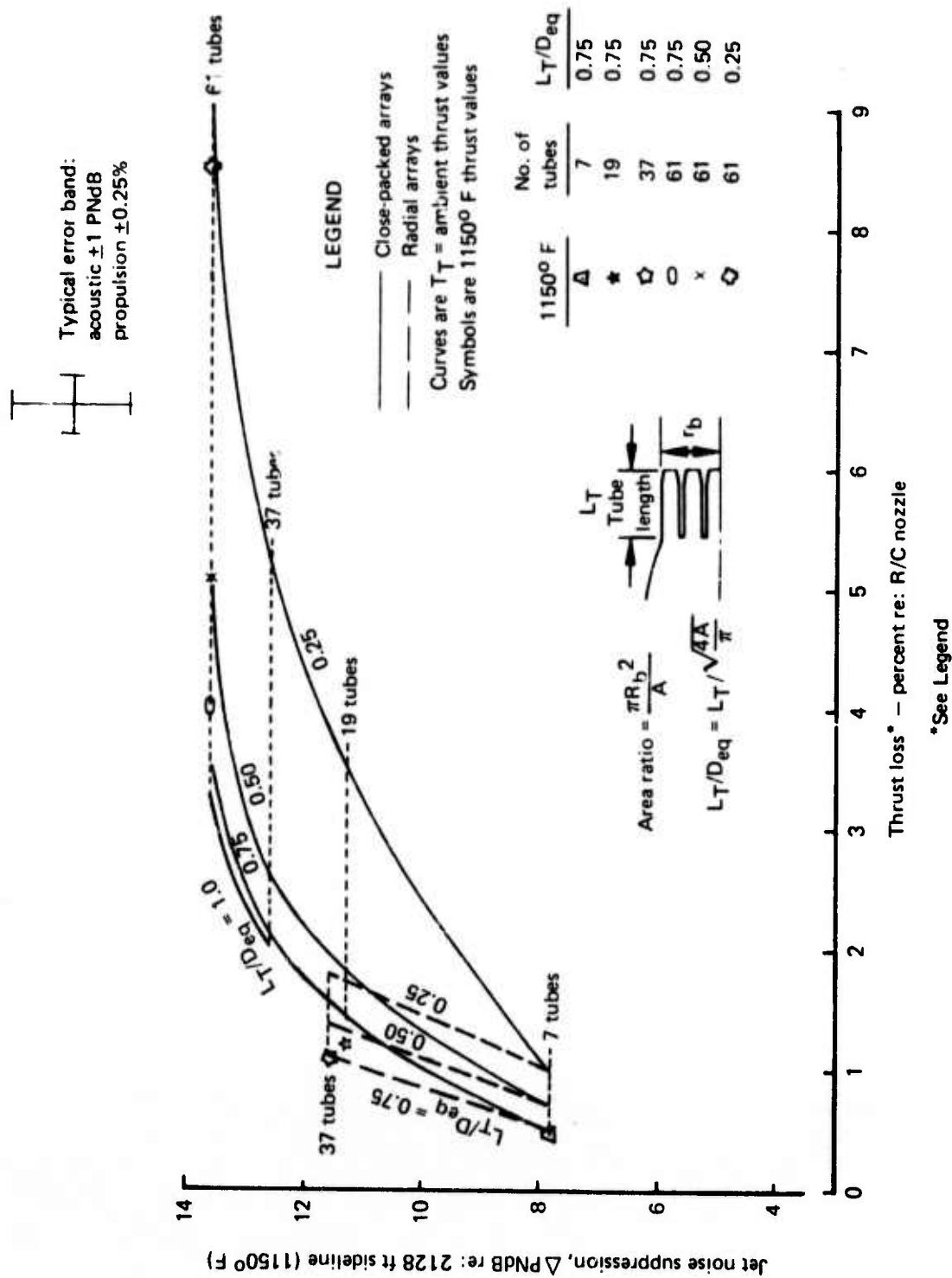
Figure 100.—Summary of Suppression Versus Thrust Loss—Area Ratio 3.3, Pressure Ratio 3.0
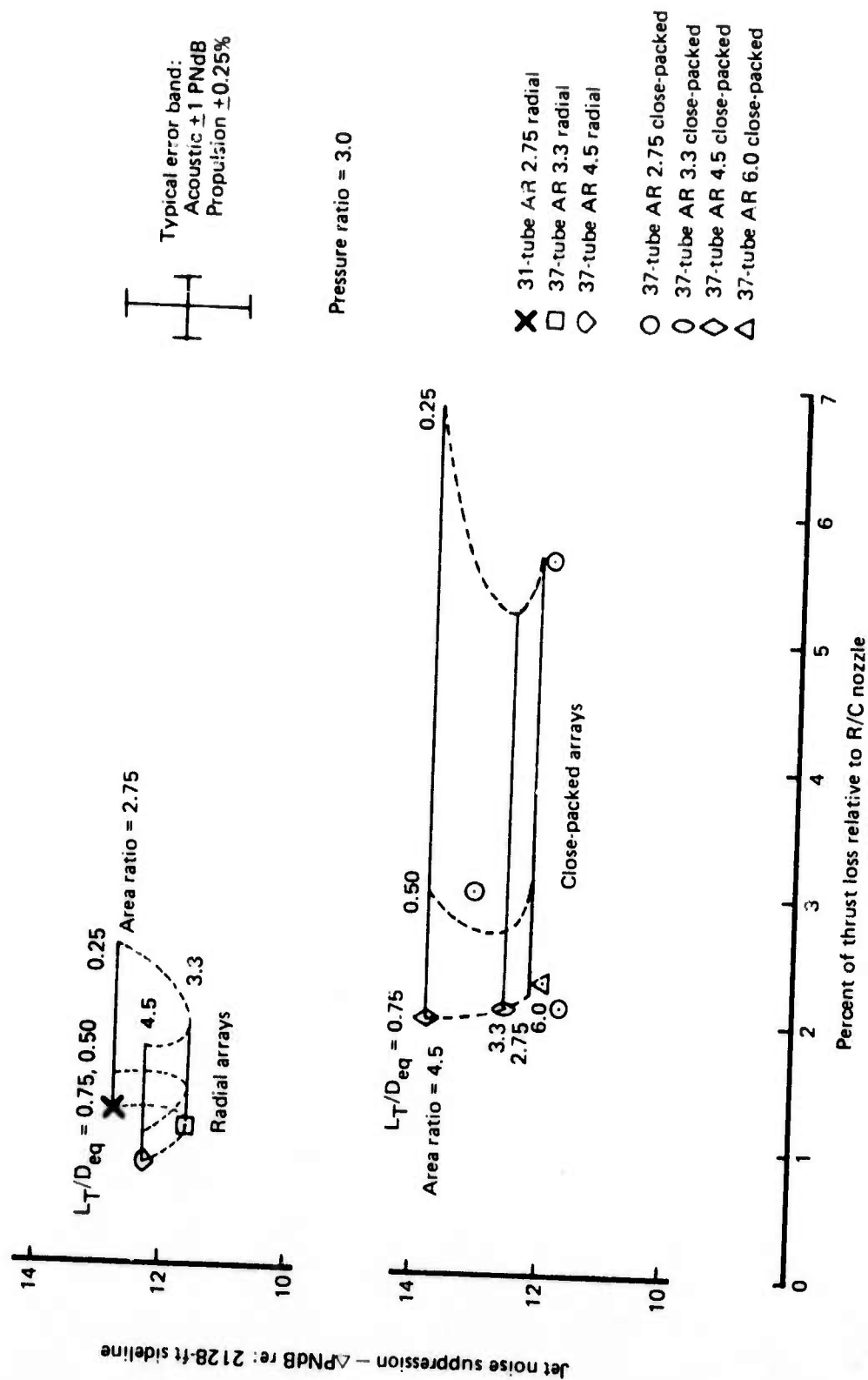
140

Figure 101.—Jet Noise Suppression Versus Thrust Loss

141

REFERENCES

1. J. Atvars, et al. *SST Technology Follow-On Program — Phase II — Noise Suppressor Nozzle Development — Volume II — Noise Technology*, FAA-SS-73-11-2 Federal Aviation Administration, Washington D.C.

2. H. Lu, D. Morden, R. Benefiel, and C. Simcox, *SST Technology Follow-On Program — Phase I: Performance Evaluation of the NCS-119B Nozzle System, Volume I: Suppressed Mode*, FAA AD-900-399L, February 1972.

3. C. Wright, D. Morden, and C. Simcox, *SST Technology Follow-On Program — Phase I: A Summary of the SST Noise Suppression Test Program*, FAA AD-900-401L, February 1972.

4. J. Campbell, D. Harkonen, R. Lawrence, and J. O'Keefe, *Design Integration and Noise Studies for Jet STOL Aircraft — Noise Suppression of Improved Augmentors for Jet STOL Aircraft*, NASA GR-114534, January 1973.

5. F. Strout and R. Lipke, *Multitube Suppressor Nozzle Characteristics Volume I: Generalized Nozzle Thrust Performance*, Boeing D6-A11822-1, April 1970.

6. F. Pearlman, *Thrust and Flow Characteristics of a Referee Multitube Nozzle With Ejector*, FAA-SS-73-11-6, June 1974.

7. C. W. Harris, *Elimination of Hydraulic Eddy Current Loss at Intake*, University of Washington Bulletin No. 54, October 1930.

8. *Aerodynamic Design — Air Intake Aircraft Engineering*, December 1969.

9. A. H. Shapiro, *The Dynamics and Thermodynamics of Compressible Fluid Flow Volume 1*, The Ronald Press Company, New York, 1953.

10. C. D. McClung, *Test Data Report — Parametric Test of Conical Convergent Nozzles*, Unpublished.

11. H. Schlichting, *Boundary Layer Theory*, trans. J. Kestin, McGraw-Hill, 1960.

12. A. R. Barbin and J. B. Jones, "Turbulent Flow in the Inlet Region of a Smooth Pipe," *Journal of Basic Engineering*, paper number 62-Hyd-10, presented at ASME Hydraulics Convention, Worcester, Massachusetts, 21-23 May, 1962.

13. W. Kays and A. Landon, *Compact Heat Exchangers*, table 17, The National Press, 1955.